Dynamics of Excited Molecules: Predissociation

Hajime Katô*

Department of Chemistry, Faculty of Science, Kobe University, Nada-ku, Kobe 657, Japan

Masaaki Baba

Faculty of Integrated Human Studies, Kyoto University, Sakyo-ku, Kyoto 606, Japan

Received November 10, 1994 (Revised Manuscript Received July 18, 1995)

Contents

I. Introduction

Direct photodissociation occurs when a molecule is excited by light to a dissociative continuum. However, if a certain discrete energy level has the same energy as a dissociative continuum and certain selection rules for the coupling are fulfilled, the molecules excited to a discrete level can dissociate. This phenomenon is called *predissociation*. In this case, the molecule is excited to a bound state which is coupled to a dissociative continuum. An absorption line of a transition to a predissociative level is usually broadened, and the lifetime of the excited level is shorter than that of a nonpredissociative level. Because a transition to a single predissociative level

0009-2665/95/0795-2311$15.50/0

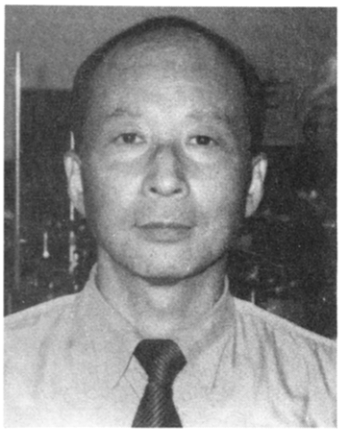

Hajime Katô was born in Gifu, Japan, in 1941. He obtained his B.S., M.A., and Ph.D. at the Faculty of Science, Kyoto University, and is currently a Professor at the Faculty of Science, Kobe University. He did graduate research on theoretical calculations on molecular properties by using a semiempirical LCAO-MO-SCF method with T. Yonezawa. In 1968, he moved to the Faculty of Science, Kobe University as a research associate and studied the MCD spectra of transition metal complexes. As a Japanese Ramsay Fellow (1972–1975), he spent 18 months working with A. D. Buckingham at Cambridge University and 6 months working with A. J. McCaffery at Sussex University. During a short period of work with Tony McCaffery, he was attracted by the beautiful world of laser spectroscopy. His research interests include molecular structure and dynamics and high-resolution laser spectroscopy now made possible to measure the Zeeman and Stark splittings in an electronic spectrum. He enjoys studying small molecules using various techniques of laser spectroscopy, molecular beams, electric or magnetic field, and theory.

Masaaki Baba was born in Fukuoka, Japan, in 1955. He obtained both his B.Sc. and Sc.D. at the Faculty of Science, Kyoto University. After studying the molecular spectroscopy for the triplet state of organic molecules with Professor Noboru Hirota, he joined the research group of Professor Ichiro Hanazaki in the Institute for Molecular Science, Okazaki, and began the work on laser spectroscopy in a supersonic jet. In 1986, he moved to Faculty of Science, Kobe University as a research associate of Professor Hajime Katô. Since then he has been concerned with high-resolution spectroscopy of small molecules. His research interests include the perturbation in the electronic excited states and dynamical processes of the excited molecule. Now he is an Associate Professor at the Faculty of Integrated Human Studies, Kyoto University.

can be selectively excited with narrow bandwidth laser light, we can study decomposition from a given electronic–vibrational–rotational (e,v,J) level. If AB is a molecule that dissociates into fragments A and B, a chemical reaction starting from a single level AB(e,v,J) can be studied if an appropriate system is chosen: AB(e,v,J) + $h\nu$ → AB(e',v',J') → A(e_a,v_a,J_a) + B(e_b,v_b,J_b). Furthermore, the translational vector and the orientation of products can be measured by various spectroscopic methods. Thus, the dynamics responsible for photofragment internal state distribution and angular momentum alignment can be studied by starting from the simplest initial state. Because predissociation is one of the simplest chemical reactions, studies on predissociation may be a useful approach for understanding chemical reaction dynamics.

In the early stage of establishment of quantum mechanics, Wentzel[1] has shown that the transition probability from a discrete state n to a dissociative continuum c of equal energy is given by

$$(4\pi^2/h)|\int \Phi_c^* H' \Phi_n \, d\tau|^2 \qquad (1)$$

where Φ_c and Φ_n are, respectively, properly chosen wave functions of c and n states, H' is the Hamiltonian of the perturbation responsible for the predissociation, and h is Planck's constant. A number of theoretical and experimental studies have been reported,[2–6] and very good summaries and reviews have also been published.[7–13]

Predissociation manifests itself by the appearance of line broadening, a decrease in lifetime, an abrupt decrease of fluorescence quantum yield, and generation of dissociation products. Lasers and synchrotron radiation have enabled us to excite a molecule to a specific energy region. Pulsed lasers of short duration have made it easy to measure time-resolved dynamics. Tunable lasers with narrow line widths enable us to measure line widths. More direct measurements of predissociation by the simultaneous detection of the absorption spectra and the dissociation products have been reported.[14,15]

In this work we review the studies that emphasize the predissociation confirmed by the detection of the dissociation products. We try to review the articles up to the beginning of 1994, but we shall confine this review to molecules which are extensively studied. Predissociations of ions and van der Waals molecules are not included.

A short summary of the theory of predissociation will be given in section II. Classifications of predissociations are summarized in section III. Experimental methods for studies of predissociation are reviewed in section IV. Practical studies of predissociation are reviewed for diatomic molecules in section V and for polyatomic molecules in section VI.

II. Theory of Predissociation

A general theory of predissociation has been given by Fano,[16] and a brief summary is described here. We let the φ_m and ψ_E be wave functions in the Born–Oppenheimer approximation. When a set of discrete states φ_1, φ_2, ..., φ_n, etc. and a set of ψ_E, belonging to one continuum (a dissociative continuous state) interact, we need to diagonalize the Hamiltonian matrix

$$\langle \varphi_m | H | \varphi_n \rangle = E_n \delta_{mn}$$

$$\langle \psi_{E'} | H | \varphi_n \rangle = V_{E'n}$$

$$\langle \psi_{E''} | H | \psi_{E'} \rangle = E' \delta(E'' - E') \qquad (2)$$

The interaction between φ_m and ψ_E can occur through interactions described in section III.C. The eigen-

functions within the continuum are expressed as

$$\Psi_E = \sum_n a_n(E)\varphi_n + \int b(E')\psi_{E'}\,dE' \qquad (3)$$

If the energy spacings between the discrete levels are much larger than the interaction energy $V_{E'n}$, it is a reasonable approximation to take into account of the perturbations between only one discrete state and one continuum. This is the case of an isolated resonance. If a discrete state φ_n lies within a continuum $\psi_{E'}$, the wave function of the mixed state of energy E is expressed as

$$\Psi_E = a(E)\varphi_n + \int b(E')\psi_{E'}\,dE' \qquad (4)$$

where

$$a(E) = \frac{V_{En}}{E - E_n - F(E) - i\pi|V_{En}|^2} \qquad (5)$$

$$b(E') = \left[\frac{1}{E - E'} + z(E)\delta(E - E')\right]V_{E'n}a(E) \qquad (6)$$

$$z(E) = \frac{E - E_n - F(E)}{|V_{En}|^2} \qquad (7)$$

and $F(E)$ is the shift of the resonance position with respect to E_n:

$$F(E) = \mathrm{P}\int \frac{|V_{E'n}|^2}{E - E'}\,dE' \qquad (8)$$

P indicates "the principal part of". Numerical methods to calculate the principal part of this integral are given in refs 17–19.

A. Optical Transition Allowed Only to a Discrete Level

When an optical transition between an initial state i and a continuum ψ_E is forbidden, $\langle\psi_E|\mathbf{T}|i\rangle$ equals 0 and the transition probability of the optical transition is proportional to

$$|\langle\Psi_E|\mathbf{T}|i\rangle|^2 = \frac{|V_{En}|^2}{[E - E_n - F(E)]^2 + \pi^2|V_{En}|^4}\,|\langle\varphi_n|\mathbf{T}|i\rangle|^2 \qquad (9)$$

where $\mathbf{T}$ is the electric dipole moment. The probability is maximum at an energy including the predissociation-induced energy shift: $E = E_n + F(E)$. The predissociation rate (the probability per unit time) k_{pr} is given by

$$k_{\mathrm{pr}} = (2\pi)^2|V_{En}|^2/h \qquad (10)$$

and is equal to the expression presented in eq 1. The lifetime τ of the excited level φ_n is given by

$$1/\tau = (2\pi)^2|V_{En}|^2/h + 1/\tau_r \qquad (11)$$

where τ_r is the radiative lifetime of the excited level φ_n. The spectroscopic absorption line shape has

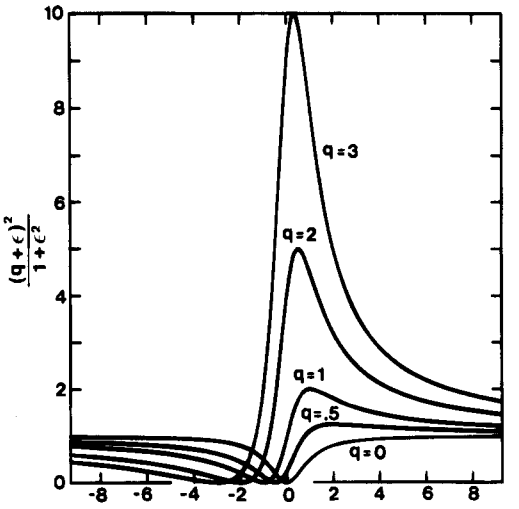

Figure 1. The Fano line shapes for different values of the Fano index q. Reverse the scale of abscissas for negative q. (Reprinted from ref 16. Copyright 1961 American Institute of Physics.)

Lorentzian form, and the width Γ (full width at half maximum) is related to the lifetime τ by

$$\Gamma(\mathrm{cm}^{-1}) = \frac{1}{2\pi c\tau\,(\mathrm{s})} = \frac{5.3 \times 10^{-12}}{\tau\,(\mathrm{s})} \qquad (12)$$

where c is the velocity of light.

B. Optical Transition Allowed Both to a Discrete Level and a Continuum

When optical transitions from an initial state i to both a discrete level and the continuum are allowed, the transition probability of the optical transition is proportional to

$$|\langle\Psi_E|\mathbf{T}|i\rangle|^2 = \frac{(q + \epsilon)^2}{1 + \epsilon^2}|\langle\psi_E|\mathbf{T}|i\rangle|^2 \qquad (13)$$

where $\langle\psi_E|\mathbf{T}|i\rangle$ is the transition moment to the unperturbed continuum

$$\epsilon = [E - E_n - F(E)]/(\pi|V_{En}|^2) \qquad (14)$$

$$q = |\langle\Phi_n|\mathbf{T}|i\rangle|/(\pi V^*_{En}|\langle\psi_E|\mathbf{T}|i\rangle|) \qquad (15)$$

and

$$\Phi_n = \varphi_n + \mathrm{P}\int \frac{V_{E'n}\psi_{E'}}{E - E'}\,dE' \qquad (16)$$

modifies φ_n by an admixture of the continuum. q characterizes the asymmetric line broadening of the absorption line.

The values of $|\langle\Psi_E|\mathbf{T}|i\rangle|^2/|\langle\psi_E|\mathbf{T}|i\rangle|^2$ are plotted as a function of ϵ in Figure 1 for a number of q. If the values of q and $|V_{En}|^2$ are obtained from the spectral data, we can determine the ratio of the transition probabilities to the "modified" discrete state Φ_n and to the unperturbed continuum (dissociative continuous state) ψ_E from the relation

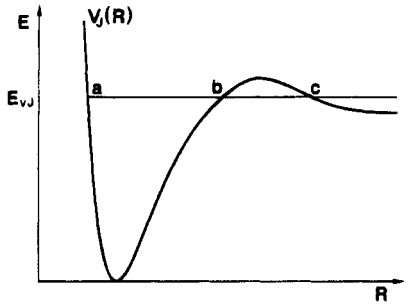

Figure 2. Potential energy curve of a quasi-bound state separated by a potential barrier; a, b, and c denote the classical turning points.

$$q^2\pi = \frac{|\langle\Phi_n|\mathbf{T}|i\rangle|^2}{\pi|V_{En}|^2|\langle\psi_E|\mathbf{T}|i\rangle|^2} \tag{17}$$

Fano[16] has studied the mixing between one discrete state and two or more continua and also the mixing between a number of discrete states and one continuum, but we shall omit them here.

C. Quasi-Bound State Separated from the Continuum by a Potential Barrier

The predissociation of a quasi-bound state separated from the continuum by a potential barrier can be treated by semiclassical scattering theory.[11,20] The potential function $V_J(R)$, where J is a rotational quantum number and R is an internuclear distance, is schematically depicted in Figure 2. The resonance energy position E_{vJ} of a (v, J) level, where v is a vibrational quantum number, is determined by the condition

$$\pi(v + {}^1/_2) = (1/\hbar)\int_a^b [2\mu(E_{vJ} - V_J(R))]^{1/2}\,dR - {}^1/_2\Phi \tag{18}$$

where μ is the reduced mass. Φ is a correction for the tunneling and is expressed as[11]

$$\Phi = \arg\Gamma({}^1/_2 + i\epsilon) - \epsilon\ln|\epsilon| + \epsilon \tag{19}$$

where $\Gamma(x + iy)$ is the complex gamma function,[21] and

$$\epsilon = -(1/\pi)\int_b^c [2\mu(V_J(R) - E_{vJ})]^{1/2}\,dR \tag{20}$$

The width of the resonance is calculated by

$$\gamma = (\hbar\omega/2\pi)\ln[1 + \exp(2\pi\epsilon)] \tag{21}$$

with

$$\hbar\omega = \partial E_{vJ}/\partial v \tag{22}$$

By observing the transition lines up to the quasi-bound region, the values of γ, E_{vJ}, and $\hbar\omega$ can be determined. The potential barrier can be determined by a least-squares optimization by varying the potential function $V_J(R)$ at positions, where observed data are available.

D. Intermediate Coupling Strength

In this section we consider the wave functions and potential curves that are well described using the Born–Oppenheimer approximation. The terms neglected in the Born–Oppenheimer approximation are considered as perturbing terms, which can cause predissociation. Very strong predissociation can occur when the potential curves of two electronic states of the same symmetry approach each other or when the spin–orbit interaction is very strong. In such cases, neither a noncrossing (adiabatic) potential curve representation nor a crossing (diabatic) potential representation is appropriate. Child[22] introduced an intermediate coupling picture that takes advantage of both the diabatic and adiabatic pictures for two interacting states 1 and 2 of a diatomic molecule. By a semiclassical calculation, the actual energy level in the region of the curve crossling lies intermediate between approximate energies of the adiabatic level E_{ad} and the diabatic level E_d close in energy:

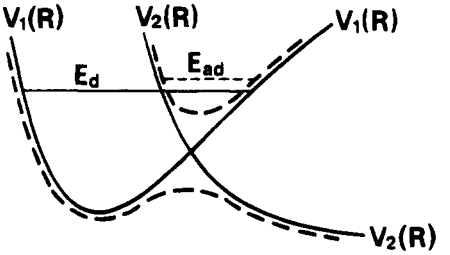

Figure 3. Diabatic (crossing) potential energy curves $V_1(R)$ and $V_2(R)$ are shown by solid lines. Adiabatic (noncrossing) potential energy curves are shown by dashed lines.

$$E = \frac{E_d + xE_{ad}}{1 + x} \tag{23}$$

where

$$x = (\bar{\omega}_d/\bar{\omega}_{ad})[\exp(2\pi\epsilon) - 1] \tag{24}$$

$\bar{\omega}_d$ and $\bar{\omega}_{ad}$ are, respectively, the local vibrational spacing for the diabatic and adiabatic potentials, and ϵ is the Landau–Zener parameter

$$\epsilon = \frac{|V_{12}|^2}{\hbar\bar{v}\Delta F} \tag{25}$$

where V_{12} is the interaction matrix element of the bound state 1 and the repulsive state 2 in the diabatic potentials, $\bar{v}$ is the radial velocity of the nuclear motion at the crossing point, and ΔF is the difference of the potential gradients of the diabatic potentials V_1 and V_2 at the crossing point. The potential curves using these parameters are schematically shown in Figure 3. The line width varies as[22]

$$\Gamma = \frac{2\pi x}{\hbar\bar{\omega}_d}\frac{[(\bar{\omega}_d/\bar{\omega}_{ad}) + x]}{(1 + x)^3}(E_d - E_{ad})^2 \tag{26}$$

The level energy and the line width can be calculated exactly by solving the following coupled equations for the vibrational wave functions:[23]

$$\left\{-\frac{\hbar^2}{2\mu}\frac{d^2}{dR^2} + V_1(R) - E\right\}\psi_1(R) = V_{12}\psi_2(R)$$

$$\left\{-\frac{\hbar^2}{2\mu}\frac{d^2}{dR^2}+V_2(R)-E\right\}\psi_2(R)=V_{12}\psi_1(R) \quad (27)$$

The result of semiclassical calculation was shown to be in excellent agreement with the exact solution of the coupled equation.[24]

III. Classification of Predissociation

The potential curve in the Born–Oppenheimer approximation (adiabatic approximation) is called an *adiabatic* potential. In diatomic molecules, the adiabatic potentials of identical symmetry and electron spin do not cross. The nonadiabatic interaction, spin–orbit coupling, and some additional interactions (which will be discussed in section III.C) cause a transition between adiabatic potentials. If the electrostatic interaction between approximate electronic states, which are described by approximate wave functions of a simple electronic character, is small and can be neglected, the potential curves of the same symmetry can cross. This approximate potential curve is called a *diabatic* potential. Mulliken[6] classified the electronic predissociation of diatomic molecules by the locations and shapes of the potential curves, and it will be summarized in section III.B. In polyatomic molecules, two potential surfaces can in principle intersect even if they belong to states of the same symmetry and spin multiplicity.[25–27]

A. Types Classified by Herzberg

Herzberg[7,8] has classified the predissociation of three kinds of overlapping of molecular energy levels (electronic, vibrational, or rotational) with a dissociation continuum.

Type I predissociation by electronic transition is caused by the coupling between discrete levels of a given electronic state and the dissociation continuum of another electronic state. This type of predissociation occurs most often. We will review mainly this type of predissociation.

Type II predissociation by vibration is caused by the coupling between a discrete vibrational level and a continuum joining onto a lower dissociation limit of another series of vibrational level in the same electronic state. This can occur when the image point representing the vibrational motion reaches an approximate saddle point of the potential surface. Only vibrational motion is changed in this predissociation process.

Type III predissociation by rotation is caused by a coupling between higher rotational levels of a given stable vibrational level of an electronic state and a dissociation continuum belonging to the same electronic state and the same series of vibrational levels. This can occur for vibrational levels of an electronic state that lie in the neighborhood of the dissociation limit, since the higher discrete rotational levels of such vibrational levels can lie above the dissociation limit.

B. Classification by the Location and Shape of Potential Curves

As we can see from eq 1, the predissociation probability depends on

$$\int \Psi_c^* H' \Psi_n \, d\tau = \int \psi_c^{e*}\psi_c^{v*}\psi_c^{J*} H' \psi_n^e \psi_n^v \psi_n^J \, d\tau \quad (28)$$

where ψ_i^e, ψ_i^v, ψ_i^J are, respectively, the electronic, vibrational, and rotational wave functions of state i. The value of the integral of eq 28 is approximately proportional to an overlap integral of the vibrational wave functions $\langle\psi_c^v|\psi_n^v\rangle$. The magnitude of the Franck–Condon factor $|\langle\psi_c^v|\psi_n^v\rangle|^2$ is governed by the relative positions and forms of potential curves of a dissociative state c and a bound state n.

Electronic predissociations in diatomic molecules are classified for cases in which the potential energy curve of the dissociative electronic state crosses the curve of the bound state.[6,28] When the dissociation asymptote of a dissociative state lies above, approximately at, or below the crossing point, it is classified as cases b, a, and c, respectively. By comparing the internuclear distances at the crossing point R_c and the equilibrium point R_e of the bound state, three subcases $R_c < R_e$, $R_c \approx R_e$, and $R_c > R_e$ are classified by adding a superscript $-$, i, or $+$, respectively. When the potential curves do not cross but only come close to each other, a superscript o is added.

C. Classification by Causes of Predissociation

Predissociation occurs by the same interactions and selection rules as perturbations. In this section, the main interactions which cause predissociation are discussed.

1. Nonadiabatic Interaction

In a diatomic molecule, the terms neglected in the adiabatic approximation are expressed as[10]

$$\langle\psi_{e1}\chi_{v1}|T^N|\psi_{e2}\chi_{v2}\rangle = -\frac{\hbar^2}{2\mu}\left\langle\chi_{v1}\middle|\left\langle\psi_{e1}\middle|\frac{\partial^2}{\partial R^2}+\right.\right.$$
$$\left.\left.\frac{2}{R}\frac{\partial}{\partial R}\middle|\psi_{e2}\right\rangle_r\middle|\chi_{v2}\right\rangle_R - \frac{\hbar^2}{\mu}\left\langle\chi_{v1}\middle|\left\langle\psi_{e1}\middle|\frac{\partial}{\partial R}\middle|\psi_{e2}\right\rangle_r\middle|\frac{\partial}{\partial R}\chi_{v2}\right\rangle_R \quad (29)$$

where T^N is the nuclear kinetic energy operator, and R is the internuclear distance. ψ_{ei} and χ_{vi} are, respectively, the electronic and vibrational wave functions of an adiabatic state i, and the suffixes r and R of the brackets $\langle||\rangle$ represent, respectively, the integration over electronic coordinates $\mathbf{r}$ at a fixed value of R and the integration over R. The Born–Oppenheimer approximation is usually a very good approximation. However, the predissociation induced by a nonadiabatic interaction can be appreciable if the adiabatic wave functions change drastically with R. Such a case can occur when the diabatic potentials of the same symmetry and spin states cross, because the adiabatic wave functions change drastically around the crossing point.

An overview of the theoretical method for treating photodissociation processes in small polyatomic molecules was given by Schinke.[13] In a polyatomic molecule, the interaction between vibration and electronic motion (vibronic interaction) can lead to the mixing of electronic states of different species. Only states of the same vibronic species can predissociate through a nonadiabatic interaction.[8]

2. Spin–Orbit Interaction

For the perturbation between different spin states, the spin–orbit interaction is usually predominant. The Hamiltonian used to compute the spin–orbit interaction is represented by[29]

$$H_{SO} = \sum_i \xi(r_i)\mathbf{l}_i \cdot \mathbf{s}_i \tag{30}$$

where $\xi(r_i)$, $\mathbf{l}_i$, and $\mathbf{s}_i$ are, respectively, the spin–orbit coupling constant, the orbital angular momentum, and the spin angular momentum of ith electron. The contribution of the spin–other-orbit interactions between unpaired electrons is not included in eq 30.[10,30] The accurate Hamiltonian is given in ref 31.

3. Electron–Rotation Interaction

The interaction of rotation and electronic motion (the L-uncoupling interaction) can cause a perturbation between different electronic species. The Hamiltonian is represented by

$$H_{JL} = B_x J_x L_x + B_y J_y L_y + B_z J_z L_z \tag{31}$$

where B_a, J_a, and L_a are, respectively, the rotational constant, the total angular momentum, and the orbital angular momentum of electrons in a molecule about the molecule-fixed a-axis.

The Hamiltonian for the rotation and the electron spin S interaction (the S-uncoupling interaction) is represented by

$$H_{JS} = B_x J_x S_x + B_y J_y S_y + B_z J_z S_z \tag{32}$$

Heterogeneous predissociation, which is caused by the perturbation between two electronic (or vibronic) species which differ by the species of rotation, takes place by the rotational interaction.

The Hamiltonian for the spin–rotation interaction, which is the interaction between the electron spin and the magnetic field created by nuclear motion, is represented by

$$H_{SR} = \gamma(\mathbf{J} - \mathbf{L} - \mathbf{S})\cdot\mathbf{S} \tag{33}$$

4. Hyperfine Interaction

Hyperfine interaction is usually a small interaction,[32] and the predissociation caused by hyperfine interaction can be appreciable only in molecules that have lifetimes on a microsecond time scale. The first observation of the effect of this interaction on predissociation was for iodine and is reviewed in section V.C.1. Predissociation induced by the hyperfine interaction was identified by the observation of the lifetimes of individual hyperfine components.[33]

5. Interaction Induced by External Fields

The Hamiltonian of the Zeeman interaction is represented by

$$H_Z = -\boldsymbol{\mu}^m \cdot \mathbf{H} \tag{34}$$

where $\boldsymbol{\mu}^m$ is the magnetic moment of a molecule and $\mathbf{H}$ is the external magnetic field. The total electronic magnetic moment is represented by

$$\boldsymbol{\mu}^m = -\mu_B(\mathbf{L} + g_e\mathbf{S}) \tag{35}$$

where μ_B is the Bohr magneton, g_e is the g value for an electron, and $\mathbf{L}$ and $\mathbf{S}$ are the orbital and spin angular momenta of electrons in a molecule, respectively. In the perturbation by H_Z, the operator $\mathbf{L}$ can mix two different electronic species with the selection rules $\Delta\Lambda = 0, \pm1$, $\Delta\Sigma = 0$. The operator $\mathbf{S}$ can mix two electronic species with the selection rules $\Delta\Lambda = 0$, $\Delta\Sigma = 0, \pm1$ in addition to the selection rules; $\Delta S = 0$, $\Delta J = 0, \pm1$, $\Delta M = 0$, and $\Delta K = 0, \pm1$, where M and K are, respectively, the quantum numbers of the projections of $\mathbf{J}$ along the direction of the magnetic field and along the principal axis of the molecule. When an external magnetic field is applied, Zeeman splitting can occur. The resulting energy shifts can enhance predissociation when the perturbing levels become close.

An external electric field can also induce predissociation. The Hamiltonian of the Stark interaction is represented by

$$H_S = -\boldsymbol{\mu}^e \cdot \mathbf{E} \tag{36}$$

where $\boldsymbol{\mu}^e$ is the electric dipole moment of the molecule and $\mathbf{E}$ is the external electric field. The operator $\boldsymbol{\mu}^e$ can mix two different electronic species which satisfy the same selection rules as for electric dipole transitions: $\Delta\Lambda = 0, \pm1$, $\Delta\Sigma = 0$ in addition to the selection rules: $\Delta S = 0$, $\Delta J = 0, \pm1$, $\Delta M = 0$, and $\Delta K = 0, \pm1$. Gerade (g) and ungerade (u) states can mix by this interaction, and two components of the Λ-doubling can also mix.

D. Indirect Predissociation (Accidental Predissociation)

When a discrete state A which is undergoing predissociation and another discrete state B can interact, some levels of B which are accidentally close in energy with A and have a significant Franck–Condon factor $|\langle v_A|v_B\rangle|^2$ are observed to predissociate. Kovács[9] formulated the decrease of emission intensity for levels undergoing this indirect predissociation. The indirect predissociation of the $Cs_2D^1\Sigma_u^+$ state was studied extensively, and it will be described in section V.B.6a.

IV. Experimental Methods

Experimental evidence for predissociation includes line broadening in absorption, sharp decreases in emission quantum yield as a function of wavelength, decreases in radiative lifetime, and the appearance of fragments. However, aside from the appearance of fragments, these processes can occur by other causes than predissociation. Therefore, in order to identify these phenomena as originating from predissociation, we need supplemental information such as the details of the potential curves, transition moments which depend on the internuclear distance and so on. The detection of fragments as a function of photoabsorption is direct evidence of predissociation, and various techniques have been applied to characterize predissociation in this manner. Other

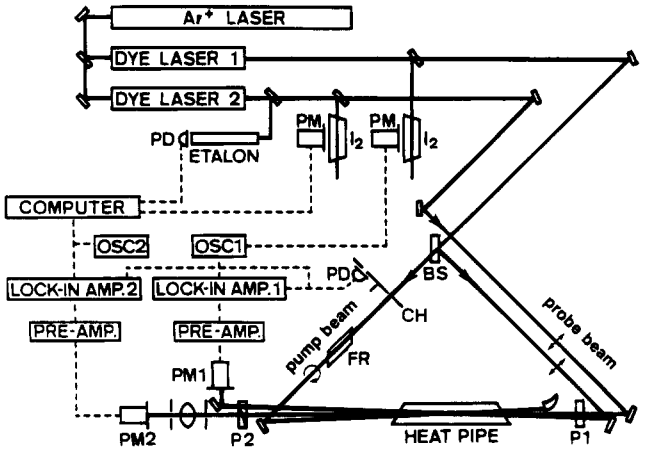

Figure 4. Experimental setup for measurement of the Doppler-free OODR polarization spectrum. Only the dye laser 1 is used for measurement of the Doppler-free polarization spectrum. (Reprinted from ref 88. Copyright 1991 American Institute of Physics.)

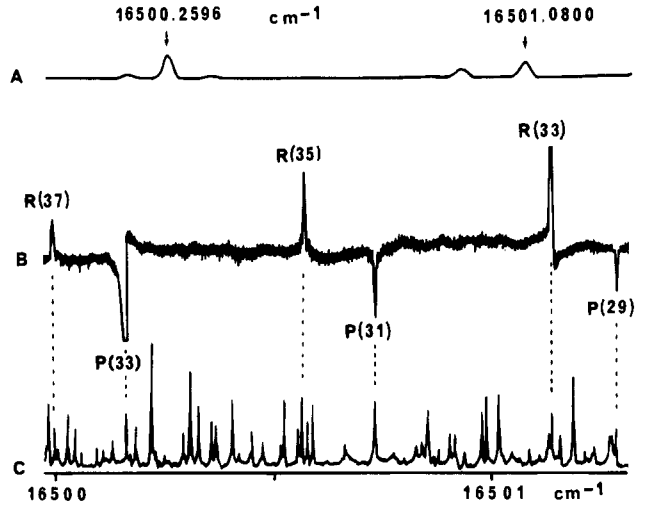

Figure 5. (A) Excitation spectrum of I_2 used for calibration of wavenumber. (B) Doppler-free OODR polarization spectrum of Cs_2, where the $C^1\Pi_u(v'=12,J'=34) \leftarrow X^1\Sigma_g^+$ $(v'' = 9,J'' = 33)$ transition is the pump transition. (C) Doppler-free polarization spectrum of Cs_2. (Reprinted from ref 15. Copyright 1991 American Institute of Physics.)

new technologies are rapidly progressing. The primary experimental methods are described in this section.

A. High-Resolution Spectroscopy

Many techniques of Doppler-free high-resolution spectroscopy[34] have been invented since tunable lasers of narrow line width have become available. Of these, Doppler-free polarization spectroscopy and Doppler-free optical–optical double resonance (OODR) polarization spectroscopy are very useful, because they are highly sensitive and can be used in the absence of emission from the excited state.[35] The setup for this method is shown in Figure 4. A representative spectrum of the Cs_2 molecule is shown in Figure 5. Many lines in the Doppler-free polarization spectrum are broader than sharp lines, and the upper level of the broad lines are assumed to be predissociating. Although these methods are useful for spectroscopic studies, the line shape is not accurate because it is very sensitive to optical adjustment, especially in the Doppler-free OODR polarization spectrum.

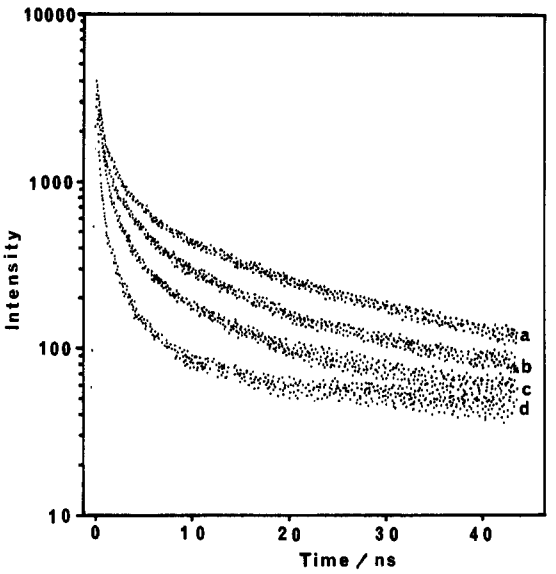

Figure 6. Time-resolved fluorescence intensity from the Cs_2 $D^1\Sigma_u^+(v' = 47)$ level excited by a pulse laser (a single-pulse time duration of 10 ps) at 17 485 cm^{-1} and monitored by the fluorescence in the 15220–15080 cm^{-1} region, and the dependence on the magnetic field (a, 0 G; b, 2 kG; c, 4 kG; d, 10 kG.) The sample is in a gas cell at 474 K with the vapor pressure Cs (0.10 Torr) and Cs_2 (1.7×10^{-4} Torr). (Reprinted from ref 103. Copyright 1992 Elsevier.)

If the excited molecule fluoresces, we can obtain a more accurate line shape by measuring the fluorescence intensity as a function of frequency of the excitation laser. The resulting spectrum is called *(fluorescence) excitation spectrum*. In order to eliminate Doppler broadening, a tunable single-mode laser beam was propagated to a collimated molecular beam at right angles and the resulting fluorescence is detected.[36] The molecular vibrational and rotational temperature is cooled in a supersonic beam. Because hot bands are eliminated, the spectrum becomes simple.[37] The effects of collision can be neglected in an excitation spectrum using a laser crossed with a molecular beam.

B. Time-Resolved Spectroscopy

The development of pulsed lasers has made it easy to measure the lifetime of predissociating levels. If one uses a pulsed laser of a single-pulse time duration of τ (s), it can be calculated from the uncertainty principle that its line width Γ (cm^{-1}) must be greater than $5.3 \times 10^{-12}/\tau$ (s). When one uses a laser of a single-pulse time duration of $\tau < 10^{-10}$ s, the laser line width will be larger than 0.053 cm^{-1}. In many cases, several lines are within the laser line width, and the resulting fluorescence decay curve is composed of the overlapped decay curves of the fluorescence from the simultaneously excited levels. Some of these lines may be distinguished by dispersing the fluorescence and detecting the light at a specific wavelength. An example of the time-resolved fluorescence intensity of the Cs_2 molecule is shown in Figure 6. Even if several states are simultaneously excited and the fluorescence from these states are

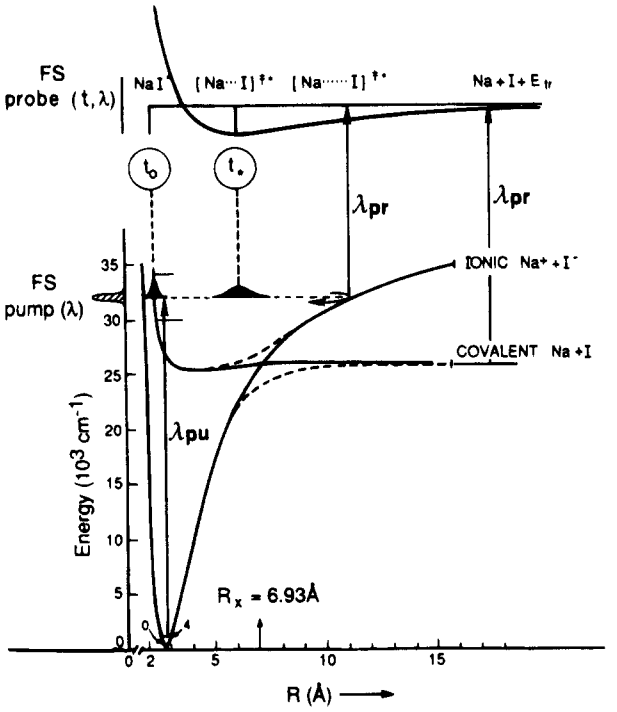

Figure 7. The method of femtosecond transition-state spectroscopy (FTS) and the relevant low-lying potential energy curves of NaI.[39] The pump pulse at wavelength λ_{pu} prepared a coherent wave packet on the predissociative state. A femtosecond probe pulse was used at different delay times (t) and wavelengths (λ_{pr}). The probe pulse excites either the molecule in the predissociative state to the second excited state which decomposes into $Na(3p^2P_{1/2\text{ or }3/2})$ $+I(5p^2P_{3/2})$ or the dissociated atom $Na(3s^2S_{1/2})$ to $Na(3p^2P_{1/2\text{ or }3/2})$ depending on the wavelength λ_{pr}. The atomic fluorescence $Na(3p^2P_{1/2\text{ or }3/2}) \rightarrow Na(3s^2S_{1/2})$ was used to detect the probability of the second excitation.

overlapped, the multicomponent decay profile may be decomposed to estimate the shortest lifetime. This can be used to confirm whether the line width observed by high-resolution spectroscopy is really due to lifetime broadening. However, we must be careful because a fast decay component may arise from a fast dephasing of the quantum beats.

The dynamics of predissociation in real time has been studied by using femtosecond transition-state spectroscopy (FTS).[39,40] The experimental methodology of this technique is presented in ref 39. If the duration of the laser pulses is shorter than the lifetime of the curve crossing, we can monitor the evolution from the bound state to the dissociative state. This may be understood by referring the potential curves of NaI molecule shown in Figure 7. A predissociative level is excited by a femtosecond pulse laser. A femtosecond probe pulse is used at different delay times and wavelengths to detect the dissociation products or the predissociating molecules. From this, the real-time dynamics of the period of the wavepacket motion, the dephasing of the wavepacket, and the curve crossing probability can be measured. Thus, a direct view of the evolution of the quantum mechanical wavefunctions, the potential energy curves, and the coupling strength between the bound state and the dissociative state are provided from these experiments.

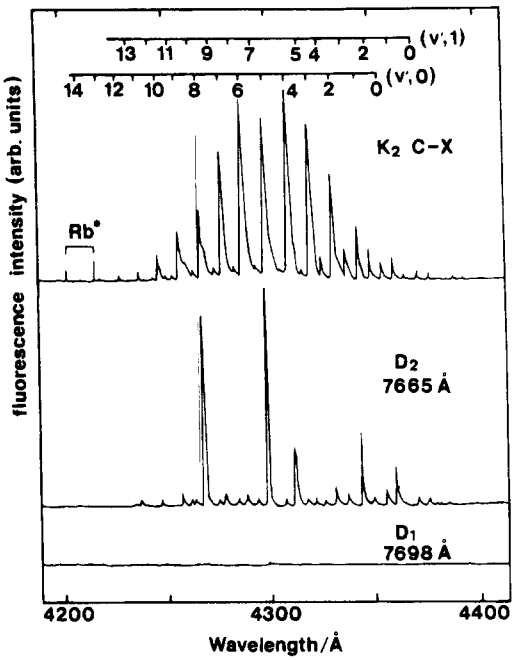

Figure 8. The excitation spectra for the crossed laser and molecular beams of K_2, which were measured by selectively detecting the molecular fluorescence K_2 $C^1\Pi_u \rightarrow X^1\Sigma_g^+$ (top), the atomic fluorescence K D_2 (middle), and the atomic fluorescence K D_1 (bottom). (Reprinted from ref 14. Copyright 1981 Chemical Society of London.)

C. Photofragment Spectroscopy

Photofragments of alkali metal dimers excited by light of visible or ultraviolet wavelengths often emit visible light. Breford, Engelke, Ennen, and Meiwes[14] have measured excitation spectra using a laser crossed with molecular beams of K_2 and Rb_2 by selectively detecting the atomic fluorescence (the D_2 or D_1 line) and the molecular fluorescence. The observed spectrum is shown in Figure 8. The dependence of the predissociation rate on the vibrational quantum number v' is clearly observed, and the selective dissociation into $K(4p^2P_{3/2})$ + $K(4s^2S_{1/2})$ atoms is also observed. The excitation spectrum measured by selectively detecting the fluorescence from the fragments was found to be orders of magnitude more sensitive than the classical method of absorption for tracking and studying predissociation.

A part of the Doppler-free excitation spectrum[15] of the Cs_2 $D^1\Sigma_u^+ \leftarrow X^1\Sigma_g^+$ transition measured by detecting selectively the intensities of the molecular fluorescence Cs_2 $D^1\Sigma_u^+ \rightarrow X^1\Sigma_g^+$ and the atomic fluoresence Cs $6p^2P_{3/2} \rightarrow 6s^2S_{1/2}$ is shown in Figure 9. In this work, the v and J dependences of the predissociation $D^1\Sigma_u^+(v,J) \rightarrow Cs(6p^2P_{3/2})$ + $Cs(6s^2S_{1/2})$ are observed. The rate of predissociation, which depends on v and J, can be determined from the spectral line width. The quantum yield of the predissociation can be determined by comparing the intensities of the molecular and atomic fluorescence.

When the photofragments are in the ground state or in a nonradiative excited state, they may be excited by a second laser. The fluorescence intensity may be measured as a function of frequency of the dissociation laser light, and the resulting spectrum is called a PHOFEX (photofragment excitation) spec-

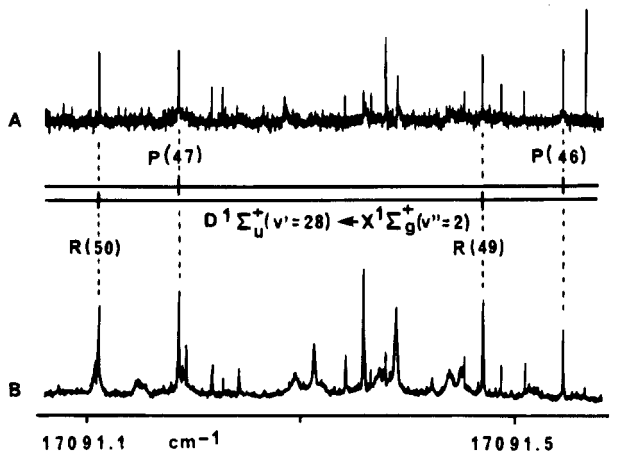

Figure 9. Doppler-free excitation spectra near the Cs_2 $D^1\Sigma_u^+(v' = 28, J' = 45) \leftarrow X^1\Sigma_g^+(v'' = 2, J'' = 46)$ transition. Upper trace (A) is the excitation spectrum measured by detecting selectively the intensity of the molecular fluorescence. Lower trace (B) is the excitation spectrum measured by detecting selectively the intensity of the atomic fluorescence Cs $6p^2P_{3/2} \rightarrow 6s^2S_{1/2}$. (Reprinted from ref 15. Copyright 1991 American Institute of Physics.)

trum.[41] From the excitation spectra of the photofragments, we can get information on the distribution of molecules in each electronic, vibrational, and rotational level as well as the velocity vector of the photofragments.[42] For example, the Doppler profile of the fluorescence from $Na(3^2P_{3/2})$ fragments[43] resulting from predissociation of the quasi-bound level Na_2 $B^1\Pi_u(v'=31, J'=42)$ was observed. The photofragments can also be detected by ionizing the neutral fragments. If the fragments are charged species, they may be detected by a mass spectrometer.

V. Predissociation of Diatomic Molecules

A. Hydrogen Molecule

The hydrogen molecule H_2 is the lightest molecule, and the departure from the Born–Oppenheimer approximation is large, although the spin–orbit coupling is small. H_2 is also the simplest molecule, and its potential curves can be calculated with reasonable accuracy. Nonadiabatic interactions can also be easily calculated. Hence, many experimental results on H_2 can be compared with the theoretical results. The potential energy curves of the low singlet state[44-47] are shown in Figure 10. In this section we discuss the important findings which have developed our understanding of the molecular structure and the dynamical behavior of H_2.

Beutler, Deubner, and Jüngen[48] have found that the $D^1\Pi_u$–$X^1\Sigma_g^+$ absorption lines are broadened, and suggested that the line broadenings were due to predissociation of the $D^1\Pi_u$ state. Monfils[47] found that the P and R branch lines are broadened and the Q branch lines are not: the *e* levels of the $D^1\Pi_u$ state were perturbed but the *f* levels were not perturbed. Using the selection rules for the perturbation, $e \leftrightarrow e$ and $f \leftrightarrow f$, the perturbing state which causes the predissociation of the $D^1\Pi_u$ state is identified as a $^1\Sigma_u^+$ state. The absorption spectrum of the hydrogen molecule in the 84.0–93.0 nm region was also studied

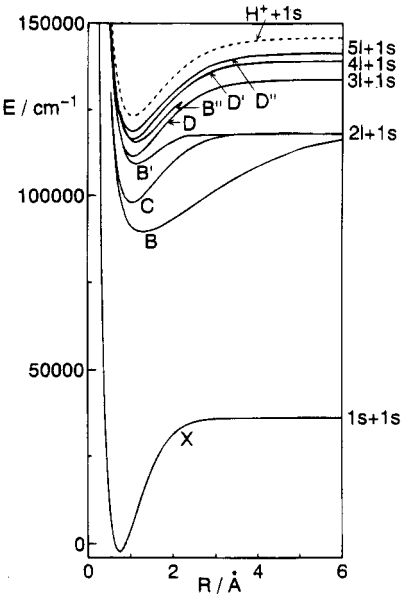

Figure 10. The potential energy curves of the singlet states of H_2. The curves of the $X^1\Sigma_g^+(1s\sigma)^2$, $B^1\Sigma_u^+(1s\sigma)(2p\sigma)$, and $C^1\Pi_u(1s\sigma)(2p\pi)$ states are from ref 44. The ones of the $D^1\Pi_u(1s\sigma)(3p\pi)$ and $D'^1\Pi_u(1s\sigma)(4p\pi)$ states are from ref 45. The one of the $B'^1\Sigma_u^+(1s\sigma)(3p\sigma)$ state is from ref 46. The ones of the $B''^1\Sigma_u^+(1s\sigma)(4p\sigma)$ and $D''^1\Pi_u(1s\sigma)$-$(5p\pi)$ states are from ref 47. The curve of the $X^2\Sigma_g^+(1s\sigma)$ state of H_2^+ is from Sharp, T. E. (*At. Data* **1971**, *2*, 119).

by Namioka.[46] The P and R lines of transitions to levels with $v \geq 3$ of the $D^1\Pi_u$ state were observed to be broadened. The RKR curves (potential curves obtained by the Rydberg–Klein–Rees method[49-51]) of the $D^1\Pi_u$ and $B'^1\Sigma_u^+$ states cross at about the $v = 3$ level of the $B'^1\Sigma_u^+$ state and the $v = 1$ level of the $D^1\Pi_u$ state. In addition to a strong heterogeneous ($\Delta\Lambda \neq 0$) perturbation between the $B'^1\Sigma_u^+$ and $D^1\Pi_u$ states, a weak heterogeneous perturbation between the $B'^1\Sigma_u^+$ and $D'^1\Pi_u$ states and a medium strength homogeneous ($\Delta\Lambda = 0$) perturbation between the $B'^1\Sigma_u^+$ and $B''^1\Sigma_u^+$ states were observed. Dalgarno and Allison[52] have calculated the absorption cross sections for transitions to the dissociative $B'^1\Sigma_u^+$, $C^1\Pi_u$, and $B^1\Sigma_u^+$ states. The calculations show that the direct photodissociation dominates in absorption to the $B'^1\Sigma_u^+$ continuum.

More direct measurements of H_2 predissociation were accomplished by measuring selectively the intensity of emission from the dissociated atom (Lyman-α) as a function of absorption wavelength (Lyman-α excitation spectrum).[53] Mentall and Gentieu[54] studied the photodissociation and absorption cross sections in the 70.0–86.0 nm region by measuring the Lyman-α excitation spectrum and the absorption spectrum. The photodissociation quantum efficiency was found to be unity from 85.0 nm to the photoionization threshold at 80.4 nm. The dissociation efficiency was about 10% at the shorter wavelengths.

High-resolution measurements of the line widths and the line shapes of isolated absorption lines have been carried out for the $D^1\Pi_u$–$X^1\Sigma_g^+$ transition of H_2 and D_2.[55] The *v* and *J* dependence of the line widths $\Gamma(v,Je)$ of the $D^1\Pi_u(v,Je)$ levels in H_2 and D_2 is

Table 1. Line Widths Γ (v, Je) in Wavenumber (cm^{-1}) of the $D^1\Pi_u(v,Je)$ levels in H_2 and D_2

	v	$J = 1$	ref	$J = 2$	ref	$J = 3$	ref	$J = 4$	ref	$J = 5$	ref
H_2	3	3.7	9	11.5	9	22.7	9				
		4.83 ± 0.23	19	14.5 ± 0.7	13						
H_2	4	3.8	9	11.9	9	24.6	9				
		4.83 ± 0.23	18	14.5 ± 0.7	13						
H_2	5	3.9	9	12.2	9						
		4.60 ± 0.03	18	13.8 ± 0.9	13						
H_2	7			11.0 ± 1.0	13						
		3.67 ± 0.37	18	11.3 ± 1.5	14						
H_2	8			10.2 ± 0.2	13						
		3.40 ± 0.30	18	12.3 ± 1.5	14						
H_2	9			9.0 ± 0.6	13						
		3.00 ± 0.20	18	9.4 ± 1.0	14						
H_2	10			9.0 ± 0.5	13						
		3.00 ± 0.17	18								
H_2	11			9.9 ± 0.9	13						
		3.00 ± 0.30	18								
D_2	4	2.3	9	3.5	9	7.4	9	13.9	9		
D_2	5	2.3	9	3.6	9	7.6	9	14.2	9		
D_2	6	2.3	9	3.7	9	7.7	9	12.8	9		
D_2	7	2.3	9	2.3	9	7.5	9	14.8	9	27.7	9
D_2	9			3.9 ± 1.0	14	7.7 ± 1.5	14				
D_2	10			3.9 ± 1.0	14						
D_2	12			3.9 ± 1.0	14						

summarized in Table 1. The line widths were observed to increase with increasing J and were greater for H_2 as compared with D_2. The predissociation of the $D^1\Pi_u$ state was confirmed as originating from the L-uncoupling interaction between the $D^1\Pi_u$ and $B'^1\Sigma_u^+$ states.

Simultaneous measurements of the absorption spectrum and the Lyman-α excitation spectrum have also proved to be very useful for studying predissociation. Because only predissociating levels can be observed in the Lyman-α detection, the Lyman-α excitation spectra are considerably simpler than the absorption spectra.

By assuming the L-uncoupling interaction between the $D^1\Pi_u$ and $B'^1\Sigma_u^+$ states, the line widths of the dissociating levels have been calculated, and the results are in good agreement with the observed line widths.[56,57] The calculated results indicate that the line width decreases monotonically as the vibrational quantum number of the $D^1\Pi_u$ state increases, and this is caused primarily by a decrease in the vibrational overlap integral. Conversely, the line widths around $v' = 10$ and 11 are observed to increase. In order to interpret the observed increase of predissociation at large v' levels, the influence of the $B''\bar{B}^1\Sigma_u^+(1s\sigma)(4p\sigma)$ is suggested.[58,59] However, because the accuracies of the reported line widths are very low, more precise experimental data, especially the Lyman-α excitation spectra of the $D^1\Pi_u$ and $B''\bar{B}^1\Sigma_u^+$ states are necessary to be definitive.

The vacuum UV continuum of the synchrotron radiation has made it possible to observe the highly excited levels of H_2 at improved resolution. The predissociation of the $D'^1\Pi_u$ state was observed[60] and is thought to be due to accidental predissociation. Two channels of this accidental predissociation have been suggested: vibronic interaction between the $D'^1\Pi_u$ and $D^1\Pi_u$ states followed by electron−rotation interaction between the $D^1\Pi_u$ and $B'^1\Sigma_u^+$ states, and the electron−rotation interaction between the $D'^1\Pi_u$ and $B''\bar{B}^1\Sigma_u^+$ states followed by vibronic interaction between the $B''\bar{B}^1\Sigma_u^+$ and $B'^1\Sigma_u^+$ states. The excitation spectra were observed by detecting selectively the atomic Lyman-α and Balmer-α, -β, and -γ lines in the 68.0−86.0 nm region.[61] By comparing the absorption spectra with the Lyman-α excitation spectra, it was found that the $D^1\Pi_u(e)$ levels were fully predissociated even above the ionization limit.

Predissociation of molecular Rydberg states was found above the dissociation threshold of the dissociation to H(1s) + H*(n = 2, 3, 4, and 5). The predissociation yields of the $^1\Pi_u(1s\sigma)(np\pi)$ (n = 3−9) levels were deduced from a peak-to-peak comparison of the simultaneously observed absorption spectrum and Lyman-α excitation spectrum.[62] The spectra in the 77.0−85.0 nm region were measured,[63] and the contribution of the predissociation to the production of H(n=2) + H(1s) atoms for the white-light excitation is found to be more than two times efficient than the direct photodissociation. The absorption spectrum in the 76.5−85.0 nm region and the excitation spectra were measured by detecting separately the Lyman-α emission and the molecular fluorescence with a resolution of 0.005−0.007 nm, and the predissociation yields of the rotational and vibrational levels of the $^1\Pi_u(e)(1s\sigma)(np\pi)$ state and the $^1\Sigma_u^+(1s\sigma)(np\sigma)$ state were determined.[64]

Laser spectroscopy is superior in resolution, and the application to the spectroscopy in the VUV region is in rapid progress. The high-resolution spectra of the $D^1\Pi_u$, $D''^1\Pi_u$, and $B''^1\Sigma_u^+$ states in H_2, HD, and D_2 were measured by using tunable laser light around 83 nm, and predissociative lines with line width as narrow as 0.3 cm^{-1} were observed.[65] By exciting the $E^1\Sigma_g^+ \leftarrow X^1\Sigma_g^+$ two-photon transition with the 201.7 nm laser light and then further exciting to high Rydberg states with a narrow-band laser, transitions to high singlet np Rydberg states were observed with sub-Doppler resolution.[66] Decay processes of the singlet gerade Rydberg states, which were pumped sequentially by the VUV and UV laser beams, through autoionization, predissociation, or electric field ionization have been studied.[67]

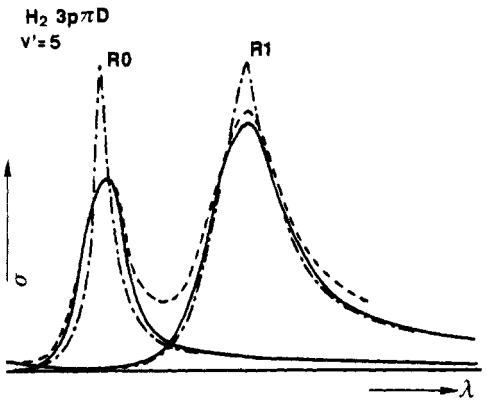

Figure 11. Absorption spectrum of the R(0) and R(1) lines of the $D^1\Pi_u(v=5)-X^1\Sigma_g^+(v=0)$ band of H_2 and the profile analysis from ref 55.

Spectroscopic studies on the triplet states of H_2 were performed by observing the optical transitions from the metastable $c^3\Pi_u(1s\sigma_g)(2p\pi_u)$ state. H_2 molecules in the $c^3\Pi_u$ state are commonly formed by electron-impact excitation of H_2 or charge exchange collision of H_2^+. Spectra of very high resolution were measured by using a tunable single-mode laser crossed with a collimated beam of metastable H_2 molecules formed by electron-impact excitation, and predissociation in the 4s and 4d triplet states were detected via Lyman-α emission.[68] Fast-beam photofragment spectroscopy was applied to study the photodissociation of the metastable H_2 formed by charge exchange of H_2^+ with Cs vapor,[69] and a very rapid ($\tau \simeq 10^{-13}$ s) predissociation of the $j^3\Delta_g(v\geq 5)$ levels and relatively slow ($\tau \simeq 10^{-8}$ s) predissociations of the quasi-bound levels of the $h\Sigma_g^+(v = 4)$ and $i^3\Pi_g(v=4,5)$ states were observed.

The optical transitions from the ground state to both the dissociative continuum of the $B'^1\Sigma_u^+$ state and the bound levels of the $D^1\Pi_u$ state are symmetry allowed. The line shapes of the R(0) and R(1) lines of the $D^1\Pi_u(v=5)-X^1\Sigma_g^+$ band were found to be asymmetric. They were analyzed by fitting them to a Fano profile (see Figure 11).[55] Fano profiles of the R(0) and R(1) lines from $v' = 3$ to $v' = 11$ were studied extensively.[58,59,64] Although the two lines of $J = 1$ and 2 are overlapping, especially, at small values of v, the values of the Fano parameter q for transitions to $J = 1$ and $J = 2$ levels of the $D^1\Pi_u$ state were determined from eq 17 as $q = -18 \pm 2$ and -9 ± 1, respectively.[58,64] The photodissociation cross section for transitions to the dissociative continuum of the $B'^1\Sigma_u^+$ state at several excitation wavelengths was obtained directly from the analysis of the Fano profiles.[63] Rotational coupling of the $j^3\Delta_g(v\geq 5,N)$ level with the vibrational continuum of the $i^3\Pi_g$ state induces predissociation of the $j^3\Delta_g(v\geq 5,N)$ levels. Both of the $j^3\Delta_g$ and $i^3\Pi_g$ states are optically allowed from the $c^3\Pi_u$ state, and asymmetric lines with widths of around 50 cm^{-1} were observed for transitions to $j^3\Delta_g(v\geq 5,N=2)$ levels.[69] Fano profiles were measured for the $j^3\Delta_g \leftarrow c^3\Pi_u$ transitions[70] by using a double-resonance technique which monitors all photoabsorption from a selected $c^3\Pi_u(v,N)$ level by detecting a reduction of the ionization rate in a transition to an autoionizing level.

The H_2 molecule in the $D^1\Pi_u$ state predissociates into H(1s) and H(2p or 2s) atoms. The H(2s) and H(2p) branching ratio in the predissociation of the $D^1\Pi_u(v=3,J=1$ and 2) levels, which are near dissociation threshold, have been measured by Comes and Wenning,[71] Mentall and Gentieu,[54] and Mentall and Guyon.[72] Mentall and Guyon[72] determined the branching ratio by observing the effect of an electric field on the Lyman-α emission. The electric field can cause a mixing of the $2p^2P_{1/2}$ and $2s^2S_{1/2}$ states, which are separated by only 0.036 cm^{-1}. In their analysis they assumed that atoms initially formed in the $2s^2S_{1/2}$ state acquire a 2p character and radiate the Lyman-α emission. However, it is expected that the electric field can change the H(2s) and H(2p) branching ratio, especially near the threshold.

Quantum mechanical calculations on the predissociation $D^1\Pi_u \rightarrow H(1s) + H(2s)$ and $H(1s) + H(2p)$ have been extensively studied.[73-76] A very accurate calculation is possible for this simplest molecule. However, more extensive experimental studies are necessary. A combination of synchrotron radiation, as a strong light source for predissociation, and a laser, as a high-resolution light source to probe the dissociation products, will be a promising future study. A tunable narrow line laser can be used to detect separately $H(2s^2S_{1/2})$, $H(2p^2P_{1/2})$, and $H(2p^2P_{3/2})$ atoms by measuring the excitation spectrum of the dissociation products. Combination of these experimental data with theoretical calculations will be promising more complete understanding of the predissociation.

Comes and Wenning[77] found that H_2 predissociation could be induced by an external electric field and that this predissociation was enhanced for states near and above the ionization limit. Qin, Bistransin, and Glab[78] studied the Stark effect of high Rydberg states of para-H_2 in the l-mixing regime through detection of predissociation, and the predissociation of the high Rydberg states was found to be induced by the electric field. From further work it will become clear how the electric field affects the dynamics of these excited states.

B. Alkali Metal Molecules

Alkali metal molecules have absorption bands in visible and ultraviolet (UV), and the photodissociated atoms often emit visible radiation. Therefore, alkali metal molecules are very suitable for studying predissociation, and many extensive studies have been reported.

1. Li_2

The predissociation of the $b(1)^3\Pi_u$ state by the electron–rotation interaction with the repulsive $a(1)^3\Sigma_u^+$ state has been predicted by Uzer and Dalgarno.[79] Rice, Xie, and Field[80] measured the $^6Li_2$ $(1)^3\Delta_g \rightarrow b(1)^3\Pi_u$ rotationally resolved dispersed fluorescence spectra following perturbation-facilitated optical–optical double resonance (PFOODR) excitation to the $(1)^3\Delta_g(N,J)$ level. They found the f-symmetry Λ-components of $b(1)^3\Pi_u(F_1)$ were broadened owing to predissociation through the $a(1)^3\Sigma_u^+$ state. Spectra of the $^6Li_2$ $(1)^3\Delta_g \rightarrow b(1)^3\Pi_u$ dispersed fluorescence

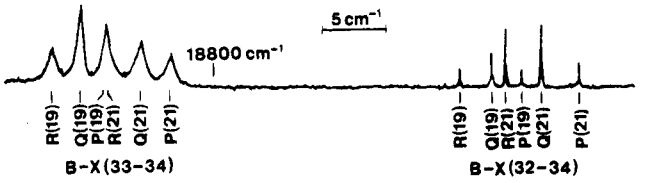

Figure 12. Spectrum of the Na_2 $B^1\Pi_u(v'=33$ and $32,J')$–$X^1\Sigma_g^+(v''=34,J''=19$ and $21)$ transitions. The $X^1\Sigma_g^+(v''=34,J''=19$ and 21 levels were populated by the first laser, which pumped the $A^1\Sigma_u^+(v=20,J=20)$–$X^1\Sigma_g^+(v=0,J=19)$ line. The line broadening caused by predissociation increases with v' and J'. (Reprinted from ref 87. Copyright 1991 Elsevier.)

measured at high resolution using a Fourier transform spectrometer, and the line widths and energy level shifts were obtained as a function of v, J, and N.[81]

Uzer and Dalgarno[79] predicted the indirect predissociation of the $A^1\Sigma_u^+$ state, which was caused by the spin–orbit coupling with predissociating levels of the $b(1)^3\Pi_u$ state. Experimental evidence of this indirect predissociation was reported by Preuss and Baumgartner.[82] After a systematic check of lifetimes of more than 2000 individual rotation–vibration levels of the $A^1\Sigma_u^+$ state, the lifetimes of 46 levels were found to be much shorter than expected. In order to understand these results, rotational coupling matrix elements between the $b(1)^3\Pi_u$ and $a(1)^3\Sigma_u^+$ states, line shifts of rovibrational levels of the $b(1)^3\Pi_u$ state, and spin–orbit coupling matrix elements between the $b(1)^3\Pi_u$ and $A^1\Sigma_u^+$ states were evaluated.[83,84]

2. Na_2

The $B^1\Pi_u$ state of homonuclear alkali metal diatomic molecules has a potential barrier, which arises from a repulsive dipole–dipole interaction at large internuclear distances and an attractive electron-exchange interaction which increases at small internuclear distances. When a molecule is excited to the region above the dissociation limit but below the top of the potential barrier, predissociation by tunneling arises. This is similar to the predissociation by rotation (type III). Keller and Weiner[85] determined the barrier height of the Na_2 $B^1\Pi_u$ state to be 366 ± 8 cm^{-1}. In their experiments, a laser was used to populate a low-lying vibrational level of the $B^1\Pi_u$ state. Via radiative transitions from this state, high vibrational levels of the ground $X^1\Sigma_g^+$ state are populated. A second laser was then used to transfer the population of these levels to states near the dissociation limit of the B state. The form of the potential curve near the top of the barrier was estimated from the observed spectral feature due to tunneling. Using the method of modulated gain spectroscopy, the uppermost vibrational level of the B state was determined to be $v' = 33$, and the position and the height of the potential barrier could be calculated from the line widths and level energies.[86] The uppermost quasibound rovibrational levels were extensively studied by a molecular beam experiment using a three-step excitation with Franck–Condon pumping and spatially separated laser fields.[87] A portion of the observed spectra is shown in Figure 12, where the increase of the line width with v is clearly observed. The increase of the line width with J was also observed, and some of the level energies and widths are listed in Table 2.

Table 2. Level Energies and Line Widths Γ (v, J) in Wavenumber (cm^{-1}) of the Predissociative Na_2 $B^1\Pi_u(v,J)$ levels (from ref 77)

		e level		*f* level	
v	J	energy	line width	energy	line width
33	4	3031.520	0.0504	3031.516	0.0521
33	5	3032.102	0.0558	3032.107	0.0555
33	6	3032.806	0.0635	3032.803	0.0646
33	8	3034.545	0.0752	3034.546	0.0737
33	9	3035.588	0.0895	3035.583	0.0913
33	10	3036.750	0.1112	3036.744	0.1043
33	11	3038.002	0.1235	3038.006	0.1315
33	12	3039.367	0.1462	3039.376	0.1382
33	13	3040.841	0.159	3040.853	0.189
33	14	3042.430	0.214	3042.429	0.201
33	16	3045.892	0.306	3045.895	0.304
33	17	3047.761	0.344	3047.766	0.319
33	18	3049.742	0.517	3049.762	0.449
33	19	3051.815	0.600	3051.844	0.658
33	20	3053.984	0.751	3054.009	0.666
33	21	3056.180	0.97	3056.300	0.91
33	22	3058.633	1.13	3058.632	1.06
33	23	3061.099	1.32	3061.042	1.35
33	24	3063.56	1.71	3063.570	1.57
33	25	3066.18	2.03	3066.245	1.93
33	26	3068.84	2.16	3068.90	2.36
33	27	3071.96	2.68	3071.67	2.47

3. NaK

The Doppler-free high-resolution spectrum of the $B^1\Pi$–$X^1\Sigma^+$ transition of $^{23}Na^{39}K$ was measured by optical–optical double resonance polarization spectroscopy.[88] The $B^1\Pi$ state is correlated with the atomic asymptote $Na(3s^2S_{1/2}) + K(4p^2P_{3/2})$. Remarkable line broadening was observed for transitions to levels above the dissociation limit to $Na(3s^2S_{1/2}) + K(4p^2P_{1/2})$. This broadening was identified as originating from the predissociation to $Na(3s^2S_{1/2}) + K(4p^2P_{1/2})$ atoms caused by spin–orbit interaction between the $B^1\Pi$ and $(2)^3\Sigma^+$ states. The potential curves were estimated to cross around the inner turning point of the $B^1\Pi(v'=34)$ level.

4. K_2

By detecting separately the intensities of the molecular fluorescence and of the atomic fluorescence (either D_1 or D_2 line), the K_2 $C^1\Pi_u(v')$ – $X^1\Sigma_g^+(v'')$ transitions between 420 and 440 nm were studied by Meiwes and Engelke.[89] The $C^1\Pi_u$ state was found to predissociate selectively to $K(4p^2P_{3/2}) + K(4s^2S_{1/2})$ atoms, and a dependence of the predissociation rate on v' was clearly observed (see Figure 8). The dissociative state was identified as $c^3\Sigma_u^+$. The $E^1\Pi_u$ state was observed to predissociate in the energy region 26600–28000 cm^{-1}.[90]

5. Rb_2

By studying the laser photoluminescence, Brom and Broida[91] found that the $C^1\Pi_u$ state predissociated strongly. When a molecular beam of Rb_2 was irradiated by the 4765 Å line of the Ar^+ laser, the resulting emission was observed to consist of molecular fluorescence belonging to the $C^1\Pi_u \rightarrow X^1\Sigma_g^+$ transition

and atomic fluorescence from the $Rb(5p^2P_{3/2})$ fine structure component (the Rb D_2 line).[92] The atomic fluorescence was caused by partial predissociation of the $C^1\Pi_u$ state. By exciting Rb_2 in a supersonic beam with a pulsed dye laser, Breford and Engelke[93] observed that (a) the $C^1\Pi_u$ state predissociates selectively to $Rb(5p^2P_{3/2}) + Rb(5s^2S_{1/2})$ atoms, and (b) the low vibrational levels of the $D^1\Pi_u$ state predissociate selectively to $Rb(5p^2P_{3/2}) + Rb(5s^2S_{1/2})$ atoms, whereas the high vibrational levels of the $D^1\Pi_u$ state predissociate selectively to $Rb(4d^2D_{3/2}) + Rb(5s^2S_{1/2})$ atoms. The predissociation of the $C^1\Pi_u$ state and of the low vibrational levels of the $D^1\Pi_u$ state were identified as caused by potential curve crossing with the $c^3\Sigma_u^+$ state. The predissociation of the high vibrational levels of the $D^1\Pi_u$ state were believed to be caused by an unknown molecular state, most probably the $d^3\Pi_u$ state. The population of the magnetic sublevels M_J of $Rb(5p^2P_{3/2,M_J})$ atoms produced by predissociation of the $C^1\Pi_u$ state was determined from the intensities of atomic fluorescence lines split by the Zeeman effect.[94] The spin–orbit coupling between an excited level of the $C^1\Pi_u$ state and levels of the $c^3\Sigma_u^+$ state and the effects of the external magnetic field were studied.

6. Cs_2

When Cs_2 is excited by Ar^+ laser lines, molecular fluorescence as well as the atomic emissions are observed.[95] The intensity of the Cs $6p^2P_{3/2} \rightarrow 6s^2S_{1/2}$ transition (D_2 line) is about 10 times larger than that of the Cs $6p^2P_{1/2} \rightarrow 6s^2S_{1/2}$ transition (D_1 line), and it is identified as originating from the predissociation of the $E^1\Pi_u$ state. When the $C^1\Pi_u$ state is excited by the 632.8 nm line of a He–Ne laser, the selective predissociation to $Cs(6p^2P_{3/2}) + Cs(6s^2S_{1/2})$ atoms can be observed.[96] The predissociation is estimated to occur through the repulsive $c^3\Sigma_u^+$ state. The relevant potential curves of Cs_2 are shown in Figure 13. The $c^3\Sigma_u^+$ state is denoted for the diabatic potential; the inner part of the adiabatic potential of the $(3)^3\Sigma_u^+$ state extends diabatically to the outer repulsive part of the adiabatic potential of the $(2)^3\Sigma_u^+$ state. The relative populations of the magnetic sublevels M_J of $Cs(6p^2P_{3/2,M_J})$ atoms produced by predissociation of the $C^1\Pi_u$ state following excitation by the 632.8 nm line of a He–Ne laser, were measured from the intensities of fluorescence lines $Cs(6p^2P_{3/2,M_J}) \rightarrow Cs(6s^2S_{1/2,M_J\pm1})$ split by the Zeeman effect, and the preferential populations of the $M_J = 3/2$ and $M_J = 1/2$ were observed.[97]

A two-photon technique has been reported for the measurement of the relative cross section for the selective photolysis of Cs_2 into a particular product channel.[98,99] Two independently tunable dye lasers were used. The first laser dissociates Cs_2 by exciting in the range of 445–640 nm and the second laser excites the resulting products to Rydberg states, which are readily ionized by collision and are detected in a thermionic heatpipe. The time delay between the photodissociation laser pulse and the detection laser pulse for the photoproducts was varied to separate collisional effects from the primary dissociation process. The red band was assigned as the $C^1\Pi_u$–$X^1\Sigma_g^+$ transition, and the $C^1\Pi_u$ state was confirmed to dissociate selectively into $Cs(6p^2P_{3/2}) + Cs(6s^2S_{1/2})$. This selective photolysis was identified as originating from the predissociation of the $C^1\Pi_u$ state through the repulsive $c^3\Sigma_u^+$ potential. The occurrence of $Cs(5d^2D_{5/2})$ fragments was attributed to direct photodissociation following the excitation into the dissociative continuum of the $D^1\Sigma_u^+$ state which is correlated with the atomic asymptote $Cs(5d^2D_{5/2}) + Cs(6s^2S_{1/2})$. The occurrence of $Cs(5d^2D_{3/2})$ fragments was estimated to result from predissociation of another $^1\Sigma_u^+$ state by a repulsive $^3\Sigma_u^+$ state correlated with both the atomic asymptotes $Cs(5d^2D_{5/2}) + Cs(6s^2S_{1/2})$ and $Cs(5d^2D_{3/2}) + Cs(6s^2S_{1/2})$.

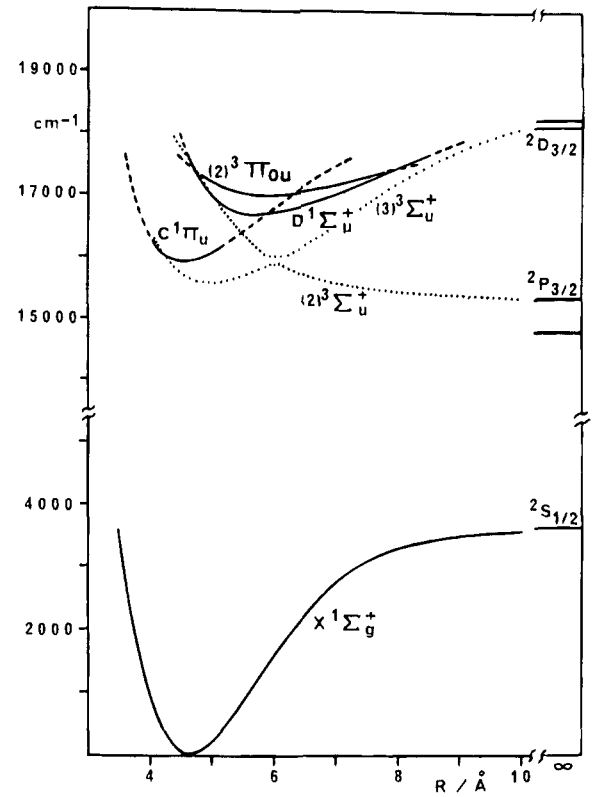

Figure 13. Adiabatic potential energy curves of Cs_2. A repulsive state of the diabatic potential, which composed of the inner part of the adiabatic potential of the $(3)^3\Sigma_u^+$ state and the outer repulsive part of the adiabatic potential of the $(2)^3\Sigma_u^+$ state, is denoted as $c^3\Sigma_u^+$. (Reprinted from ref 15. Copyright 1991 American Institute of Physics.)

Raab, Höning, Demtröder, and Vidal[100] studied the $C^1\Pi_u - X^1\Sigma_g^+$ and $D^1\Sigma_u^+ - X^1\Sigma_g^+$ bands by using techniques of Doppler-free polarization spectroscopy and optical–optical double resonance polarization spectroscopy. They observed a broadening of the lines that suggested predissociation. To avoid the effects of dissociation induced by collisions and to obtain a Doppler-free high-resolution spectrum, Baba, Nakahori, Iida, and Katô[101] used a tunable single-mode dye laser to excite Cs_2 molecules in a collimated molecular beam. The intensities of the D_2 atomic emission and of the $C^1\Pi_u - X^1\Sigma_g^+$ molecular fluorescence were measured separately as a function of laser frequency. The dependence of the predissociation on each vibrational and rotational level $C^1\Pi_u(v',J')$ was studied by comparing the intensities of the molecular fluorescence and the atomic emission. The predissociation was found to depend strongly on v' but

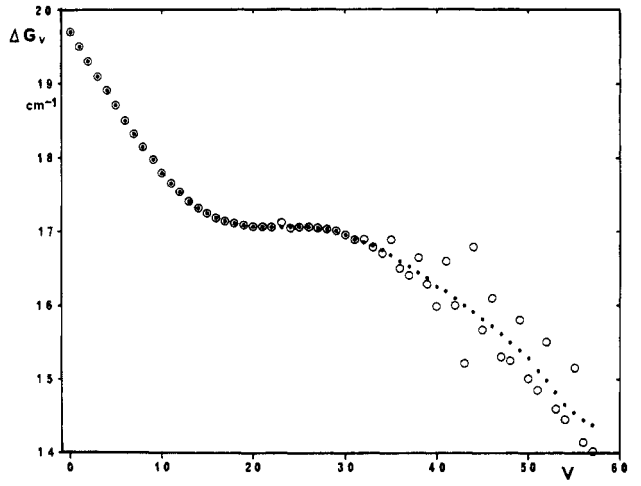

Figure 14. The variation of the vibrational spacing $\Delta G_v = G_{v+1} - G_v$ (open circles) of the $D^1\Sigma_u^+$ state of Cs_2 with v. Filled circles are the fitted values of ΔG_v, which are calculated from the molecular constants. (Reprinted from ref 15. Copyright 1991 American Institute of Physics.)

weakly on J' and occurred most strongly around the $v' = 3$ level. The Franck–Condon factors between the RKR potential curve of the $C^1\Pi_u$ state and several repulsive potential curves were calculated and were compared with the observed predissociation rates. The potential curve of the $(2)^3\Sigma_u^+$ state, whose adiabatic potential was expected to be dissociative, was estimated to cross the potential curve of the $C^1\Pi_u$ state between the left turning points of $v' = 1$ and $v' = 0$ levels. Energy level shifts and line broadenings were observed for the $C^1\Pi_u(v'>10)$ state, but more extensive studies are needed to unravel their complex behavior.

a. Indirect Predissociation of Cs_2 $D^1\Sigma_u^+$ State. Amiot, Demtröder, and Vidal[102] studied the $D^1\Sigma_u^+ - X^1\Sigma_g^+$ band by a Fourier-transform spectroscopy, Doppler-free polarization spectroscopy, and optical–optical double resonance polarization spectroscopy. They found an unusual vibrational spacings as well as line broadening in the spectra of this band. Katô, Kobayashi, Chosa, Nakahori, Iida, Kasahara, and Baba[15] studied extensively the perturbation and the predissociation within the rotational levels. The Doppler-free polarization spectra up to $v' = 58$ were measured, and the molecular constants of the $D^1\Sigma_u^+$ state were determined. The variation of the vibrational spacing $\Delta G_v = G_{v+1} - G_v$ is shown in Figure 14. Large deviations of ΔG_v from the fitted ΔG_v curve were observed for v' larger than 35. Conversely, almost all rotational levels of a vibrational state were observed to deviate uniformly. Perturbations can occur only between levels of the same total angular momentum J: the selection rule is $\Delta J = 0$.[7] The energy shift is expected to be large when the energy separation between the perturbing levels is small. The ΔG_v values observed for $v' = 35$–58 showed that some lines were shifted upward and some lines downward from the fitted values. If the perturbing state is a continuous state, such nonuniform energy shifts are not observed. Using this fact, the perturbing electronic state was concluded to be a bound state. Parallel shifts of all the rotational levels of a vibrational state can occur if the rotational constants of two perturbing vibrational state are equal. Hence, the equilibrium internuclear distance of the perturbing state was estimated to be nearly equal (within ±0.2 Å) to that of the $D^1\Sigma_u^+$ state.

The perturbing state was assigned as the $(2)^3\Pi_{0u}$ state, which asymptotically dissociates into $Cs(5d^2D_{3/2})$ + $Cs(6s^2S_{1/2})$ atoms. The perturbation between the $D^1\Sigma_u^+$ and $(2)^3\Pi_{0u}$ states is induced by spin–orbit interaction. The nonvanishing matrix elements between the three Hund's case (a) states $^3\Pi_\Omega$ (Ω = 0, 1, and 2) and a $^1\Sigma_u^+$ state are given by

$$\langle {}^1\Sigma^+ v'JM|H_{SO}|{}^3\Pi_0 evJM\rangle = \zeta \qquad (37)$$

where the symbol e refers to an e level of the Λ-type doubling, M is the quantum number of a component of $\mathbf{J}$ along the space-fixed Z axis, and ζ is a constant. For a given pair of interacting levels, the higher level is displaced upward and the lower level downward by equal amounts. From the direction of the energy shift of the $D^1\Sigma_u^+(v')$ level, the location of the $(2)^3\Pi_{0u}(v)$ level was estimated. For a given ζ, the smaller the separation between the levels is, the larger are their shifts. By analyzing a series of shifts of observed vibrational energies of the $D^1\Sigma_u^+(v' = 35 - 58)$ levels, the value of ΔG_v for the $(2)^3\Pi_{0u}$ state was estimated to be 12 cm^{-1} around $D^1\Sigma_u^+(v' = 40)$, and the value of $\omega_e x_e$ to be 0.03 cm^{-1}. The potential curve of the $(2)^3\Pi_{0u}$ state was determined to cross the potential curve of the $D^1\Sigma_u^+$ state at about $v' = 40$, because large shifts of the vibrational levels $D^1\Sigma_u^+(v')$ were observed above $v' = 35$. Since the level shifts were observed only for $v' > 32$, the potential minimum of the $(2)^3\Pi_{0u}$ state was estimated to lie above the potential minimum of the $D^1\Sigma_u^+$ state. The potential curve of the $(2)^3\Pi_{0u}$ state was calculated using the above constraints. The unperturbed level energies, which are the energies calculated from the molecular constants of the $D^1\Sigma_u^+(v',J' = 0)$ and $(2)^3\Pi_{0u}(v,J=0)$ levels are schematically shown in Figure 15. All the energy shifts ΔE of the observed $D^1\Sigma_u^+(v',J' = 0)$ levels from the unperturbed levels are explained accurately by the location of the unperturbed levels.

In order to study the predissociation at Doppler-free high resolution under collision-free condition, a collimated Cs_2 beam was crossed at right angles with the laser beam, and the excitation spectra were measured by detecting separately the intensities of the molecular fluorescence and the D_2 or D_1 atomic fluorescence. It was found that the predissociation of the $D^1\Sigma_u^+$ state occurs appreciably for $v' > 20$, and the probability of predissociation increases with increasing v'. The $D^1\Sigma_u^+(58 \geq v' > 20)$ levels decompose selectively into two atoms $Cs(6p^2P_{3/2})$ + $Cs(6s^2S_{1/2})$.

The v' and J' dependence of the line width Γ was also measured. The observed dependence of Γ on J' for $v' = 28$ is shown in Figure 16. It is possible that the line broadening is due to hyperfine splitting, but no splitting of lines was observed with the spectral resolution of 15 MHz. The predissociation rate of molecular levels, which is proportional to the intensity ratio of the corresponding lines in the two

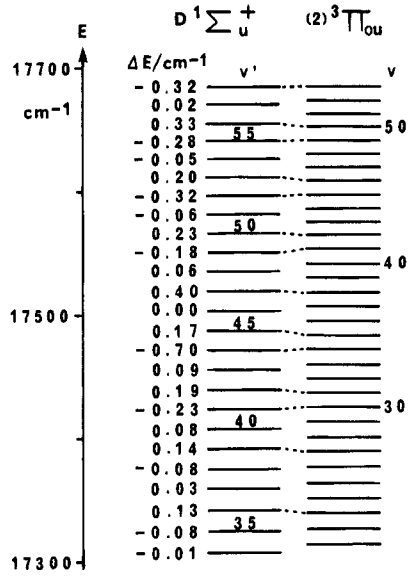

Figure 15. The unperturbed level energies (E_v) of the $D^1\Sigma_u^+(v',J'=0)$ and $(2)^3\Pi_{0u}(v,J=0)$ states of Cs_2, which are calculated from the molecular constants, are shown by full lines. ΔE is the difference between the observed level energy and the unperturbed level energy E_v. Strongly perturbing levels ($|\Delta E| \geq 0.10$ cm^{-1}) are connected by broken lines. (Reprinted from ref 15. Copyright 1991 American Institute of Physics.)

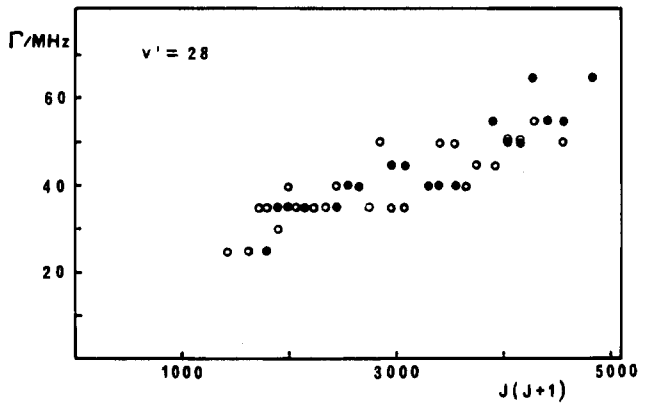

Figure 16. The line widths Γ of the $D^1\Sigma_u^+(v'=28,J)-X^1\Sigma_g^+(v''=2,J\pm1)$ transitions are plotted against $J(J+1)$. Open circles denote the R branch and filled circles denote the P branches. The difference between the P and R branches is due to the experimental uncertainty. (Reprinted from ref 15. Copyright 1991 American Institute of Physics.)

excitation spectra monitored by the atomic emission and by the molecular fluorescence, respectively, was observed to increase parallel with the increase of the line width. From these facts, the observed line width is attributed to lifetime broadening.

The lifetime τ is related to the predissociation rate k_p and the radiative decay rate k_r by

$$\tau = 1/(k_p + k_r) \qquad (38)$$

The lifetimes of the $D^1\Sigma_u^+(v' = 46,J' = 30 - 70)$ levels were evaluated to be about 1 ns from the observed line width Γ and eq 12. The increase of the line width is indicative of the increase of the predissociation rate. The radiative lifetime of the unperturbed $D^1\Sigma_u^+(v', J')$ level was reported to be about 35 ns.[103] From these facts, the observed line width is attributed to the predissociation; the predissociation rates k_p of the $D^1\Sigma_u^+(v' = 46,J' = 30)$ levels are evaluated to be 10^9 s^{-1}. The line widths were observed to increase with v'. This indicates that the predissociation in the $D^1\Sigma_u^+$ state becomes faster with increasing v'.

The $(2)^3\Pi_{0u}$ state is a bound state. Hence, the perturbation between the $D^1\Sigma_u^+$ and $(2)^3\Pi_{0u}$ states does not directly lead to predissociation of the $D^1\Sigma_u^+(v',J')$ level. The most probable repulsive state, which can contribute to predissociation, is the $c^3\Sigma_u^+$ state. Interaction between the $^1\Sigma_u^+$ and $^3\Sigma_u^+$ states is forbidden in first-order approximation. The perturbation between the $(2)^3\Pi_{0u}$ and $c^3\Sigma_u^+$ states can occur through electron-rotation (L-uncoupling) interaction. The nonvanishing matrix elements are given by[15]

$$\langle {}^3\Pi_{0u}(evJ)|H_{JL}|{}^3\Sigma_u^+(N{=}JJ)\rangle = [J(J+1)]^{1/2}B_L \qquad (39)$$

where N and J are, respectively, the quantum numbers of the rotational and the total angular momenta, and B_L is a constant. Therefore, the predissociation of the $D^1\Sigma_u^+$ state can occur by a combination of spin–orbit interaction between the $D^1\Sigma_u^+(v',J)$ and $(2)^3\Pi_{0u}(evJ)$ levels: $\langle D^1\Sigma_u^+(v'J)|H_{SO}|(2)^3\Pi_{0u}(evJ)\rangle$ and the L-uncoupling interaction between the $(2)^3\Pi_{0u}(evJ)$ and $c^3\Sigma_u^+(N = JJ)$ levels: $\langle {}^3\Pi_{0u}(evJ)|H_{JL}|{}^3\Sigma_u^+(N{=}JJ)\rangle$.

The linewidth Γ, and hence the predissociation rate k_p of the $D^1\Sigma_u^+(v' = 25 - 30)$ levels, was observed to increase proportionally to $J(J + 1)$. This is in agreement with eq 39, which shows that L-uncoupling induces the predissociation and the rate is proportional to $J(J + 1)$. From these results, the predissociation of the $D^1\Sigma_u^+$ state was identified as indirect predissociation, which is caused by a combination of spin–orbit interaction between the $D^1\Sigma_u^+(v'J)$ and $(2)^3\Pi_{0u}(evJ)$ levels and L-uncoupling interaction between the bound $(2)^3\Pi_{0u}(evJ)$ and dissociative $^3\Sigma_u^+(N = JJ)$ levels. The potential curve of the $c^3\Sigma_u^+$ state, which is repulsive and decomposes into $Cs(6p^2P_{3/2})$ and $Cs(6s^2S_{1/2})$ atoms, was presumed to extend to the inner wall of the $D^1\Sigma_u^+$ state potential curve and to cross near the $D^1\Sigma_u^+(v' = 40)$ level. At this position, crossing with the $(2)^3\Pi_{0u}$ state also occurs (see Figure 13).

b. Magnetic Predissociation of the Cs_2 $D^1\Sigma_u^+$ State. Time-resolved fluorescence intensities following the pulsed excitation of the $v' = 3$, 27, and 47 levels of the $D^1\Sigma_u^+$ state have been measured.[103] The lifetimes τ_0 in the collisionless limit were found to be $\tau_0 = 37$, 36, and 34 ns, respectively, for the $D^1\Sigma_u^+(v' = 3)$, $D^1\Sigma_u^+(v' = 27)$, and $D^1\Sigma_u^+(v' = 47)$ levels. When an external magnetic field was applied, a remarkable change in the decay profiles of the fluorescence intensity was observed for the excitation to $v' = 27$ and 47 levels (see Figure 6). However, no change of the fluorescence intensity and of the decay profiles was observed for excitation to the $v' = 3$ level. The decay rates were found to be proportional to the square of the magnetic field (H^2), and the decay rate

of $v' = 47$ was observed to be faster than that of $v' = 27$. This shortening of the lifetime was identified as originating from magnetic predissociation (predissociation induced by a magnetic field).

The Zeeman interaction, which is responsible for the magnetic predissociation, has nonvanishing matrix element only between the same spin states: the selection rule is $\Delta S = 0$. Hence, the magnetic predissociation of the $D^1\Sigma_u^+$ state does not occur through the direct Zeeman interaction between the $D^1\Sigma_u^+$ and $c^3\Sigma_u^+$ states. The $D^1\Sigma_u^+$ state is known to interact with the $(2)^3\Pi_{0u}$ state via spin–orbit interaction.[15] The nonvanishing matrix elements of this interaction are given by eq 37. The perturbation between the $(2)^3\Pi_{0u}(evJM)$ level and the $c^3\Sigma_u^+$ state occurs by the Zeeman interaction H_Z, and the nonvanishing symmetric matrix elements are given by[103]

$$\langle {}^3\Pi_o evJM|H_Z|{}^3\Sigma^+ v_c N{=}JJ{+}1M\rangle = \frac{J+2}{2J+3}\left[\frac{(J-M+1)(J+M+1)}{2(J+1)(2J+1)}\right]^{1/2} CH$$

$$\langle {}^3\Pi_o evJM|H_Z|{}^3\Sigma^+ v_c N{=}JJM\rangle = -\frac{M}{[2J(J+1)]^{1/2}} CH$$

$$\langle {}^3\Pi_0 evJM|H_Z|{}^3\Sigma^+ v_c N{=}JJ{-}1M\rangle = -\frac{J-1}{2J-1}\left[\frac{(J-M)(J+M)}{2J(2J+1)}\right]^{1/2} CH$$

$$\langle {}^3\Pi_0 evJM|H_Z|{}^3\Sigma^+ v_c N{=}J{+}2J{+}1M\rangle = \frac{1}{2J+3}\left[\frac{(J+2)(J-M+1)(J+M+1)}{2J(2J+1)}\right]^{1/2} CH$$

$$\langle {}^3\Pi_0 evJM|H_Z|{}^3\Sigma^+ v_c N{=}J{-}2J{-}1M\rangle = -\frac{1}{2J-1}\left[\frac{(J-1)(J-M)(J+M)}{2(2J+1)}\right]^{1/2} CH \quad (40)$$

where

$$C = 2^{-1/2}\langle v|\langle 1|L_+|0^+\rangle|v_c\rangle\mu_B \quad (41)$$

The predissociation in the presence of an external magnetic field, accompanying the $D^1\Sigma_u^+(v'JM) \leftarrow X^1\Sigma_g^+(v''J-1M)$ excitation, is induced by a combination of the spin–orbit interaction between the $D^1\Sigma_u^+(v'JM)$ and $(2)^3\Pi_{0u}(evJM)$ levels, and the $H_{JL} + H_Z$ interaction between the $(2)^3\Pi_{0u}(evJM)$ and $c^3\Sigma_u^+$ $(v_cN = JJ'M)$ levels. The rate $k_p(v'JM)$ is calculated to be

$$k_p(v'JM) = |\langle X^1\Sigma_g^+(v''J{-}1M)|\mu_Z|D^1\Sigma_u^+(v'JM)\rangle|^2 \times |\langle D^1\Sigma_u^+(v'JM)|H_{SO}|(2)^3\Pi_{0u}(evJM)\rangle|^2 \times |\langle (2)^3\Pi_{0u}(evJM)|H_{JL} + H_Z|c^3\Sigma_u^+(v_cN{=}JJ'M)\rangle|^2 \quad (42)$$

where μ_Z is the electric dipole operator along the space fixed Z-axis with the electric vector of the laser beam and the external magnetic field pointing into the same direction. By averaging over all molecular orientations and summing over $J' = J + 1$, J, and $J - 1$, we obtain

$$k_p(J) = \mu^2\zeta^2C^2H^2J(16J^3 + 2J^2 - 23J + 11)/30(2J-1)^3(2J+3) + \mu^2\zeta^2B_L{}^2J^2(J+1)/3(2J-1) \quad (43)$$

where μ is the electronic transition moment along the molecular axis. Thus, the predissociation rate is expressed as a sum of the rate induced by the Zeeman interaction and the rate induced by the L-uncoupling interaction. Equation 43 shows that the rate of the magnetic predissociation is proportional to H^2 in accordance with the observed results. Both the C and B_L values are approximately proportional to the overlap integral $\langle v|v_c\rangle$. The fact that both the rates of the magnetic predissociation and the predissociation in the absence of the magnetic field increased with v' can be explained if the overlap integral increases with v'. Thus, the shortening of the lifetime by an external magnetic field was identified as originating from the magnetic predissociation caused by a combination of the spin–orbit interaction between the $D^1\Sigma_u^+$ and $(2)^3\Pi_{0u}$ states and the electronic Zeeman interaction between the $(2)^3\Pi_{0u}$ and $c^3\Sigma_u^+$ states.[103]

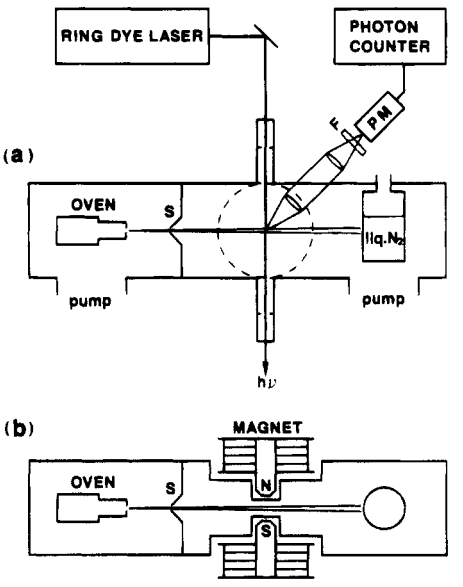

Figure 17. Experimental setup for the Doppler-free excitation spectroscopy in the presence of an external magnetic field. The fluorescence from the dissociated atom $Cs(6p^2P_{3/2})$ was selected by placing appropriate interference filter (F) in front of the photomultiplier (PM). Cross-sectional view of the molecular beam apparatus: (a) longitudinal section, (b) cross section. (Reprinted from ref 104. Copyright 1993 American Institute of Physics.)

The line shapes of transitions to the predissociative levels $D^1\Sigma_u^+(v',J')$ and the effects of magnetic field were studied by measuring the excitation spectra obtained from selective detection of the fluorescence intensity from dissociated atoms $Cs(6p^2P_{3/2})$.[104] The experimental setup is shown in Figure 17. The spectra of the $D^1\Sigma_u^+(v' = 46, J' = 54) \leftarrow X^1\Sigma_g^+(v'' = 0, J'' = 55)$ transition in the absence and presence of the magnetic field are shown in Figure 18. The Lorentzian line shapes were observed to increase in

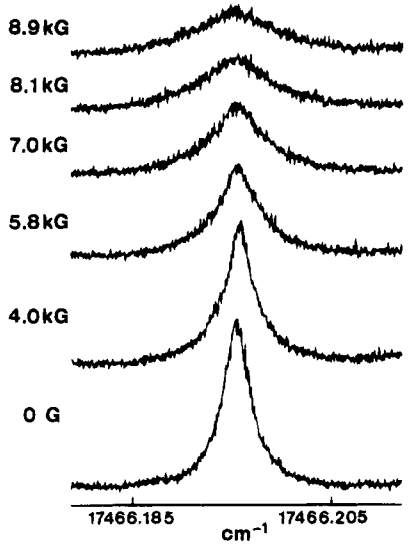

Figure 18. Spectral line of the $D^1\Sigma_u^+(v' = 46,J' = 54) \leftarrow X^1\Sigma_g^+(v''=0,J''=55)$ transition, and the change with the magnetic field. (Reprinted from ref 104. Copyright 1993 American Institute of Physics.)

width proportional to H^2, which agrees with the results of the time-resolved studies.[103] However, some lines were observed to change from a Lorentzian to an asymmetric line shape accompanied by an energy shift of the intensity maximum, and the line width increased abruptly with the magnetic field.[104] This is thought to be due to the Zeeman interaction between the $(2)^3\Pi_{0u}$ and $(2)^3\Pi_{1u}$ states.

C. Halogens

The electric transitions of the diatomic halogens and interhalogens are in an experimentally convenient spectral region, and therefore many excellent studies on their predissociation have been reported. A review on the fluorescence decay dynamics has been given by Heaven.[105]

1. I_2

a. Predissociation Induced by Rotational and Hyperfine Interactions. Predissociation of the $B^3\Pi_{0^+u}$ state was found by detection of $I(^2P_{3/2})$ atoms by electron spin resonance.[106] Chutjian and James[107] found a significant amount of predissociation occurring within the $B^3\Pi_{0^+u}$ state by comparing the purely radiative decay rate with the total decay rate for the $v' = 14 - v'' = 1$ and $v' = 25 - v'' = 0$ band of the $B^3\Pi_{0^+u}-X^1\Sigma_g^+(0^+)$ transition. The former was obtained from the line strength of the absorption spectrum, and the latter was obtained from the lifetime of the fluorescence decay. Chutjian[108] calculated the rate of predissociation which was induced by the rotational interaction (see section III.C.3) between the $B^3\Pi_{0^+u}(v',J')$ bound level and the 2431 $^1\Pi_{1u}$ continuum level. The notation 2431 is defined in ref 109 and indicates the electronic configurations of the molecular orbitals in I_2. The rate of predissociation is then given by

$$\Gamma_{pred} = k_{v'}J'(J' + 1) \qquad (44)$$

where $k_{v'}$ is a rate constant which depends on v'. The dependence of the rate on the rotational level J' was studied, and the predissociation was identified as originating from the rotational interaction between the $B^3\Pi_{0^+u}(v',J')$ and $2431^1\Pi_{1u}$ states. The potential curve of the $2431^1\Pi_{1u}$ state was estimated from the v' dependence of the predissociation, and excellent agreement between the calculated and observed relative predissociation rates for $v' = 14$, 25, and 50 was obtained. By applying technique of photodissociation translational spectroscopy, Busch, Mahoney, Morse, and Wilson[110] observed the predissociation of the discrete $B^3\Pi_{0^+u}$ level under molecular beam conditions with no collisional perturbation.

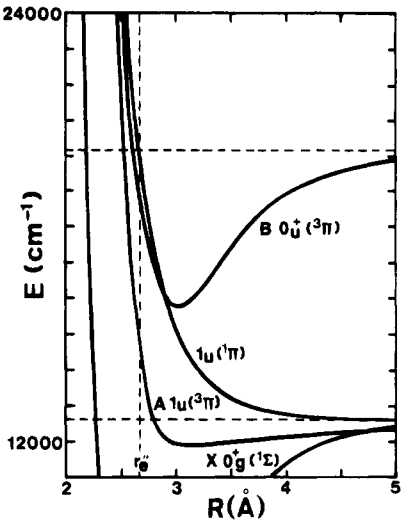

Figure 19. Potential energy curves of I_2 in the region of interest.

Photodissociation quantum yields in the 500–630 nm region were determined by measuring atomic emission.[111] By analyzing the lifetimes and photodissociation yields, a plot of Γ versus vibrational quantum number shows a sharp peak at $v' \sim 5$, negligibly small near $v' = 14$, and a broad weak maximum around $v' = 26$.[112] The absorption coefficient of I_2 in the 420–800 nm was measured, and by referring to the above results, the contributions of the $2431^1\Pi_{1u} \leftarrow X^1\Sigma_g^+$, $B^3\Pi_{0^+u} \leftarrow X^1\Sigma_g^+$, and $A^3\Pi_{1u} \leftarrow X^1\Sigma_g^+$ transitions to this absorption were extracted.[113] Potential energy curves of the relevant states of I_2 deduced by Tellinghuisen are shown in Figure 19.

Lifetimes of individual rovibrational levels in the $B^3\Pi_{0^+u}$ state were measured systematically.[114,115] As alluded to eq 11, the inverse of the lifetime τ is related to a radiative decay rate Γ_{rad} and the predissociation rate Γ_{pred} by

$$1/\tau = \Gamma = \Gamma_{rad} + \Gamma_{pred} \qquad (45)$$

From the $J(J + 1)$ dependence of Γ_{pred}, the predissociation was demonstrated as originating from the rotational interaction, and the rate constants k_v defined by eq 44 were determined. Γ_{rad} obtained by extrapolation of Γ to $J = 0$ showed a similar v dependence with k_v. From this fact, Broyer, Vigue, and Lehmann[115] estimated that the value of Γ_{rad} were not the true radiative decay rate and still included a predissociation term. The predissociation was thought to occur through an interaction with the $2431^1\Pi_{1u}$

state because of the same v dependence with k_v. This predissociation was caused by the hyperfine interaction, and the total decay rate is expressed as

$$\Gamma = \Gamma_{rad} + \Gamma_{hf} + \Gamma_{int} + k_v J(J+1) \quad (46)$$

The hyperfine predissociation rate Γ_{hf} and the interference term Γ_{int} were expressed as

$$\Gamma_{hf} = \frac{|a_v|^2}{3}\left[\mathbf{I}^2 + \frac{3(\mathbf{I}\cdot\mathbf{J})^2 + {}^3/_2\mathbf{I}\cdot\mathbf{J} - \mathbf{I}^2\cdot\mathbf{J}^2}{(2J-1)(2J+3)}\right] \quad (47)$$

$$\Gamma_{int} = -\sqrt{2}a_v c_v \mathbf{I}\cdot\mathbf{J} \quad (48)$$

where a_v is the hyperfine predissociation coefficient and $k_v = |c_v|^2$. The lifetimes of the hyperfine sublevels for a given J are expected to be different and depend on whether J is even or odd. This was experimentally confirmed by the observation that the lifetimes of ortho (J: even, $I = 1$, 3, and 5) and para (J; odd, $I = 0$, 2, and 4) levels, which were averaged over hyperfine sublevels, were different and that the decay was nonexponential.[116] More directly, the lifetimes and fluorescence yields of individual hyperfine components were measured for a number of $B^3\Pi_{0^+u}(v',J')$ levels, and the rotational and hyperfine predissociation parameters c_v^2 and a_v^2 were determined.[28,117-123]

b. Predissociation Induced by a Magnetic Field. In 1913, Steubing[124] discovered that the $B^3\Pi_{0^+u} \rightarrow X^1\Sigma_g^+$ fluorescence was quenched by an external magnetic field. Turner[125] suggested that this quenching originated from magnetic predissociation. Van Vleck[126] suggested that the mixing of the $B^3\Pi_{0^+u}$ state with the $^3\Pi_{0^-u}$ state caused the magnetic predissociation. The rate constants were determined by studying the quenching of fluorescence intensity and the shortening of the lifetime by the magnetic field.[127-129] A quantum interference effect between the magnetic predissociation and natural predissociation were observed.[130,131] Such an interference occurs only if the natural and magnetic predissociations of the $B^3\Pi_{0^+u}$ state are both induced by interaction with the same state, which was accordingly assigned as the $2431^1\Pi_{1u}$. However, the theory[132] was not completely correct because the matrix element of the coupling between the $B^3\Pi_{0^-u}$ and $2431^1\Pi_{1u}$ states was evaluated to be zero. The matrix element of the Zeeman interaction between the $B^3\Pi_{0^+u}$ and $2431^1\Pi_{1u}$ states was later shown to be nonzero because the $2431^1\Pi_{1u}$ state was mixed with the $2431^3\Pi_{1u}$ state by spin–orbit coupling.[133]

c. Predissociation Induced by an Electric Field. Predissociation induced by the application of an electric field was first predicted by Zener.[134] The Stark interaction eq 36 between two states i and j can occur if an electric dipole transition is allowed *i.e.* $\langle i|\mu^e|j\rangle \neq 0$. Sullivan and Dows[135] found that the fluorescence from the $B^3\Pi_{0^+u}$ state was quenched when an electric field was applied, and concluded that this was caused by the electric field-induced predissociation. Dalby, Levy, and Vanderlinde[136] studied the v' and J' dependence, and concluded that the unbound 1_g state crossed the $B^3\Pi_{0^+u}$ state near $v' = 0$ on the inner limb of the potential curve. The transition dipole moment between the two states was estimated to be 0.13 ± 0.07 Debye.

2. Br_2

The $B^3\Pi - X^1\Sigma^+$ transition of halogen molecules is caused by the partial $^1\Sigma^+$ character of the $B^3\Pi$ state.[7] A smaller absorption coefficient for the B–X transition is expected for Br_2 than for I_2, since the $B^3\Pi - X^1\Sigma^+$ transition is more strongly forbidden for Br_2 because of the smaller spin–orbit interaction. Therefore, longer lifetime of the $B^3\Pi$ state is expected for Br_2 than for I_2. A tunable dye laser was used to excite selected vibrational levels between $v' = 1$ and 31 of the $B^3\Pi_{0u}$ state of Br_2.[137] The lifetime was about 1.2 μs near $v' = 27$ and 0.15 μs near $v' = 14$, and the two minima near $v' = 1$ and 14 were explained as due to predissociation. The observed short lifetimes indicate that the radiative lifetime contributes little to the measured lifetime and that nonradiative processes are very important. This large effect of predissociation in Br_2 as compared to I_2 is consistent with the conclusion that the predissociation is induced by the rotational interaction, whereas the interaction should be proportional to the inverse of the square of the molecular mass. The existence of a strong predissociation, which was induced by rotational interaction between the $B^3\Pi_{0u}$ and $^1\Pi_{1u}$ states, was confirmed by measurements of rotationally dependent lifetimes.[138,139] The potential curve of the continuum state $^1\Pi_{1u}$ was deduced from the analysis of the v' dependence of the predissociation rates.[140,141] It should be noted that the curve crossing is the c^- case in I_2, and the c^+ case in Br_2 in Mulliken's notation[6] (the crossing point lies at the inner limb of the $B^3\Pi_{0u}$ state in I_2, but at the outer limb in Br_2). Hyperfine predissociation was also observed from the intensity anomalies between the components of resolved hyperfine structure of rotational lines.[142-145] The effect of an electric quadrupole hyperfine interaction to the predissociation was observed, and the parameters associated with rotational, magnetic dipole hyperfine and electric quadrupole hyperfine interactions were determined.[146]

3. Cl_2

Clyne and McDermid[147-149] observed rotationally resolved excitation spectra of the $B^3\Pi_{0^+u} - X^1\Sigma_g^+$ transition of Cl_2, and found that the quantum yields of the laser-induced fluorescence were unity for excitations to $v' \leq 12$ and about 3×10^{-5} for excitations to $v' \geq 13$. The $v' \geq 13$ levels of $B^3\Pi_{0^-u}$ were observed to undergo fast predissociation at the crossing of the outer limb of the $B^3\Pi_{0^+u}$ state and the $^1\Pi_{1u}$ repulsive state between $v' = 12$ and 13. The rotationally dependent portion of the predissociation was found to be described by eq 44, but the rate constant k_v was found to be much greater than those of Br_2 and I_2. Heaven and Clyne[150] calculated the predissociation rate constants in order to investigate the form of the repulsive potential of the $^1\Pi_{1u}$ state, and showed that the experimentally observed vibrational dependence of the predissociation rate cannot be accounted for by predissociation via the $^1\Pi_{1u}$ state. They demonstrated that the $A^3\Pi_{1u}$ state provides the

dissociation channel. By studying the lifetimes for $B^3\Pi_{0^+u}(J=0,v'>13)$, the existence of a hyperfine predissociation via the $A^3\Pi_{1u}$ state was proved.[151]

4. IBr

The discrete absorption from the $X^1\Sigma^+$ ground state to the $B^3\Pi_{0^+}$ state was found to break off at a false dissociation limit due to a crossing of the diabatic potential curves of the bound $B^3\Pi_{0^+}$ state which is correlated with the atomic asymptote $I(^2P_{3/2})$ + $Br(^2P_{1/2})$ and the repulsive 0^+ state which is correlated with the atomic asymptote $I(^2P_{3/2})$ + $Br(^2P_{3/2})$. Another weak diffuse band was observed at higher frequencies.[152,153] This band was assigned as the transition to the adiabatic state $\bar{B}_{0^+}$ whose inner limb was the one of the 0^+ diabatic potential and the outer limb was the attractive part of the $B^3\Pi_{0^+}$ diabatic potential. The P and R branches extending over narrow ranges of J were sharp and intense, but the lines on both sides of the band system were diffuse. Donovan and Husain[154] found that photodissociation from the $B^3\Pi_{0^+}$ state continuum leads predominantly to excited $Br(^2P_{1/2})$ atoms. This shows that the photodissociation is largely a diabatic process governed by the diabatic potential curve of the $B^3\Pi_{0^+}$ state. Child[22] successfully explained the observed results by applying the semiclassical theory for the case of intermediate coupling strength (see section II.D), and showed that both diabatic and adiabatic characteristics must be taken into account. The line widths of rotational lines of the $\bar{B}_{0^+}-X^1\Sigma^+$ transition were measured by using a laser excitation spectroscopy, and the change of the line width with J was attributed to predissociation.[155] The results were in excellent agreement with the theoretical results given by Child.[22] Using Doppler-free laser polarization spectroscopy, the hyperfine structure of the sharpest lines of several bands was measured, and the magnitude of the hyperfine parameters and their variation with v' were studied.[156]

5. ICl

Brown and Gibson[157] found a faint set of irregular bands on the short wavelength side of the $v' = 4 - v'' = 1$ and $v' = 4 - v'' = 0$ bands of the $B^3\Pi_{0^+}-X^1\Sigma^+$ system. The rotational lines in narrow ranges of J were sharp and intense, but other lines became diffuse. Brown and Gibson gave an explanation of why transitions to only a few rotational levels were observed: Above the point of intersection of the potential curves of the $B^3\Pi_{0^+}$ state and the repulsive 0^+ state, certain "virtual" rotational levels of the diabatic (crossing) potential of the $B^3\Pi_{0^+}$ state coincide with the rotational levels of the adiabatic (noncrossing) bound potential of the 0^+ state with the same J. However, more accurate interpretation was given by applying Child's theory[22] in the case of intermediate coupling strength.[158] The curve crossing and the repulsive part of the $B^3\Pi_{0^+}$ potential curve were studied by photofragment spectroscopy.[159] Orson and Innes[160] determined the lifetimes of single rotational levels of the $B^3\Pi_{0^+}(v' = 3, J')$ from measurements of line widths. A striking increase in line widths occurred for $J' > 37$ due to homogeneous predissociation, and the crossing of a repulsive curve of the 0^+ state at the outer limb of the potential curve of the $B^3\Pi_{0^+}$ state was suggested. Fluorescence lifetimes of the $B^3\Pi_{0^+}(v' = 1, 2,$ and $3, J')$ levels were measured by selective excitation, and the homogeneous predissociation that occurred for $v' = 3$ was not observed for $v' = 2$.[161,162] The hyperfine structure of the $B^3\Pi_{0^+}(v' = 3, J')$ levels was studied by measuring the excitation spectra using a molecular beam.[163] The relative intensities of the hyperfine components revealed a hyperfine predissociation of these levels, and the corresponding hyperfine predissociation parameter a_v was determined.

6. IF

The excitation spectra of IF was measured, and the onset of predissociation was observed at $v' = 10$, $J' = 12$ of the $B^3\Pi_{0^+}$ state.[164] The predissociation of the $B^3\Pi_{0^+}(v'=10,J')$ state was estimated as due to the interaction of the B state with a repulsive $Y0^+$ state. A shortening of lifetimes was observed for $v' = 8$, $J' > 52$ and $v' = 9$, $J' > 7$.[165] The predissociations of the $B^3\Pi_{0^+}(v'=8,J')$ and $B^3\Pi_{0^+}(v'=9,J')$ levels were estimated as due to the interaction of the B state with a weakly-bound $C^3\Pi_{0^+}$ state, which crossed the repulsive potential of the 0^+ state at a large internuclear distance.

D. Alkali Halides

The ground state $X^1\Sigma^+$ of alkali halides is an ionic state which decomposes into $M^+ + X^-$ atoms. The excited states of low energy are covalent states and decompose into $M(^2S_{1/2})$ + $X(^2P_{3/2})$ and $M(^2S_{1/2})$ + $X(^2P_{1/2})$. The potential curves of the ionic ground state and the covalent excited states are known to cross (see Figure 7). Berry[166] discussed the coupling of these states and the resulting predissociation. Davidovits and Brodhead[167] reported the absorption spectra of alkali halides in the vapor phase in the region of 200−400 nm. By applying the photofragmentation spectroscopy method,[168] the ratio of the $A0^+ \leftarrow X0^+$ parallel transition to the $A1 \leftarrow X0^+$ perpendicular transition was measured for KI and NaI in the 300−337 nm region and for KBr and NaBr in the 265−310 nm region, and the potential curves were constructed.[169]

1. NaI

In the absorption spectrum of NaI, Berg and Skewes[170] observed a discrete band structure with spacings of about 36 cm^{-1} and a broad pattern of weakly alternating dark and bright intensities in the region from 294.5 to 540 nm. Schaefer, Bender, and Tiemann[171,172] measured a high-resolution excitation spectrum in the range of 26900−33175 cm^{-1} by detecting molecular fluorescence. Fragmentary rotational structures, which have a strong central line and symmetrically decreasing intensities of the neighboring lines, were observed in the vibrational bands and were explained by predissociation originating from the interaction between the ionic ground state $X0^+$ and the covalent state $A0^+$. Such fragmentary structure occurs in predissociation which can be interpreted as the case of an intermediate coupling strength (see section II.D). By adopting the semi-

classical model of Child[22] for the predissociation, the molecular parameters of the diabatic state $X0^+$ and the adiabatic state $A0^+$, the RKR potential curves, and the interaction matrix element were determined. The emission spectrum from a molecular beam of NaI was measured following excitation by the 248 nm line of a KrF excimer laser.[173] Excitation spectra of NaI excited by a frequency doubled pulsed dye laser were recorded in the range of 239–256 nm, and the molecular constants and the RKR potential curve of the $C0^+$ state of the atomic asymptote $Na(3p^2P) + I(5p^2P_{3/2})$ were determined.[174]

Femtosecond real-time observation of wave packet oscillations in the predissociation of NaI has been extensively studied.[39,175–178] The scheme of the femtosecond transition state spectroscopy (FTS) is shown in Figure 7. Because of the crossing between the ionic ground state and the covalent excited state, there are two limiting possibilities for the behavior of the excited state. Either the wave packet produced by a pump laser is trapped on the adiabatic surface without crossing or it crosses on the diabatic surface and dissociates. The actual behavior can be expected to fall between these diabatic and adiabatic extremes.

If the probe wavelength λ_{pr} is varied, the dynamics of the dissociative process at different positions along the reaction coordinate can be studied. 590 nm light is resonant with the Na D-line transition. The transition $Na(3p^2P) \leftarrow Na(3s^2S_{1/2})$ occurs at very large internuclear distances R. The signal of the product $Na(3p^2P)$ atoms showed an initial sharp rise with a series of stair-step plateaus (see Figure 20c). The probe light was used to detect the leakage of the wave packet; each time it passes through the interaction region, the time dependence of the Na atom population was effectively integrated. At $\lambda_{pr} = 575$ and 615 nm (Figure 20, parts a and d), the probe light is off-resonance and the oscillation of the signal is a manifestation of the propagation of the wave packet (initially generated by the pump) as it traverses back and forth across the well. At $\lambda_{pr} = 580$ nm (Figure 20b), the probe light is off-resonance, but not far enough to entirely eliminate the on-resonance contribution. The periods of the oscillation were the same for a fixed pump wavelength. Thus, the on- and off-resonance data are complementary measurements of the dynamics of the system.

When the pump wavelength λ_{pu} was varied, different wave packets were produced. If the trapping well is harmonic, the period of oscillation will be the same for all pump wavelengths. If the well is anharmonic, the period is expected to change. An example of this effect is shown in Figure 21. The FTS probed at off-resonance are shown for $\lambda_{pu} = 300$, 311, 321, and 339 nm. The period becomes shorter as the wavelength of the pump laser is tuned to longer wavelengths. The damping time changes as well, and becomes slower for longer wavelengths. From the period of the oscillation τ_o, the vibrational frequency is calculated: $\nu = 1/\tau_o$. The damping time τ_d gives the cross section for a transition from the adiabatic (bound) potential curve to the diabatic (dissociative) potential curve. The ratio τ_o/τ_d gives the average probability of the crossing per oscillation. Many theoretical studies[179–183] have been reported on these phenomena. The data obtained by the FTS method and the data obtained by high-resolution spectroscopy complement each other.

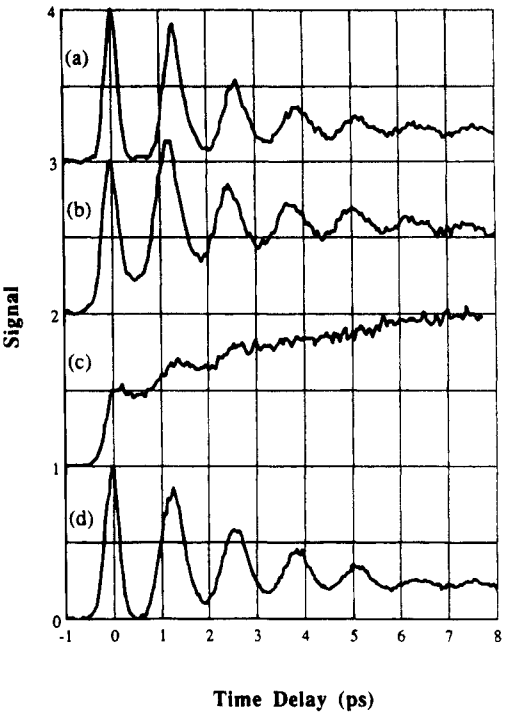

Figure 20. Experimental results of the femtosecond transition-state spectroscopy of NaI as a function of probe wavelength: (a) 575 nm; (b) 580 nm; (c) 590 nm; and (d) 615 nm. The probe beam was passed through an approximate 10 nm bandwidth filter and the pulse duration was approximately 250 fs. The pump beam of a pulse duration of about 50 fs and a bandwidth of 3 nm was fixed at 307 nm. The 590 nm signal (c), which probes $Na(3p^2P_{3/2}) \leftarrow Na(3s^2S_{1/2})$ transition, shows a production of $Na(3s^2S_{1/2})$ atom with an initial sharp rise and a series of stair-step plateaus. (Reprinted from ref 176. Copyright 1989 American Institute of Physics.)

2. Other Alkali Halides

Schaefer, Bender, and Tiemann[184] observed the high-resolution excitation spectrum of the $A0^+ \leftarrow X0^+$ transition of LiI. The analysis was performed along the lines of the semiclassical model of predissociation originating from the coupling of ionic and covalent states. The molecular constants and potential curves are given for the limiting diabatic state $X0^+$ and for the adiabatic state $A0^+$ and the coupling matrix element is in good agreement with the model of charge-transfer reactions by Grice and Herschbach.[185] FTS results have been reported for NaBr and LiI.[176] The FTS signals of NaBr were similar to those of NaI except that the rise time was shorter and no apparent oscillation was measured. The damping time was very short and only a faint recurrence was observed. The Landau–Zener parameter of NaBr was found to be at least 1 order of magnitude larger than that of NaI. Thus, NaBr should behave diabatically.

E. O_2, S_2, Se_2

1. O_2

In the Schumann–Runge bands ($B^3\Sigma_u^- - X^3\Sigma_g^-$) of O_2, diffuse lines occur, suggestive of predissociation

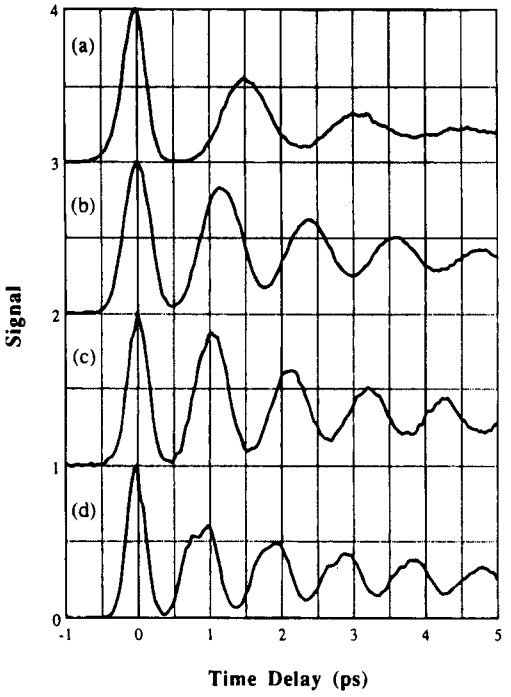

Figure 21. Experimental results of femtosecond transition-state spectroscopy of NaI as a function of pump wavelength: (a) 300 nm; (b) 311 nm; (c) 321 nm; and (d) 339 nm. The wavelength of probe beam was chosen at off-resonance. (Reprinted from ref 176. Copyright 1989 American Institute of Physics.)

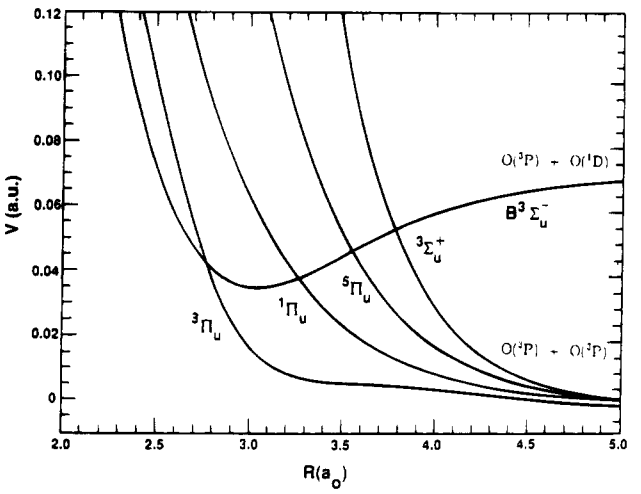

Figure 22. Potential energy curves of O_2 relevant to predissociation of the $B^3\Sigma_u^-$ state. (Reprinted from ref 199. Copyright 1992 American Institute of Physics.)

in the $B^3\Sigma_u^-$ state.[186] Murrell and Taylor[187] studied the relation between the potential energy curves and the v dependence of the predissociation rates, and suggested that a repulsive state crosses the $B^3\Sigma_u^-$ state at the outer turning point of $v' = 4$. The rotational dependence due to the centrifugal term was also shown to change with v'.[188] However, the *ab initio* calculation of Schaefer and Miller[189] suggested that the $B^3\Sigma_u^-$ state correlating with $O(^3P) + O(^1D)$ crosses four close-lying repulsive states, $^1\Pi_u$, $^5\Pi_u$, $^3\Sigma_u^+$, and $^3\Pi_u$ which correlate with $O(^3P) + O(^3P)$ (see Figure 22). The $^1\Pi_u$, $^5\Pi_u$, and $^3\Sigma_u^+$ states can couple with the $B^3\Sigma_u^-$ state by spin–orbit coupling, and the $^3\Pi_u$ state can couple with the $B^3\Sigma_u^-$ state mainly by L-uncoupling interaction. Julienne and Krauss[190] studied theoretically the v' dependence of the observed lifetimes and level shifts and concluded that the predissociation was caused primarily by the interaction with the $^5\Pi_u$ state. Julienne[191] suggested that the $^3\Sigma_u^+$ state contributed appreciably to the predissociation at $v' \geq 6$. In a later study, the analysis of laser-induced fluorescence of O_2 where the fine-structure levels were partially resolved[192] showed that the L-uncoupling interaction with the $^3\Pi_u$ state was significant at high J' for $v' = 10$ and 11.

The lifetimes of the vibrational and rotational levels were determined by the analysis of high-resolution absorption spectra for the $^{16}O_2$, $^{16}O^{18}O$, and $^{18}O_2$ isotopes.[193–195] The level shifts due to the interaction with each repulsive state was also analyzed.[196–198] Chiu, Cheung, Finch, Jamieson, Yoshino, Dalgarno, and Parkinson[199] obtained the best-fit potential energy curves and the interaction strengths to reproduce the experimental v' dependence of the predissociation rates. The spin–orbit interaction with the $^5\Pi_u$ state was shown to be the main channel causing the predissociation of the $B^3\Sigma_u^-$ state, but the other three repulsive states were also shown to contribute.

The translational energy release distribution of two O $^3P_{J_1}$ and $^3P_{J_2}$ (J_1, J_2 = 0, 1, 2) atoms, which is produced from the predissociation of O_2 $B^3\Sigma_u^-(v' = 7)$, was measured by Leahy, Cyr, Osborn, and Neumark.[200a] The observed (J_1, J_2) distribution is not completely consistent with dissociation along the adiabatic Hund's case c potential curves and is also inconsistent with completely statistical distribution. They suggested that the strength of the coupling of the $^3\Pi_u$ and $^1\Pi_u$ states was underestimated in ref 199.

Cosby, Park, Copeland, and Slanger[200b] observed the transitions from the vibrationally excited $O_2(X^3\Sigma_g^-)$ molecules produced by photodissociation of O_3, and measured the line widths of transitions to the rotational and fine-structure levels of the $B^3\Sigma_u^-(v' = 0$ and 2) state. The line widths of the $F_2(N'=J')$ and $F_3(N'=J'+1)$ levels were found to be remarkably larger than the line width of the $F_1(N'=J'-1)$ level and to increase as the rotational quantum number N' increased. For low v' levels, the L-uncoupling interaction with the $^3\Pi_u$ state was shown to be crucial for this fine-structure dependence. The potential energy curve of the $^3\Pi_u$ state obtained by *ab initio* calculations[201] was found to give better fits to the line widths of the rotational and fine-structure levels in $v' = 0$ and 2.

Predissociation in the gerade state of O_2 was observed by van der Zande, Koot, Los, and Peterson[202] and van der Zande, Koot, and Los.[203] They measured the distribution of kinetic energy released to the fragments from the O_2 molecules in the $^{1,3}\Pi_g$ Rydberg states using translational spectroscopy. From the observed v' and N' dependence of the dissociation rate, the predissociations of the $d^1\Pi_g$ and $C^3\Pi_g$ states were both shown to be induced by the interaction with the valence $^{1,3}\Pi_g$ states. Friedman, Du, and Dalgarno[204] explained these experimental results using the Landau–Zener model. Strong predissociations of the $3d\pi$, $^1\Delta_g$, $^3\Delta_g$,[205] $ns\sigma$, and $nd\lambda$ states ($n = 3–5$), where $nl\lambda$ denotes a Rydberg state

by the main single electronic configuration, were observed using multiphoton ionization.[206]

2. S_2

In 1924, Henri and Teves[207] measured the UV absorption spectrum of S_2 and found that several sharp bands disappeared abruptly and were replaced by broad bands suggestive of predissociation. The emission spectrum was observed using a high-voltage discharge,[208] and a break off of the intensity was found. Lochte-Holtgreven[209] measured the emission spectrum of S_2 and pointed out that strong predissociation occurred at $v' = 11$ and 18. Herzberg and Mundie[210] discovered the predissociation onset at $v' = 10$, and suggested that the predissociation was case c from the v' dependence of the line widths. The upper state was identified as the $B^3\Sigma_u^-$ state, which corresponds to the upper state of the Schumann–Runge bands of O_2. Ricks and Barrow[211] observed the high-resolution absorption spectrum of the $B^3\Sigma_u^- - X^3\Sigma_g^-$ transition. They found that the rotational quantum number at the threshold for predissociation decreased as v' increased. Therefore, the predissociation was identified as case b^+. This $B^3\Sigma_u^-$ state was found to be strongly perturbed by a nearby $B''^3\Pi_u$ state, which induced level shifts and lifetime variation.[212] The potential curve of the $B''^3\Pi_u$ state was estimated to cross the $B^3\Sigma_u^-$ state at the inner limb. Therefore, if the B″ state is responsible for the predissociation, it would be case b^-. It was also suggested that the predissociating state was another electronic state which crossed the $B^3\Sigma_u^-$ state at the outer limb. From the analysis of the dissociation energy and from theoretical calculations, the predissociation in the $B^3\Sigma_u^-$ state is thought to be caused by the interaction with a 1_u state correlating with $S(^3P_2) + S(^3P_1)$.[211] Quick and Weston[213] observed weak emission from the predissociating $v' = 10$ level by the laser-induced fluorescence method and the lifetime was found to be shorter than 3 ns. There has been no quantitative study on the predissociation rate. More extensive studies are necessary to understand the predissociation in the $B^3\Sigma_u^-$ state of S_2.

Narasimham and Gopal[214] observed the emission spectrum of the $f^1\Delta_u - a^1\Delta_g$ transition, and, from the decrease of the emission intensity, the predissociation was estimated to occur at $v' = 10$ and 11 in the $f^1\Delta_u$ state. Carleer and Colin[215] observed the high-resolution absorption spectrum and reported that the broadening in the predissociating level was small and did not increase with J'. Therefore, the predissociation was identified as the case c^+ and the potential energy curve was expected to cross the outer limb of the $f^1\Delta_u$ state. From symmetry considerations, the perturbating state was estimated to be a repulsive $^3\Delta_u$ state correlated with $S(^1D) + S(^3P)$.

3. Se_2

Diffuseness in the absorption spectrum of Se_2 has been observed in the region of 27000–31000 cm^{-1}.[216,217] Barrow, Chandler, and Meyer[218] studied the vibrational and rotational structure of $^{80}Se_2$ and analyzed the v' and J' dependence of the predissociation. The rotational levels are approximately expressed by Hund's case c. Strong predissociation was observed for $v' = 13$, 14, and 15, and $v' = 4$, 5, and 6 in the $B0_u^+$ state. All of the predissociation was shown to be the case b^+. In the $B1_u$ state, the predissociation was found at $J' \sim 72$ in $v' = 5$. This predissociation was suggested to be the case c^+.

F. NO, CO

Predissociation of NO and CO in the Rydberg states via the interaction with a valence state were observed, and the Rydberg–valence interaction has been extensively studied.

1. NO

The dissociation limit of $NO \rightarrow N(^4S) + O(^3P)$ is equal in energy to the $v' = 0$ level of the $C^2\Pi$ state, a short-lived Rydberg state. This $C^2\Pi(v' = 0)$ level is strongly perturbed by the $v' = 7$ level of the valence $B^2\Pi$ state.[219,220] Callear and Pilling[221] found that the $C^2\Pi$ state predissociated strongly via an interaction with the $a^4\Pi$ state. The lifetime of each rotational level was measured by Rottke and Zacharias[222] using the two-color resonantly enhanced multiphoton ionization technique. It was shown that the predissociation onset was at $J' = 2.5$ ($^2\Pi_{3/2}$) and $J' = 3.5$ ($^2\Pi_{1/2}$) in the $C^2\Pi(v'=0)$ state, and at $J' = 4.5$ ($^2\Pi_{3/2}$) and $J' = 7.5$ ($^2\Pi_{1/2}$) in the $B^2\Pi(v'=7)$ state. The rate was determined to be 1.5×10^9 s^{-1} at $J = 9.5$. Tsukiyama, Munakata, Tsukakoshi, and Kasuya[223] confirmed this result by measuring the fluorescence lifetimes in a supersonic jet. The radiative decay rate at $J' = 3.5$ was reported to be 1.06×10^8 s^{-1}. de Vivie-Riedle, van Hemert, and Peyerimhoff[224] calculated theoretically the predissociation rate and suggested that the predissociation in the $C^2\Pi(v'=0)$ state was caused solely by the spin–orbit interaction with the $a^4\Pi$ state. The lifetime of the $v' = 1$ level was calculated to be 0.27 ns, which was consistent with the observation by d'Azy, Lopez-Delgado, and Tramer.[225]

The lifetime of the $D^2\Sigma^+(v'=0)$ state, which lies very close to the $C^2\Pi$ state is about 20 ns, and the predissociation via the $\lambda^4\Pi$ state is negligible.[222,223] However, predissociation occurs in the $D^2\Sigma^+(v'=1$ and 2) levels.[226]

Strong predissociation has been found in several Rydberg states of NO. Using the two-color multiphoton optical–optical double-resonance technique, Ashfold, Dixon, Prince, Tutcher, and Western[227] measured the line shapes of the transitions to the $E^2\Sigma^+(\sigma^2\pi^4 4s\sigma^1)$ Rydberg state, and found that only the transition lines to $N' = 8-12$ were remarkably broadened and asymmetric. It is believed that this effect is caused by predissociation originating from the interaction with the $I^2\Sigma^+(v'=4)$ state, which strongly predissociated via the repulsive $A'^2\Sigma^+$ state. Both of the $E^2\Sigma^+ \leftarrow X^2\Pi$ and $I^2\Sigma^+ \leftarrow X^2\Pi$ transitions are allowed transitions, so that absorption lines can show asymmetric profiles by the interference of transition amplitudes (Fano profile). Miller, Li, Wang, Chupka, and Colson[228] found that the lifetime of the $(4p\pi)K^2\Pi(v'=2)$ state was very short, and concluded that this arose from the predissociation via the $(4p\sigma)M^2\Sigma^+$ state and/or the $a^4\Pi$ state. The $N(^2P)$ atoms produced by predissociation in the $5s\sigma$, $4d\pi^-$, and $5d\pi^-$ Rydberg states were found by Gadd,

Jusinski, and Slanger[229] using the two-photon dissociation and multiphoton–ionization techniques. Fujii and Morita[230] also detected N(4S) and N(2D) atoms to study the predissociation in the superexcited 7f Rydberg state of NO. They found that only odd $\mathcal{L}$ level generated the N(4S) atom ($\mathcal{L}$ is the projection of the orbital angular momentum onto an axis of the core rotation) via the $A'^2\Sigma^+$ state, and concluded that N(2D) atoms were produced by predissociation that was caused mainly through the interaction with the $I^2\Sigma^+$ state. The decay of the superexcited np Rydberg states was also identified to be predominantly governed by predissociation, not by autoionization.[231]

2. CO

The $B^1\Sigma^+$ state is a 3sσ Rydberg state. Line broadening caused by predissociation was found by Coster and Brons.[232] The $B^1\Sigma^+$–$X^1\Sigma^+$ transition was analyzed for the four isotopic species $^{12}C^{16}O$, $^{13}C^{16}O$, $^{12}C^{18}O$, and $^{13}C^{18}O$.[233,234] Eidelsberg, Roncin, Le Floch, Launay, Letzelter, and Rostas[234] found (i) a weakening of emission from $v' = 0$ and 1 above a critical rotation number J_c ($J_c = 37$ for $v' = 0$, and $J_c = 17$ for $v' = 1$) and another weakening at $J' \sim 60$ for $v' = 0$, and $J' \sim 40$ for $v' = 1$ in $^{12}C^{16}O$, (ii) no detectable emission bands originating from $v' = 2$, (iii) the broadening of absorption lines for $v' = 2$. They concluded that this experimental evidence was indicative of predissociation that was caused by the interaction with the repulsive part of the $D'^1\Sigma^+$ state. This was theoretically predicted by Cooper and Langhoff.[235] The $D'^1\Sigma^+$–$X^1\Sigma^+$ transition was measured and analyzed by Wolk and Rich.[236] Cooper and Kirby[237] carried out theoretical calculations and confirmed that the predissociation was mainly caused by the interaction between the $B^1\Sigma^+$ and $D'^1\Sigma^+$ states. By comparing the experimental results with theoretical calculations based on the close coupling method, Tchang-Brillet, Julienne, Robbe, Letzelter, and Rostas[238] concluded that the predissociation occurred through the Rydberg-valence predissociative interaction. The energy where the emission yield decreases at $v' = 0$ and 1 corresponds to the dissociation limit to C(3P) + O(3P). The decrease in emission yield at $v' = 2$ was attributed to the predissociation through the long-range potential barrier.

In the $E^1\Pi(v'=0)$ state of CO, Simmons and Tilford[239] observed the effects of accidental predissociation. The R(30) lines of the $E^1\Pi$–$X^1\Sigma^+$ (0–0) band were split by the perturbation in the absorption spectrum, but were missing in emission. Klopotek and Vidal[240] reinvestigated this band using two-step vacuum-ultraviolet visible excitation spectroscopy, and suggested that the most probable perturbing state was a $^1\Sigma^+$. Amiot, Roncin, and Verges[241] found accidental predissociations for the f, $J' = 6$ sublevel in ^{12}CO, and f, $J' = 19$ and e, $J' = 41$ sublevels in ^{14}CO by using Fourier spectroscopy.

G. CH, NH, OH

1. CH

The absorption spectrum of CH was extensively studied by Herzberg and Johns[242] and the predissociation was observed for several electronic states in the UV region. van Dishoeck[243] used *ab initio* SCFCI methods to calculate the potential energy curves of CH and studied theoretically the predissociation in each electronic state. The calculated adiabatic potential curves of CH are shown in Figure 23.

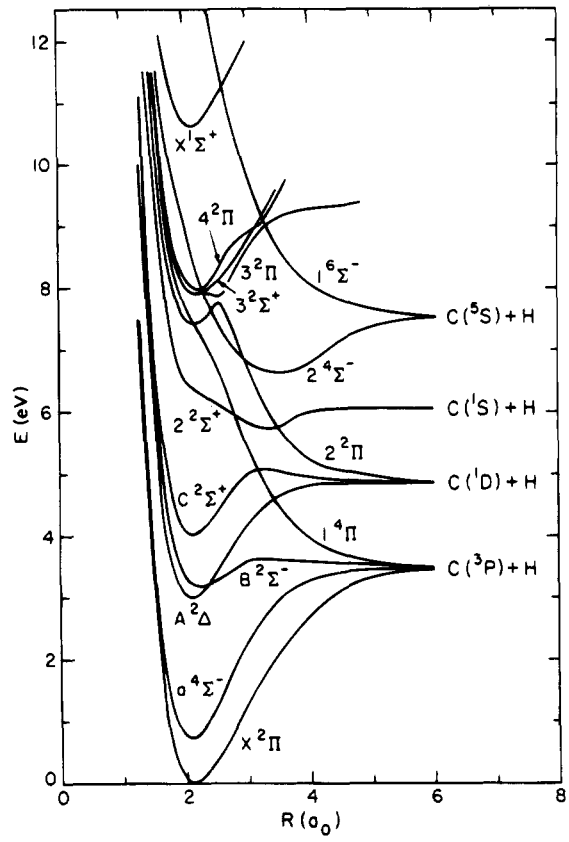

Figure 23. The calculated adiabatic potential energy curves of CH. (Reprinted from ref 243. Copyright 1987 American Institute of Physics.)

The lifetimes of the vibrational and rotational levels in the $A^2\Delta$ state were measured by Brzozowski, Bunker, Elander, and Erman.[244] The lifetime τ was 534 ± 5 ns for $N' = 6$–23 in the $v' = 0$ level, and decreased sharply for $N' \geq 12$ in $v' = 1$. These observations were attributed to predissociation induced by the coupling with the $X^2\Pi$ ground state. The $A^2\Delta$ and $X^2\Pi$ states can couple through rotational interactions.[243] The lifetime of one of the λ-doublet components was remarkably short for $N' = 17$–19 in $v' = 1$ and this was attributed to the perturbation by the nearby $B^2\Sigma^-$ state.[244]

Shidei[245] observed the emission spectrum of the $B^2\Sigma^-\rightarrow X^2\Pi$ transition, and found the diffuseness and breaking-off of the intensity for $N' \geq 15$ in $v' = 0$, and $N' \geq 6$ in $v' = 1$. These facts were confirmed by Herzberg and Johns.[242] Brzozowski, Bunker, Elander, and Erman[244] measured the lifetimes of the vibrational and rotational levels and showed that the predissociation was caused by tunneling through a barrier (see Figure 23).

The $C^2\Sigma^+$–$X^2\Pi$ transition was observed between 300–320 nm.[246] Because the fluorescence of CH is five times weaker than that of CD, Herzberg and Johns[242] pointed out that the $C^2\Sigma^+$ state of CH was predissociative, and suggested that the predissociation was caused by the interaction with the $B^2\Sigma^-$, $a^4\Sigma^-$, and $X^2\Pi$ states. Brzozowski, Bunker, Elander,

and Erman[244] measured the lifetimes of the rotational lines for $v' = 0$ and 1. The lifetime of the $v' = 1$ level was observed to be almost constant (3−4 ns), but that of the $v' = 0$ level was found to become longer as N' increased (10−25 ns). Ubachs, Meyer, ter Meulen, and Dymanus[247] measured the lifetime of each doublet level F_1 ($J=N+1/2$) and F_2 ($J=N-1/2$) separately. The lifetime of the F_1 level was found to be independent of N', but that of the F_2 level was found to become remarkably longer as N' increased. Only the spin−rotation interaction with a $^2\Sigma^-$ state is expected to cause this difference. Therefore, the predissociation of the $C^2\Sigma^+$ state is thought to be primarily caused by spin−rotation interaction with the $B^2\Sigma^-$ state. This was supported by theoretical calculations,[243] but the calculated values were not quantitatively consistent with the observed lifetimes. It is suggested that the $a^4\Sigma^-$ or $^4\Pi$ states cause a perturbation and affect the lifetimes of these states.

van Dishoeck[243] also performed theoretical calculations for the $D^2\Pi$ state, and showed that the three $^2\Pi$ states were strongly interacting. Wang, Li, and Chupka[248] confirmed this by using resonance-enhanced multiphoton ionization and found a sudden onset of predissociation for $N' \geq 12$ in $v' = 2$.

2. NH

Predissociation in the $A^3\Pi$ state of NH and ND was investigated by measuring the decay rate of the vibrational and rotational levels.[249,250] Smith, Brzozowski, and Erman[249] measured the lifetimes of the rotational levels of $v' = 0$ and 1 in the $A^3\Pi$ state by using a high-frequency deflection technique. The lifetime was appreciably short for $N' \geq 27$ in $v' = 0$, and $N' \geq 16$ in $v' = 1$. The predissociation was estimated to be caused by the spin−orbit interaction with the repulsive $1^5\Sigma^-$ state, and the $A^3\Pi$ state was estimated to cross at $R = 2.57\ a_0$ where a_0 is the Bohr radius. Goldfield and Kirby[251] calculated the crossing point to be at $R = 2.912\ a_0$. Patel-Misra, Parlant, Sauder, Yarkony, and Dagdigian[252] observed the lifetime of each e or f fine-structure level for $v' = 2$ for NH, and of $v' = 1-3$ for ND in a pulsed supersonic beam. They estimated the potential curves by modifying the calculated ones so as to fit the observed lifetimes. The resulting potential curve of the $1^5\Sigma^-$ state crossed the $A^3\Pi$ state at $R = 2.962\ a_0$ and $E = 12612\ cm^{-1}$. The break-off point was much lower than $12612\ cm^{-1}$. From this, it was estimated that quantum mechanical tunneling was important in the predissociation of the $A^3\Pi$ state.

The lifetimes of the vibrational and rotational levels in the $c^1\Pi$ state of NH were observed by Smith, Brzozowski, and Erman.[249] No transition could be found for $N' \geq 17$ in $v' = 0$, and $N' \geq 11$ in $v' = 1$. This was attributed to predissociation caused by the $1^5\Sigma^-$ state. Kenner, Rohrer, and Stuhl[253] observed the lifetimes to be almost constant; 460 ± 20 ns for $J' = 2-9$ in $v' = 0$ and 67 ± 7 ns for $J' = 1$ and 4 in $v' = 1$. They estimated that the $v' = 0$ level was not predissociative. The predissociation of the $v' = 0$ level at low J' was suggested by Parlant, Dagdigian, and Yarkony[254] and was confirmed by more accurate measurement and calculations of the lifetime.[255] The predissociation rate increased with J', but the radiative decay rate decreased by almost the same amount. The invariance of the total decay rate was explained by cancellation of these opposite J' dependences.

3. OH

The spectrum of OH $A^2\Sigma^+-X^2\Pi$ emission in a flame was observed by Gaydon and Wolfhard.[256] The intensity was found to decrease abruptly at high J' in $v' = 1$ and was very weak in $v' = 2$. The lifetimes of the $A^2\Sigma^+(v',J')$ levels were also subsequently measured.[257-263] Sink, Bandrauk, and Lefebvre[264] performed a theoretical analysis using multichannel scattering theory and showed that the predissociation in low v' levels of the $A^2\Sigma^+$ state was mainly attributed to the coupling with the repulsive $^4\Sigma^-$ state. For low J' levels in $v' = 0$ and 1, predissociation was negligible and the radiative decay rate decreased gradually with increasing N'. However, the lifetime was shortened abruptly for $N' \geq 24$ in $v' = 0$ and $N' \geq 15$ in $v' = 1$.[260] This shortening was caused by the potential curve crossing with the $^4\Sigma^-$ state. In contrast, predissociation was found for all rotational levels of $v' = 2$ with a lifetime of 150 ns at $N' = 0$, which decreased with increasing N'.[260] For the $v' = 3$ level, the lifetime was on the order of picoseconds and decreased rapidly with N'.[262,263] The lifetime of the F_1 ($J'=N'+1/2$) level was found to be slightly shorter than that of the F_2 ($J'=N'-1/2$) level.[263] The lifetime of OD also decreased for several J' levels of $v' = 0-2$, and all the rotational levels of $v' = 3$ were observed to be strongly predissociative.[261] Yarkony[265] has theoretically examined the perturbation induced by spin−orbit coupling and the geometry dependence of the coupling matrix elements. The calculated predissociation rates are in good agreement with the observed values for $v' = 0-3$ of OH and OD.

H. MgCl

Bourguignon, Gargoura, Rostas, and Taieb[266] studied the vibrational population of MgCl molecules produced by the reaction

$$Mg(^1S) + Cl_2 \rightarrow MgCl(X^2\Sigma^+) + Cl(^2P)$$

Spectral lines to upper level $v' \geq 7$ were found to be absent in the fluorescence excitation spectrum of the $A^2\Pi(v')-X^2\Sigma^+(v'')$ transition. Shafizadeh, Rostas, Taieb, Bourguignon, and Prisant[267] measured the fluorescence excitation spectra of MgCl formed in a Broida oven by the reactions of $Mg(^1S)$ with chlorine-containing molecules. From this work, molecular constants of the $X^2\Sigma^+$ and $A^2\Pi$ states were determined. The sudden cutoff of the vibrational structure at $v' \geq 7$ was interpreted as arising from an avoid crossing between the $A^2\Pi$ bound state and $(D)^2\Pi$ repulsive state, which results in the predissociation of the $A^2\Pi$ state. In addition, they observed that the fine structure splitting parameter $A_{SO} = E(A^2\Pi_{3/2}) - E(A^2\Pi_{1/2})$ decreased anomalously as v' increased. Chemiluminescence from $MgCl(A^2\Pi)$ produced by the reaction

$$Mg(^3P) + Cl_2 \rightarrow MgCl(A^2\Pi) + Cl(^2P)$$

was observed only for $v' \leq 5$.[268]

Parlant, Rostas, Taieb, and Yarkony[269] theoretically examined the electronic structure and the predissociation of MgCl. The adiabatic electronic wave functions of the $A^2\Pi$ and $(D)^2\Pi$ states were calculated by using the *ab initio* multiconfiguration self-consistent field/first and second-order configuration interaction methods, and from these wave functions diabatic wave functions were derived using a diabatization procedure. The $A^2\Pi$ bound state [the $1^2\Pi^d$ diabatic state correlating with $Mg^+(^2P) + Cl^-(^1S)$] was shown to predissociate by crossing with the repulsive $(D)^2\Pi$ state [$2^2\Pi^d$ diabatic state correlating with $Mg(^1S) + Cl(^2P)$]. By taking into account the spin–orbit and spin–other orbit interactions between the $1^2\Pi^d$ and $2^2\Pi^d$ states, the coupled-state quantum scattering calculations were able to reproduce the observed v dependence of the fine structure splittings. The predissociation lifetimes and energy shifts of the $A^2\Pi_{1/2}$ and $A^2\Pi_{3/2}$ vibrational levels were calculated on the basis of a coupled diabatic state representation. The predissociation rates for the $A^2\Pi_{1/2}(v')$ levels were calculated to be 3.6 times the radiative rate for $v' = 6$ and 700 times the radiative rate for $v' = 7$. This is consistent with the observed cutoff of the vibrational structure at $v' > 6$.[268]

VI. Predissociation of Polyatomic Molecules

In polyatomic molecules, predissociation of the electronically excited molecule can often occur by vibronic interaction and rovibronic interaction in addition to type I, type II, and type III predissociations classified by Herzberg for diatomic molecules. In most cases, the predissociation mechanism is discussed on the basis of the dependence of the observed quantum yield on the rotational and vibrational levels. The electronic spectrum is sufficiently sparse in some triatomic molecules, so that single rotational levels can be selectively excited.

A. HCO, HNO, H_2O, HCN, SO_2

1. HCO

The rotational dependence of the predissociation rate in the A^2A'' state of HCO was observed by Brown and Ramsay[270] from the line-width analysis of the absorption spectrum of the A^2A''–X^2A' transition. Degenerate states in the linear geometry are split by a vibronic interactuion (Renner–Teller effect) to bent X^2A' and A^2A'' states. Since HCO in the A^2A'' state is nearly linear, the vibrational state is represented using a linear molecule expression (v_1,v_2^K,v_3) where v_1, v_2, and v_3 are the vibrational quantum numbers of CH stretching, bending, and CO stretching, respectively. In a linear molecule, the quantum number K is given by $K = |\Lambda + l|$ where Λ is the projection of the electronic angular momentum to the molecular axis and $\Lambda = \pm 1$ for $^2\Pi$. l is the vibrational angular momentum with $|l| = v_2', v_2' - 2, ..., 1$, or 0. Therefore, the smallest value of K' is 0 for an odd v_2' level and 1 for an even v_2' level. The $(0,v_2'^{K'},0)$–$(0,0,0)$ progression is prominent in the visible A–X transition.

Vasudev and Zare[271] observed the high-resolution spectrum by using a single-mode laser and an optogalvanic method. The rotational structure was expressed as a prolate symmetric top $|N,K\rangle$. The transition to $K' \neq 0$ was diffuse, which is suggestive of a fast predissociation. In contrast, sharp rotational lines could be observed for the transition to $K' = 0$, and the line width of the $A(0,9^0,0)$–$X(0,0,0)$ band was observed to be strongly dependent on N' (see Figure 24). The primary process of the predissociation in the A^2A'' state was assigned as

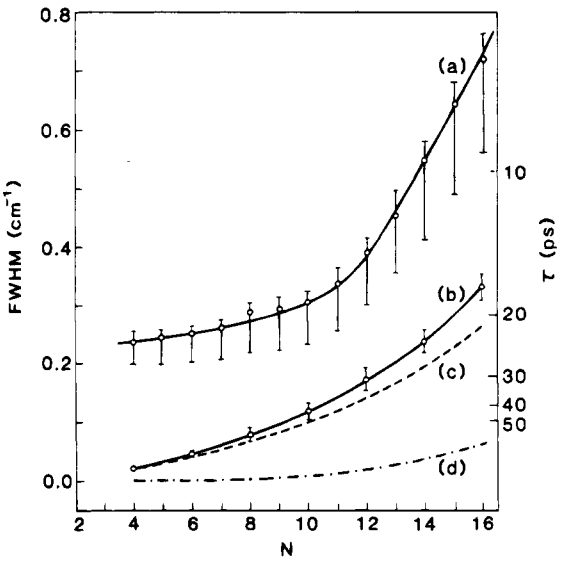

Figure 24. Variation of the line width with the rotational quantum number N' for the $(0,9^0,0)$–$(0,0,0)$ band of HCO; a is the observed line widths, and b is the sum of Coriolis interaction given in c and K-type resonance given in d. (Reprinted from ref 271. Copyright 1982 American Institute of Physics.)

$$HCO(A^2A'') \rightarrow H(^2S) + CO(^1\Sigma^+) \qquad (49)$$

For the $K' = 0$ level, a weak predissociation was observed.[270,271] The N'-dependent part in this $K' = 0$ level was attributed to the mixing with the strongly predissociative $K' \neq 0$ level. Brown and Ramsay[270] considered a K-type resonance, which mixes the $\Sigma(K'=0)$ level with the $\Delta(K'=2)$ level. The line width of the Σ level was expressed as

$$\Gamma_\Sigma = |\Delta D'|\frac{[N'(N'+1)]^2}{(E_\Sigma - E_\Delta)}\Gamma_\Delta \qquad (50)$$

where Γ_Δ is the line width of the Δ level and $\Delta D' = D'_{eff} - D'_{000}$. Vasudev and Zare[271] measured the line width of the $(0,9^0,0)$ level, which can interact with a Δ level $(0,9^2,0)$. In this case, $\Delta D'$ was expressed as

$$\Delta D' = -\frac{4B^4}{\omega_2^2}\left(1 + \frac{\zeta_{23}^2\omega_2^2}{\omega_3^2 - \omega_2^2}\right)^2 \times \left\{\frac{(v_2+1) + [(v_2-1)(v_2+3)]^{1/2}}{32(E_\Sigma - E_\Delta)}\right\} \qquad (51)$$

where B is the rotational constant, ζ_{23} is a Coriolis coupling constant, and ω_i is the vibrational frequency of the ith normal mode. The calculated width for the $(0,9^0,0)$ level is shown in Figure 24d. This contribution has a quartic dependence on N'. They also demonstrated that the mixing with a $\Pi(K'=1)$ level

was not negligible. It is caused by the b,c-axis Coriolis coupling which connects $\Delta v_2 = \pm 1$ and $\Delta v_n = \pm 1$ levels. The $(0,8^1,1)$ level couples with the $(0,9^0,0)$ level and the line width is given by

$$\Gamma_\Sigma = \frac{1}{2}(v_2+1)\frac{(\omega_3+\omega_2)^2}{\omega_2\omega_3}\zeta_{23}^2 B^2[N'(N'+1)]\frac{\Gamma_\Pi}{(E_\Sigma - E_\Pi)^2} \quad (52)$$

This contribution is shown in Figure 24c with a quadratic dependence on N'. Thus, the N'-dependent part of the observed width in the $K' = 0$ level was ascribed to these two effects. The residual N'-independent part was considered to be due to spin–orbit coupling with other high-lying levels of the X^2A' state.

Concerning the strong predissociation in the $K' \neq 0$ level, Dixon[272] studied the time-dependent wave-packet evolution and performed a model calculation for the predissociation through radiationless transitions between the Renner–Teller components X^2A' and A^2A''. The crossing probability was calculated assuming a $V(s) = {}^1/_2 f' s^2$ harmonic potential for the upper A'' surface and a negative force constant f'' for the lower A' state along the bending coordinate s. An empirical equation for the full width at half maximum was obtained as

$$\Delta\nu_{1/2} = -\left(\frac{\nu'}{\pi}\right)\ln[1 - {}^1/_2\{1 - \exp(-1.83K'^2 f/n^{3/2})\}] \quad (53)$$

where ν' is the bending vibrational frequency, $f = (f' - f'')/f'$, and $n = \langle\psi(0)|H|\psi(0)\rangle/\hbar\omega$ is equal to $v_2' + 1$ for a stationary state of an unperturbed harmonic oscillator. This equation shows that the predissociation rate increases drastically with K', and decreases slightly with v_2'.

For HCO and DCO cooled in a supersonic jet, Kable, Loison, Houston, and Burak[41,273] measured the PHOFEX spectrum, in which the wavelength of the first photolysis laser was scanned by monitoring the fluorescence intensity of the CO fragment excited by a second laser. The predissociation rate was determined from the rotational line width. Figure 25 shows the PHOFEX spectrum of HCO monitoring the transition intensity from the $CO(v''=0,J''\simeq 30)$ level. According to eq 53, predissociation should be slow and the rotational lines sharp for odd v_2' levels, whereas the predissociation should be fast and the spectrum diffuse for even v_2' levels. The observed PHOFEX spectra clearly show this alternation.[41] The N' dependence was weak and the averaged (Coriolis mediated) line widths versus v_2' for each K' (see Figure 26) reproduce the calculated widths of eq 53 with a fitting parameter $f = 5.0$.

The vibrational–rotational distribution of the nascent CO was determined from the intensity of the fluorescence excitation spectrum of the A–X transition, and was found to depend on v_2' of the parent HCO molecule.[41] The $CO(v''=0)$ yield was 83% for $A^2A''(0,v_2',0)$. The rotational quantum number J_p at the peak of the fluorescence yield increased with v_2': $J_p = 14$ for (0,6,0) and $J_p = 35$ for (0,16,0). The $(1,v_2',0)$ level with CH stretching excitation was observed to give a similar CO distribution with an 80% yield of $CO(v''=0)$, although J_p increased remarkably. In contrast, the (0,12,1) level with CO stretching excitation yielded more than 67% of $CO(v''=1)$, but nearly the same rotational distribution as for the (0,12,0) level was observed. *Ab initio* classical trajectory calculations could explain these results qualitatively.[274] However, Renner–Teller vibronic coupling calculations using a Hamiltonian model with a parity-adapted wave packet representation gave a hotter and narrower CO rotational distribution than the experimental result. This discrepancy was attributed to inadequacy of the calculated X^2A' potential energy surface.[275] Manaa and Yarkony[276,277] performed *ab initio* calculations of the potential surface by using a MCSCF/CI method, and predissociation of the B^2A' state of HCO was suggested.

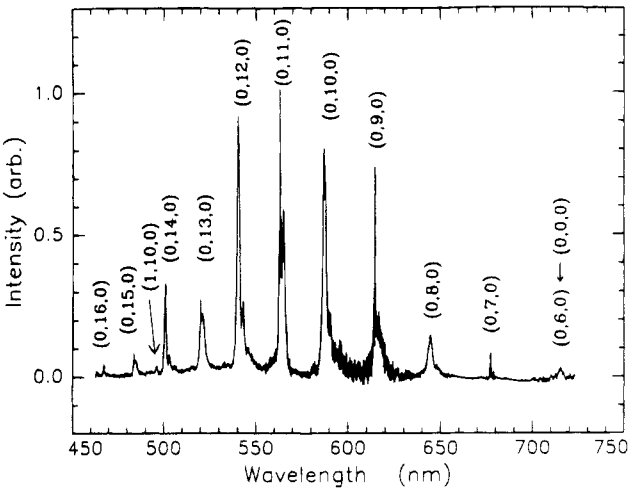

Figure 25. PHOFEX spectrum of jet-cooled HCO monitoring $CO(v''=0,J''\simeq 30)$. Assignments shown correspond to $A^2A''(v_1,v_2,v_3)$. All transitions originate from $X^2A'(0,0,0)$. (Reprinted from ref 41. Copyright 1991 American Institute of Physics.)

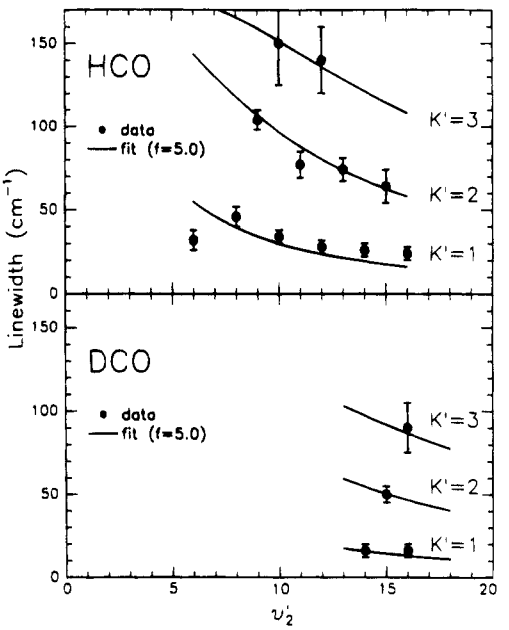

Figure 26. Observed line width $2\Gamma(v_2',K')$ plotted against v_2' for each value of K' for HCO and DCO. The solid lines are calculated using Dixon's model in eq 53. (Reprinted from ref 41. Copyright 1991 American Institute of Physics.)

2. HNO

For the HNO $A^1A''-X^1A'$ transition, line broadening was found in the absorption spectrum together with a sharp decrease in fluorescence yield.[278,279] Bancroft, Hollas, and Ramsay[279] reported that the rotational line width of the (1,0,1)−(0,0,0) band increased with increasing K'. In order to explain these experimental results, Dixon, Jones, Noble, and Carter[280] constructed the potential energy surfaces of the relevant A^1A'', a^3A'', and X^1A' states using spectroscopic data, thermochemical data, and quantum chemical calculations. The A^1A'' and X^1A' states correlate with the components of a $^1\Delta$ or a $^1\Pi$ state of linear HNO. They showed that these two states interacted by a-axis electron−rotation Coriolis coupling and that a radiationless transition was the main process of predissociation in the A^1A'' state

$$HNO(A^1A'') \rightarrow HNO(X^1A') \rightarrow H(^1S) + NO(^2\Pi) \quad (54)$$

Thus, predissociation is rotationally assisted by internal conversion to the ground-state continuum. The matrix element of the a-axis Coriolis interaction is proportional to K', which is consistent with the observed line widths. They also observed the fluorescence excitation spectrum and studied the J', K' dependence of the predissociation threshold energy. The energy of the fluorescence cutoff was found to increase with $J'(J' + 1)$. The drastic drop of the fluorescence intensity indicated that the dissociation to $H(^2S)$ + $NO(^2\Pi)$ occurred above the threshold energy. In diatomic molecules, the threshold energy should increase as J increases. Assuming that polyatomic molecules follow a similar case, they calculated the J dependence of the breaking-off point using a constructed potential surface of the X^1A' state. The calculated results were in good agreement with the experimental work.

Similar studies were performed for DNO[281,282] and supported the above predissociation mechanism. However, the energy shifts were difficult to predict, and the contribution of intersystem crossing through the spin−orbit coupling with the a^3A'' state is expected to be more significant in DNO.

3. H_2O

Predissociation of H_2O in the C^1B_1 state is suggested to occur through three different channels.[283,284]

$$H_2O(C^1B_1) \rightarrow OH(X^2\Pi) + H(^2S_g) \quad (I)$$

$$\rightarrow OH(A^2\Sigma^+) + H(^2S_g) \quad (II)$$

$$\rightarrow O(^1D_g) + H_2(^1\Sigma_g^+) \quad (III)$$

From the photofragment fluorescence excitation spectrum in which the $OH(A^2\Sigma^+ \rightarrow X^2\Pi)$ fluorescence intensity was monitored, Hodgson, Simons, Ashfold, Bayley, and Dixon[285,286] found that the predissociation channel II in the $C^1B_1(0,0,0)$ level was state selective. The total predissociation rate for a single rotational level, which was determined by the observed line width, was strongly K_a' dependent. The predissociation processes that were considered are as follows[286]

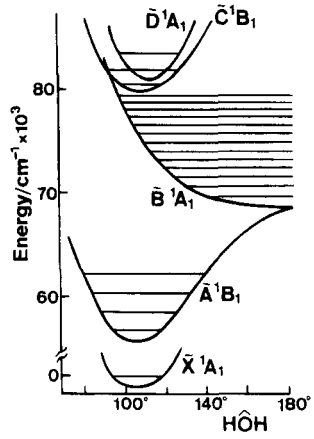

Figure 27. Schematic potential energy curves of H_2O plotted as a function of HOH bending angle. (Reprinted from ref 287. Copyright 1984 Elsevier.)

$$H_2O(C^1B_1) \rightarrow H_2O(B^1A_1) \quad \text{(heterogeneous)} \quad (55)$$

$$\rightarrow H_2O(^1B_1\text{-dark channel}) \quad \text{(homogeneous)} \quad (56)$$

$$H_2O(B^1A_1) \rightarrow OH(A^2\Sigma^+) + H(^2S_g) \quad (\phi) \quad (57)$$

$$\rightarrow OH(X^2\Pi) + H(^2S_g) \quad (1 - \phi) \quad (58)$$

The potential energy curves of H_2O as a function of bending angle are schematically shown in Figure 27. It has been found that the rate of the heterogeneous predissociation is proportional to $0.35K_a'^2/(1 + 0.35K_a'^2)$ for H_2O, and $0.22K_a'^2/(1 + 0.22K_a'^2)$ for D_2O. This rate is affected by the $C^1B_1 \rightarrow B^1A_1$ radiationless transition. These C^1B_1 and B^1A_1 states can couple by the a-axis electron−rotation Coriolis interaction. The probability of this coupling is expressed as[287]

$$\Gamma_{C\rightarrow B} \propto |\langle A_1;v'JK_a'|H_{Coriolis}|B_1;vJK_a\rangle|^2\rho(E) \quad (59)$$

$$\propto \bar{A}^2\langle A_1v'|B_1v\rangle^2K_a'^2\delta(K_a',K_a)\rho(E) \quad (60)$$

where $\rho(E)$ is the level density of the B^1A_1 state at an energy E, and $\bar{A}$ is a constant. Equation 60 indicates that the rate of heterogeneous predissociation is proportional to $K_a'^2$. Since K_a' is not a good quantum number for an asymmetric top molecule, the predissociation rate can be modified as $\propto cK_a'^2/(1 + cK_a'^2)$, which is in good agreement with the observed result. However, the $OH(A^2\Sigma^+)$ yield determined by the total fluorescence intensity of the OH A→X transition was very low for $K_a' \geq 2$ levels, and it was maximum for $K_a' = 2$ in D_2O. This decrease for high K_a' level was ascribed to the branching in the dissociation process of the H_2O B^1A_1 state.

The B^1A_1 state is one of the Renner−Teller components correlated with the linear $H_2O(^1\Pi)$ state. This state strongly couples with another A^1B_1 component, which is correlated with $OH(X^2\Pi)$ + $H(^2S)$ and produces ground state OH. As shown in eq 58, the crossing probability $(1 - \phi)$ increases as K_a' increases. Consequently, the quantity ϕ in eq 57 which gives the probability of $OH(A^2\Sigma^+)$ production

rapidly decreases with increasing K'_a. As a result of the heterogeneous perturbation between the C^1B_1 and B^1A_1 states and the transition to the A^1B_1 state, the branching ratio for $OH(A^2\Sigma^+)$ will have a maximum at a certain value of K'_a. Thus, the K'_a-selective predissociation of $H_2O(C^1B_1)$ is explained by both Coriolis and Renner–Teller couplings.

The nascent distribution of the $OH(A^2\Sigma^+)$ state was determined from the intensity of the dispersed fluorescence spectrum of the A→X transition.[286] The rotational distribution of $OH(N'' = 10-20)$ was found to be almost the same as that of the direct excitation to the B^1A_1 continuum of H_2O, and no considerable $J'_{K_a'K_c'}$ dependence was observed by monitoring the OH fragments.

Multiphoton ionization (MPI) has been shown to be useful for studying predissociation quantitatively.[287,288] Kuge and Kleinermanns[289] applied the MPI technique to study molecules in a molecular beam in order to measure line widths. Although the K'_a dependence was almost identical with the above-mentioned work, the J'-dependent weak c-axis Coriolis interaction and the K'_a-independent homogeneous predissociation were also observed.

4. HCN

The diffuseness in the VUV region of the absorption spectrum of HCN and DCN is attributed to fast predissociation.[290] By analyzing the line width, the predissociation rate was found to depend strongly on K'_a in the A^1A'' state. Hsu, Smith, and Wallace[291] measured the line widths of rotationally resolved transitions to the $A^1A''(0,v'_2,0)$ state by the technique of four-wave difference–frequency mixing. The predissociation rate was found to be almost independent of J' and to increase with K'_a. This strong K'_a dependence was explained by the a-axis Coriolis interaction with the X^1A' state. The lifetime of the zero-point level was extremely short, and an excitation of the bending quanta suppressed the predissociation strongly. Further, the $A^1A''\rightarrow X^1A'$ fluorescence intensity decreased drastically when the vibrational energy became greater than 2200 cm^{-1}. On the basis of theoretical calculations,[292] the main process of predissociation below the threshold energy is estimated to be

$$HCN(A^1A'') \rightarrow H + CN(X^2\Sigma^+) \qquad (61)$$

A new process

$$HCN(A^1A'') \rightarrow H + CN(A^2\Pi_i) \qquad (62)$$

is believed to occur above the threshold where the fluorescence intenstiy becomes weak.

In contrast, the K'_a dependence of the line width of DCN was found to be small above the energy threshold.[293] This is thought to be due to the contribution of J',K'_a-independent homogeneous predissociation by vibronic coupling with the higher $2^1A''$ state.

Predissociation in the C^1A' state of HCN was extensively studied by detecting the fluorescence from the product $CN(B^2\Sigma^+)$. The vibrational and rotational distributions of $CN(B^2\Sigma^+)$ were found to depend on the wavelength of the exciting light.[294–296] MacPherson and Simons[297] observed the fluorescence excitation spectrum, and determined the relative quantum yield for $CN(B^2\Sigma^+)$ production from single vibronic levels in the C^1A' state. The predissociation quantum yield in the $(0,v'_2,0)$ levels (v_2 is the vibrational quantum number of the bending mode) were almost identical for both HCN and DCN. However, a very large isotope effect was found for molecules vibrationally excited via the C–H stretching mode ($v'_1 > 0$). The $(1,v'_2,0)$ progression was missing in the HCO spectrum, and it suggests of a fast predissociation. The quantum yields in the $(0,v'_2,0)$ and $(1,v'_2,0)$ levels of DCN showed a similar dependence. This isotope effect was explained by quantum mechanical tunneling and the observed predissociation rates were well reproduced by the calculated Franck–Condon factors. Predissociation accelerated by excitation of the bending mode was also suggested to compete with the tunneling mechanism.

5. SO_2

Kanamori, Butler, Kawaguchi, Yamada, and Hirota[298] excited the C^1B_2 state of SO_2 at 193 nm and measured the spin, rotational, and vibrational distributions of the product SO. Although several rotational and vibrational levels were excited simultaneously, the predissociation was thought to occur through the repulsive $^3A_1$ state correlated with $SO(X^3\Sigma^-) + O(^3P)$. Ebata, Nakazawa, and Ito[299] excited SO_2 in a supersonic jet with narrow band laser light ($\Delta E \approx 0.2$ cm^{-1}) and observed the fluorescence excitation spectrum, in which the rotational levels were partly resolved. From the observed lifetimes and the comparison of intensities of fluorescence excitation and absorption spectra, the predissociation rate was found to depend on both J' and v'. A sharp decrease in fluorescence intensity was found at 45 400 cm^{-1} and was attributed to the onset of the predissociation channel. For the $C^1B_2(3,0,0)$ state just below the threshold, the predissociation rate was large for the high J' levels. Spin–orbit coupling between the C^1B_2 and the $^3A_1$ states was estimated to induce the predissociation. A very slow predissociation was observed for the Q transition to the $J' = K'$ level. This fact strongly supports the spin–orbit mechanism. The matrix elements for the singlet–triplet interaction were derived by Stevens and Brand:[300]

$$\Delta N = +1 \qquad \frac{(J \pm K + 2)(J \pm K + 1)}{4(J + 1)(2J + 1)} |\langle {}^{ev}\Gamma_S | H_{SO} | {}^{ev}\Gamma_T \rangle|^2 \qquad (63)$$

$$\Delta N = 0 \qquad \frac{(J \mp K)(J \pm K + 1)}{4J(J + 1)} |\langle {}^{ev}\Gamma_S | H_{SO} | {}^{ev}\Gamma_T \rangle|^2 \qquad (64)$$

$$\Delta N = -1 \qquad \frac{(J \mp K - 1)(J \mp K)}{4J(2J + 1)} |\langle {}^{ev}\Gamma_S | H_{SO} | {}^{ev}\Gamma_T \rangle|^2 \qquad (65)$$

where $N = J - S$. Ebata, Nakazawa, and Ito[299] also found that the ν_3 antisymmetric stretching mode enhanced the predissociation. This mode selectively was first suggested by Vasudev and McClain.[301]

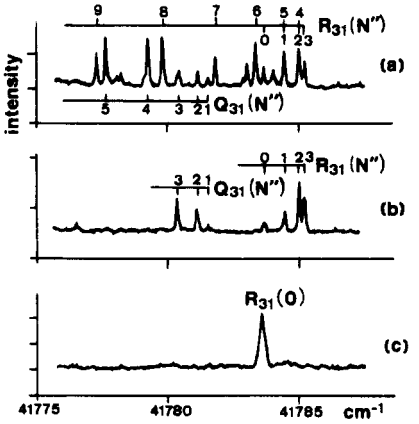

Figure 28. One-photon ionization excitation spectrum of the $A^3\Pi_2-X^3\Sigma^-$ (9−0) band of SO after excitation of the C−X(142)−(000) band of SO_2 (a) at 219 nm, (b) via the $8_{35}-7_{35}$, and (c) via the $6_{25}-5_{24}$ transition. (Reprinted from ref 302. Copyright 1993 Elsevier.)

Becker, Braatz, Lindner, and Tiemann[302] studied the predissociation of the $C^1B_2(1,4,2)$ state via the reaction

$$SO_2(C^1B_2;v_1',v_2',v_3',J'_{K_a'K_c'}) \rightarrow SO(X^3\Sigma^-,v''=0,J'',N'') + O(^3P) \quad (66)$$

The first photolysis laser with a line width of 0.06 cm^{-1} excited a single rotational line, and the distribution of $SO(X^3\Sigma^-,v''=0,J'',N'')$ levels was determined from the intensity of the one-photon ionization of SO by the second probe laser. The 1 + 1 MPI excitation spectra with the excitation (a) at 219 nm, (b) via the $8_{35}-7_{35}$, and (c) via the $6_{25}-5_{24}$ transitions of the C(1,4,2)−X(0,0,0) band are shown in Figure 28. The excitation to the 8_{35} level produced SO in the $N'' = 0-3$ state, but only the $N'' = 0$ state was produced when the 6_{25} level was excited. No predissociation was observed from the $C^1B_2(J' \leq 5)$ levels. When the $C^1B_2(1,4,2)$ state was excited, the product state distribution depended strongly on $J'_{Ka'Kc'}$. This suggests the existence of another dissociation channel than the spin−orbit coupling with the $^3A_1$ state. The curve crossing point with a repulsive $^1B_2$ state was estimated to be the threshold of this predissociation.

B. NH_3, C_2H_2

1. NH_3

Strong predissociation in the A^1A_2'' state of NH_3 was found by examining the diffuse absorption spectrum.[303] Douglas[304] analyzed the spectrum and showed that the NH_3 molecule is pyramidal (C_{3v}) in the ground state, and is planar (D_{3h}) in the A^1A_2'' state. Progression bands due to the out-of-plane bending mode ν_2 (the umbrella motion) are predominant in the absorption spectrum. The predissociation was found to be slower in $v_2' = 1$ than in $v_2' = 0$, and the rate increased again with v_2' for $v_2' \geq 2$. The predissociation was much slower in ND_3 than in NH_3. These facts were explained by the tunneling effect. McCarthy, Rosmus, Werner, Botschwina, and Vaida[305] performed *ab initio* calculations of the potential energy surface. The potential curve corresponding to the reaction

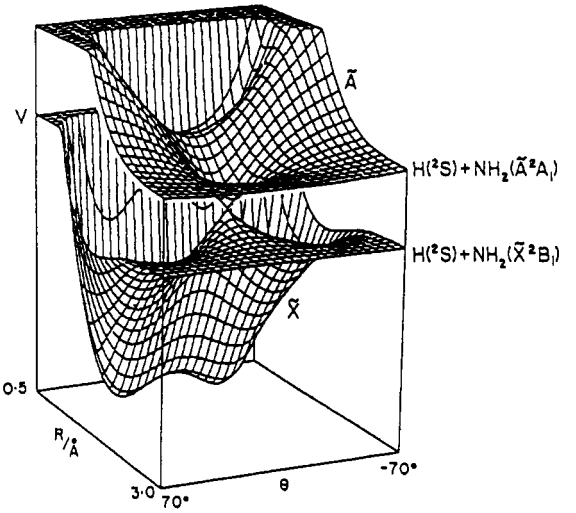

Figure 29. The dependence of the potential functions for the A and X states of NH_3 on $R(H-NH_2)$ and the out-of-plane angle θ. The mesh intervals are 0.1 Å and 5°, respectively. (Reprinted from ref 311. Copyright 1989 American Institute of Physics.)

$$NH_3\,(A^1A_2'') \rightarrow H(^2S) + NH_2(X^2B_1) \quad (67)$$

was found to cross that of

$$NH_3\,(X^1A_1') \rightarrow H(^2S) + NH_2(A^2A_1) \quad (68)$$

The A^1A_2'' state, which has a bound 3s Rydberg character, correlates with a repulsive potential which has a very low barrier. From this, there exists a conical intersection as illustrated in Figure 29.

Ashfold, Bennett, and Dixon[306] analyzed the line width of the two-photon fluorescence excitation spectrum of ND_3. They found that the predissociation rate could be described as

$$\Gamma \propto \Gamma_0\{1 + x'[J(J+1) - 0.62K^2]\} \quad (69)$$

for the slow predissociation level 2^1, in which v_2' equals 1 and other vibrational quantum numbers are zero. x' is a constant which depends on the vibrational level. These experimental results were well explained by a model calculation.[307] The relatively slow predissociation in the $v_2' = 1$ level was attributed to a high dissociation barrier. This effect is expected to become constant as the vibrational energy increases. However, the observed rate was rather fast for $v_2' \geq 2$ levels. This discrepancy was ascribed to vibrational nonadiabaticity for $v_2' \geq 2$. For example, the 2^n level can mix with 1^12^{n-1} by anharmonic coupling. This in turn promotes the N−H stretching mode (ν_1) and enhances the predissociation. The interaction between the bound and repulsive states was estimated to occur through centrifugal assistance and Coriolis coupling. Both of these effects give the same dependence on J' and K':

$$\Gamma(J,K) \propto \Gamma_0 \exp\{\gamma_b[J(J+1) - K^2] + \gamma_c K^2\} \quad (70)$$

where γ_b and γ_c are constants. This is approximately consistent with the experimental result of eq 69. The predissociation rate and the product state distribu-

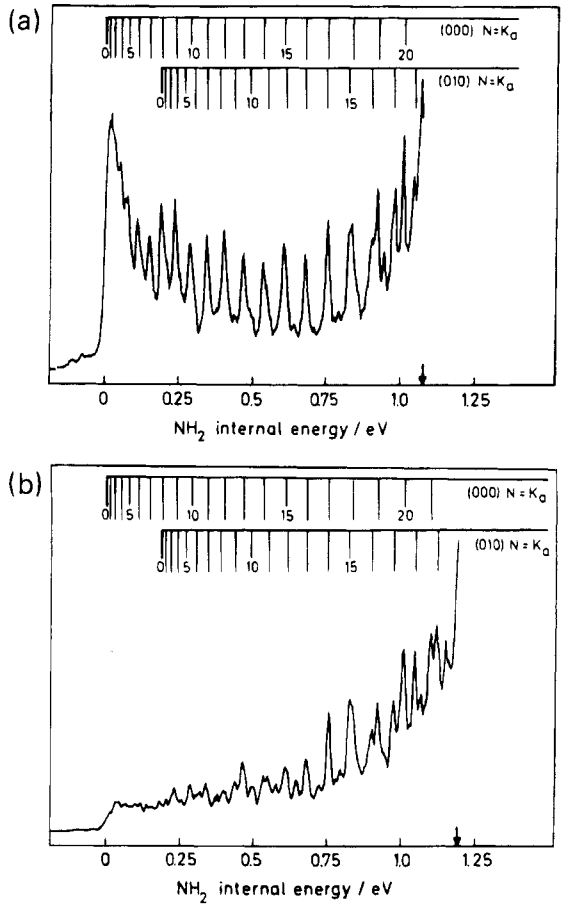

Figure 30. NH_2 internal energy spectra resulting from photolysis of jet-cooled NH_3 at (a) 46200 cm^{-1} (A–X 0_0^0 band) and (b) 47080 cm^{-1} (A–X 2_0^1 band). Indicated above the spectra are the energies of the different $N'' = K''_a$ levels of the (000) and (010) levels of NH_2 (X); indicated also on each spectrum is the energy corresponding to the maximum available [i.e., $h\nu - D_0^0(H-NH_2)$]. (Reprinted from ref 310. Copyright 1988 American Institute of Physics.)

tion were calculated, and a reasonable coincidence with the observed J', K' dependence were obtained.[307]

Endo, Iida, and Ohshima[308] measured the line widths of the rotational lines for the $v' = 0$ level by microwave-optical double resonance. They found a weak K' dependence:

$$\Gamma(J',K') \propto \Gamma_0\{1 + 0.00437J'(J' + 1) - 0.00058K'^2\} \quad (71)$$

Ashfold and Dixon[309] demonstrated that this observation was consistent with the model presented by Dixon.[307] In the $v' = 0$ level, Coriolis coupling was found to be important and the predissociation rate was less dependent on K'.[307]

Biesner, Schnieder, Schmeer, Ahlers, Xie, Welge, Ashfold, and Dixon[310] measured the state distribution of H atoms by using photofragment translational spectroscopy. Fine structure was observed in the time-of-flight spectrum of H atoms produced by the predissociation from the vibronic level of the NH_3 A^1A'' state. The flight time was transformed into the NH_2 internal energy as shown in Figure 30. The rotational lines were not resolved due to broadening by rapid dissociation, and the wavelength of the exciting laser was tuned to the center of the vibrational band of $v_2' = 0$ (Figure 30a) and $v_2' = 1$ (Figure 30b). The sharp peaks showed that NH_2 was populated specifically in the $N'' = K''_a$ level of the ground state with the maximum possible angular momentum about the a internal axis (in-plane, parallel to HNH). This indicates that the rotational excitation in NH_2 is induced by the acceleration of the out-of-plane motion in the vicinity of the conical intersection. The rotational energy of NH_2 was much higher for the excitation to the $v_2' = 1$ level of the parent NH_3 molecule than for the $v_2' = 0$ level, where an inverted distribution of the rotational levels was observed. This difference between $v_2' = 0$ and 1 was explained by the shape of the vibrational wave function. For $v_2' = 1$, the wave function of the bending mode has a node in the molecular plane. This reduces the rate of planar dissociation which produces the NH_2 fragment with little rotational excitation.

The dependence of the product state distribution on the rotational level of the parent molecule was observed for ND_3,[311] where rotational lines were resolved in the excitation because of the slow predissociation. When levels with large values of $J(J + 1) - K^2$ in the parent ND_3 molecule were excited, the rotational energy of the product ND_2 was observed to be relatively small. This rotational dependence was also explained by the same mechanism as in NH_3. The out-of-plane moment $\langle J_\perp^2 \rangle$ of ND_3 which is proportional to $J(J + 1) - K^2$ has a centrifugal contribution to the effective radial potential and consequently gives increased kinetic energy. Since it introduces a bias in favor of the more direct near-planar dissociation, the rotational excitation is suppressed for levels of large values of $J(J + 1) - K^2$.

2. C_2H_2

By probing photolysis[312] and measuring fragment translational energies,[313] the primary predissociation process of C_2H_2 in the vacuum UV region was shown to be

$$C_2H_2 \rightarrow C_2H + H \quad (72)$$

From the analysis of the absorption spectrum,[314,315] C_2H_2 was found to be linear in the ground state, and *trans*-bent in the A^1A_u state. Fujii, Haijima, and Ito[316,317] found that the fluorescence excitation spectrum of the transition to the A^1A_u state was dominated by progression bands of $V_0^nK_0^1$ ($n = 0-3$), where the mode V is the *trans*-bending vibration. The fluorescence intensity abruptly decreases at wavelengths shorter than the $V_0^4K_0^1$ band at 215.970 nm. By comparing the intensity of the absorption spectrum with that of the fluorescence excitation spectrum, the rotational dependence of the predissociation yield was found to differ above and below the threshold. In the $V_0^4K_0^1$ band just below the threshold, the predissociation yield increased proportionally to $J'(J' + 1)$, but changed irregularly in the $V_0^5K_0^1$ band above the threshold. From this, it was concluded that the predissociation in the A^1A_u state of C_2H_2 was due to tunneling in which the barrier top corresponds to the predissociation threshold. The

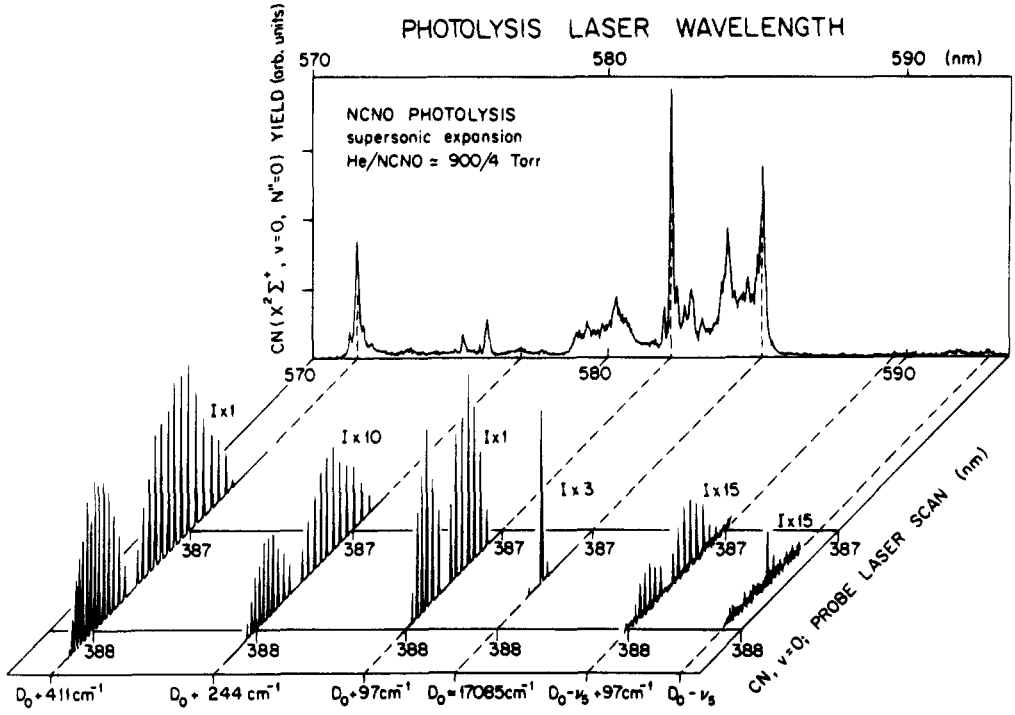

Figure 31. CN LIF spectra at different photolysis wavelengths (570–585 nm), following the photodissociation of expansion-cooled NCNO. The spectrum in the rear is obtained by monitoring $CN(X^2\Sigma^+,v''=0,N''=0)$ as the photolysis wavelength is varied. The individual CN LIF spectra, at specific photolysis wavelength, are displayed perpendicular to the horizontal axis. (Reprinted from ref 321. Copyright 1985 American Institute of Physics.)

$J'(J'+1)$ dependence below the threshold was explained by rotational interaction. It is also expected that there is no J' dependence above the threshold. These explanations are consistent with the observed rotational dependence. Although the origin of the irregularity in $V_0^5K_0^1$ is not clear, it may be attributed to accidental perturbation with another excited state such as a spin–orbit interaction with a triplet state. Haijima, Fujii, and Ito[317] performed similar experiments on C_2D_2. The threshold energies was found to be shifted by the difference in the zero-point energy, which supports the tunneling mechanism.

Osamura, Mitsuhashi, and Iwata[318] carried out *ab initio* calculations of the potential curves of C_2H_2 using the MCSCF method. They found a *cis*-bent state below the threshold and pointed out that *trans–cis* isomerization can occur before the dissociation in the A^1A_u state. Detailed product analysis will be necessary to elucidate the overall predissociation process in the C_2H_2 molecule.

C. Nitroso Molecules

Strong predissociation can occur in the S_1 state of nitroso molecules, which are induced by an internal conversion to the ground state. A prototype molecule for this type of predissociation is HNO. In this section we extend the discussion to other nitroso molecules, NCNO, CF_3NO, and $(CH_3)_3CNO$.

1. NCNO

The absorption band of the A^1A''–X^1A' transition of NCNO extends throughout the visible region.[319] Nadler, Reisler, Noble, and Wittig[320,321] observed the fluorescence excitation spectrum in a supersonic jet and found a clear cutoff of the fluorescence intensity at 583.3 nm. They also measured the PHOFEX spectrum, and some vibronic structure was observed at wavelengths above the threshold. The decrease in fluorescence was attributed to the predissociation

$$NCNO(A^1A'') \rightarrow CN(X^2\Sigma^+) + NO(X^2\Pi_i) \quad (73)$$

The PHOFEX spectrum of NCNO in a supersonic jet near the dissociation threshold is shown in Figure 31, where the fluorescence excitation spectrum of the $CN(B^2\Sigma^+–X^2\Sigma^+)$ transition was measured. Although the vibrational structure was analyzed near the origin level,[322] the vibrational quantum numbers are not assigned near the predissociation threshold of 5750 cm^{-1}. The rotation of CN was excited slightly by the excitation of NCNO at the predissociation threshold. The average rotational energy of CN was found to increase as the excess energy increased (see Figure 31). The production of CN for $v'' = 1$ and 2 was found to occur at their threshold energies. The fluorescence excitation spectrum of the $NO(A^2\Sigma^+–X^2\Pi)$ transition was observed by Qian, Noble, Nadler, Reisler, and Wittig,[323] and the rotational distribution of the $NO(X^2\Pi)$ fragment was nearly the same as for CN. For NO formed in the reaction, the spin–orbital states ($^2\Pi_{1/2}$ and $^2\Pi_{3/2}$) were almost equally populated. From these experimental results, it is concluded that the predissociation occurred following internal conversion to the ground state. The rotational distribution of the fragments was in good agreement with phase space theory calculations,[324,325] where the excess energy was assumed to be partitioned statistically among every internal degree of freedom.

As indicated by the level shifts near the origin of the A^1A'' state, the A^1A'' and X^1A' states must be vibronically coupled Renner–Teller components.[322]

Because the level density increases rapidly as the energy increases, the radiationless transition becomes faster in high vibrational levels. The top of the high barrier in the ground state is the threshold position of the predissociation. Above it, the excited NCNO molecule undergoes fast internal conversion to the ground state, and dissociates via a loose transition state. The products were found to have a statistical thermal distribution. Calculations of the unimolecular reaction based on the phase space theory could reproduce the observed distribution qualitatively. However, for high excess energy where $CN(^2\Sigma^+,v''=1)$ was produced, a modified phase space theory (SSE) provided quantitatively better fits.[326] This mechanism was confirmed by the Doppler profile of the rotational lines of CN.[327] The observed profiles were fit well by the SSE method, and the translational distribution of the CN fragment was found to be statistical and isotropic.

Khundkar, Knee, and Zewail[328] obtained the absolute reaction rate of the predissociation for several vibronic levels by observing the real-time appearance of the CN product using the technique of picosecond time-resolved spectroscopy. The results could be explained by the phase space theory. However, the calculated absolute rate and the relative yield obtained by the PHOFEX spectrum were not exactly in agreement because they depend on global and local features of the potential energy surface.

2. CF_3NO

DeKoven, Fung, Levy, Hoffland, and Spears[329] measured the excitation spectrum of the $A^1A''-X^1A'$ transition of CF_3NO in a supersonic jet, and observed well-resolved vibronic structure. From the vibrational analysis, CF_3NO was determined to be eclipsed in the ground state and staggered in the S_1 state. The torsional mode ν_{12}, the CF_3 rocking mode ν_8, and the skeletal bending mode ν_7 were prominent in the spectrum. Spears and Hoffland[330] found a breaking-off and diffuseness in the fluorescence excitation spectrum, and measured the lifetime of each vibronic level. The predissociation

$$CF_3NO\ (A^1A'') \rightarrow CF_3 + NO(X^2\Pi_i) \qquad (74)$$

was estimated to occur through A → X internal conversion. Bower, Jones, and Houston[331] observed the PHOFEX spectrum by monitoring the $NO(A^2\Sigma^+-X^2\Pi_i)$ transition intensity. Dyet, McCoustra, and Pfab[332] reinvestigated the lifetime, predissociation yield, and the state distribution of the NO fragments for several vibronic levels. By comparing the intensities of fluorescence excitation and PHOFEX spectra, the NO yield was found to be dramatically enhanced when CF_3NO was vibrationally excited via ν_7, ν_8, and combinations of the two modes. The CF_3 rocking and the skeletal bending were found to promote the predissociation in the A^1A'' state of CF_3NO. The main product was $NO(X^2\Pi_i;v''=0)$ and the production of vibrationally excited $NO(v''=1)$ was small (<1%). The rotational distribution was statistical, and the rotational energy increased as the excess energy increased. These results were interpreted by a predissociation mechanism where the A^1A'' state of CF_3NO is coupled with the X^1A' state, and the dissociation occurs through A → X internal conversion.

The observed decay was found to be biexponential for high vibrational levels of the A^1A'' state. This suggests that the a^3A'' state is considerably mixed with the A^1A'' state by spin–orbit interaction. The a^3A'' state is not well studied, although its location is well known to be about 6270 cm^{-1} above the ground state in HNO.[333] The vibrational level density was estimated to be $1 \times 10^5/cm^{-1}$ for X^1A', and $600/cm^{-1}$ for a^3A'' at the energy of the A^1A'' origin level. The internal conversion was estimated to be favorable in the lower energy region. For high vibrational levels, the level density of the a^3A'' state increases significantly. Therefore, the intersystem crossing becomes significant and the decay becomes biexponential. In both mechanisms, the ν_7 or ν_8 mode excitation was estimated to increase the Franck–Condon overlap and, hence, to enhance the mixing of the A and X states. Similar results were observed for $CClF_2NO$[334] and CCl_2FNO.[335] The contribution of the a^3A'' state was found to be more important for CCl_2FNO predissociation.

3. $(CH_3)_3CNO$ (t-BuNO)

The appearance time of the NO fragment after the excitation of $(CH_3)_3CNO$ was observed to be very fast (less than 10 ns).[336] Noble, Qian, Reisler, and Wittig[337,338] observed the fluorescence excitation spectrum and the PHOFEX spectrum by monitoring NO fragments in a supersonic jet. The *t*-Bu torsion and the CNO bending were found to be prominent in the fluorescence excitation spectrum of the parent $(CH_3)_3CNO$ molecule. Above the intensity break-off point at 689 nm, NO was found to be generated with a rise time less than 60 ns. In contrast, the NO production was much slower ($\approx$3.2 μs) for longer wavelength below the threshold. This indicates that two different channels exist for the predissociation of $(CH_3)_3CNO$. The slow channel is attributed to the dissociation in the ground state after internal conversion. The fast component is considered to be caused by intersystem crossing to the a^3A'' state. This contribution is expected to become more important in the high-energy region because the vibrational state density increases strongly with the excess energy.

From the analogy of HNO, the a^3A'' state is expected to have a barrier to dissociation. The maximum point corresponds to the fluorescence break-off point. In the long wavelength region where the slow channel was predominant, the rotational population of the NO fragments had a statistical distribution and the averaged appearance time was 3.7 μs. The level density of the ground state was estimated to be extremely high in the A^1A'' state region ($\sim 10^{12}/cm^{-1}$). As a result, the intramolecular vibrational redistribution became fast, and caused the dissociation rate to become slow. Calculations based on the RRKM theory[336] predict the dissociation time to be on the order of microseconds, which agrees well with the observed appearance time. However, the appearance curve was observed to be biexponential above the fluorescence break-off point. The level density of the a^3A'' state was estimated to be $\approx 10^8/$

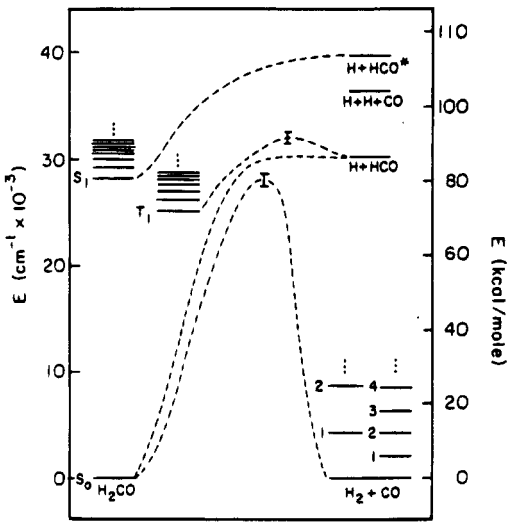

Figure 32. Energy level diagram for H_2CO. The dashed lines show the correlations between bound states and continua. (Reprinted from ref 353. Copyright 1976 American Institute of Physics.)

cm^{-1}, which corresponds to a predissociation rate $\approx 10^8$ s^{-1}. The biexponential rise was attributed to the subsequent a → X radiationless decay.

D. Carbonyl Molecules

The molecular conformation of carbonyl molecules is drastically changed by the $n \rightarrow \pi^*$ excitation, so that the Franck–Condon envelope of the transition shifts and the high vibronic levels can be excited. The vibrational mode selectivity in predissociation of the $^1(n\pi^*)$ state has been the subject of extensive studies.

1. H_2CO

Formaldehyde H_2CO was found to dissociate and yield various products when irradiated with UV light.[339] The photochemistry has been extensively investigated concerning interstellar chemistry or isotope enrichment.[340] Two predissociation paths in the S_1 state have been reported:

$$H_2CO\ (S_1{}^1A_2) \rightarrow H_2 + CO \qquad (I)$$

$$\rightarrow HCO + H \qquad (II)$$

I and II are called the "molecular mechanism" and "radical mechanism", respectively. From the study of molecular-beam time-of-flight photofragment spectroscopy, it was shown that both processes occurred via the ground state under collision-free conditions.[341] It was also shown that 65% of the available energy was transferred to the translational energy of fragments in I, while the translational energy of HCO in II was small. An interpretation of this energy partitioning was shown by Figure 32, which was constructed based on the results of *ab initio* calculations of the potential energy surfaces of H_2CO.[342–347] There is a high barrier to dissociation in the molecular mechanism I, which induces a large product translational energy. In contrast, there is no barrier in the radical mechanism II. These two processes compete when the excitation energy is greater than 32 000 cm^{-1} and high vibrational levels are excited.

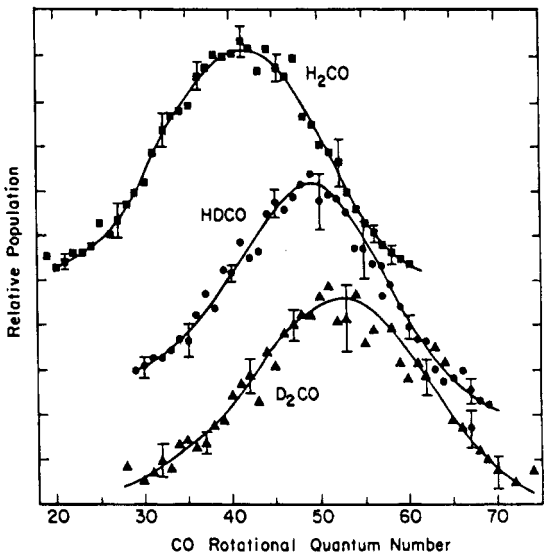

Figure 33. Effect of isotope substitution on the CO(v''=0) rotational distribution. The top trace is from H_2CO photolysis at ~29 490 cm^{-1}. The middle trace is HDCO photolysis at ~29 515 cm^{-1}. The bottom trace is D_2CO photolysis at ~29 545 cm^{-1}. The middle and top traces have been displayed by two and five vertical units, respectively, from the bottom trace. (Reprinted from ref 352. Copyright 1985 American Institute of Physics.)

The decay rates of vibronic levels in the S_1 state were observed to depend strongly on J' and K'.[348–350] Henke, Selzle, Hays, Schlag, and Lin[351] explained this effect by Coriolis coupling and the vibration–rotation coupling due to the centrifugal distortion. These two contributions were observed to depend on the vibrational state. The rate was found to increase remarkably with K'_a in the 4_0^1 level, where ν_4 is the C=O out-of-plane bending. Bamford, Filseth, Foltz, Hepburn, and Moore[352] observed the PHOFEX spectrum by monitoring the CO population. The predissociation rate for the molecular mechanism I was shown to be approximately the same as the decay rate, although it included minor contributions of the radiationless decay. The state distribution of CO was determined by measuring the excitation spectrum of CO. Figure 33 shows the rotational distribution of the nascent CO fragments ($X^2\Sigma^+$,v''=0) at the excitation of the $2^1 4^1$ band of H_2CO, HDCO, and D_2CO, where ν_2 is the C–H stretching. In H_2CO, the distribution was found to have the maximum at J'' = 40. This was considerably different from that calculated assuming statistical energy partitioning.[352] The J'' value at the peak was observed to increase with deuterium substitution. Houston and Moore[353] studied this mapping of the CO vibrational energy. The main product was CO($X^1\Sigma^+$,v''=0) and the distribution was almost independent of the vibrational mode excited. The population of CO($v''\neq 0$) increased gradually with the excess energy. If the excess energy were statistically partitioned among all internal degrees of freedom and relative translational energy, the vibrational energy of CO was estimated to be 14% of the excess energy. However, it was only 0.7% in the 4_0^3 level. This indicates that the predissociation path I is not statistical. Since these results show that the energy randomization does not effectively occur during the dissociation, the H_2 fragment is expected to be internally excited. By using

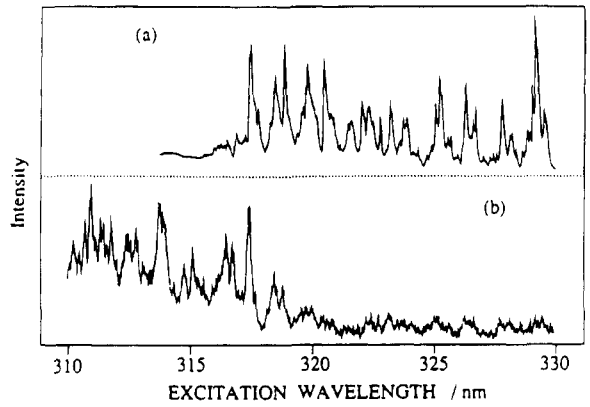

Figure 34. Fluorescence excitation spectrum of CH_3CHO (a) and PHOFEX spectrum of CH_3CHO obtained by monitoring $^QP_0(5)$ of the B(0,0,2) ← X(0,0,0) transition of HCO (b). (Reprinted from ref 363. Copyright 1993 Elsevier.)

the technique of coherent anti-Stokes Raman scattering (CARS), Debarre, Lefebvre, Pealat, Taran, Bamford, and Moore[354] measured the vibrational and rotational distribution of the nascent H_2 fragments for the excitation to the 2^14^1 level. The fractions of partitioned energy were determined to be 4% for translation, 13% for rotation, and 1% for vibration in CO, and 61%, 5%, and 16%, respectively, in H_2.[341,353,354]

Apel and Lee[355] studied the dependence of nonradiative decays on the vibronic level of the H_2CO $S_1{}^1A_2$ state for low J' levels. The fluorescence lifetimes of the 2^n4^1 and 2^n4^3 levels were found to be noticeably shorter than others. They concluded that the radiationless decay was mode-selective and that the out-of-plane bending was the promoting mode. This observed S_1 vibrational mode selectivity was consistent with the mode specificity in the unimolecular dissociation of the S_0 state obtained by theoretical calculations.[356,357] Weisshaar and Moore[358] found that the fluorescence decays of single rotational levels in 4^1 were changed irregularly by an electric field. The effect of an external magnetic field was found in D_2CO by Orita, Morita, and Nagakura,[359,360] and they suggested that the triplet state was involved with the predissociation.

2. CH_3CHO

Three dissociation channels are involved in the photolysis of acetaldehyde:[361]

$$CH_3CHO \rightarrow HCO + CH_3 \quad (I)$$

$$\rightarrow H + CH_3CO \quad (II)$$

$$\rightarrow CO + CH_4 \quad (III)$$

A fluorescence cutoff was observed at 317.5 nm in a supersonic jet.[362] Kono, Takayanagi, Nishiya, and Hanazaki[363,364] observed the PHOFEX spectrum by detecting HCO fragments. Figure 34 shows the fluorescence excitation spectrum of CH_3CHO and the PHOFEX spectrum monitoring the B(002)–X(000) $^QP_0(5)$ transition of HCO. Many vibronic bands were observed with an unresolved rotational envelope. The predissociation was found to begin at 320.5 nm and the fluorescence yield was found to decrease drastically at 317.5 nm. The rotational distribution of the HCO fragment was approximately the same for several vibronic bands above the threshold. The averaged value of the rotational energy was about 6.2 kJ mol^{-1} and the rotational temperature was about 500 K. They concluded that channel I occurred via the $T_1{}^3(n\pi^*)$ state. The excited molecule in the S_1 state is transferred to the T_1 state by intersystem crossing. The CH_3CHO molecule is pyramidal in both of the S_1 and T_1 states, and spin–orbit interaction is appreciable. The T_1 state was estimated to have a barrier to dissociation, and the top of this barrier coincides with the predissociation onset. The rotational excitation in the HCO fragment was attributed to the torque imparted to the fragments when the system moved on the exit potential surface. By a simple impulsive model, they calculated the rotational energy to be 5.8 kJ mol^{-1}. The results were in good agreement with the experimental results.

3. Cyclobutanone

In 1942, Benson and Kistiakowsky[365] studied the photochemistry of the excited cyclobutanone molecule and showed that it decomposes by two primary processes

$$\text{cyclobutanone} \rightarrow CH_2CO + C_2H_4 \quad (I)$$

$$\rightarrow c\text{-}C_3H_6 + CO \quad (II)$$

Lee, Denschlag, and Lee[366–368] analyzed the products of the photodecomposition of cyclobutanone in the $S_1{}^1(n\pi^*)$ state. They concluded that the path I occurred via internal conversion to the ground electronic state, but the path II occurred via the intersystem crossing to a triplet state.

The fluorescence quantum yield was measured[369,370] and was shown to decline suddenly at 319 nm (1200 cm^{-1} above the origin level). Tang and Lee[371] obtained the product ratio of the paths II and I, C_{II}/C_I, for a number of single vibronic levels in the S_1 state. The main path near the origin level was found to be the path II with a value of C_{II}/C_I equal to 7.0. The ratio decreased gradually at an excess energy greater than 700 cm^{-1}, which was identified to be the onset of the predissociation in the S_1 state of cyclobutanone. At the excess energy of more than 1500 cm^{-1}, the C_{II}/C_I ratio was less than 0.5. The branching ratio still depended on the excess energy. However, no appreciable vibrational mode selectivity was observed. The decrease of the C_{II}/C_I ratio with the excess energy was attributed to the increase of the $S_1 \rightarrow S_0$ internal conversion.

4. CHOCHO

By exciting a single rotational level in the $S_1{}^1A_u(n\pi^*)$ state of glyoxal, Loge and Parmenter[372] investigated CO and H_2 formation. The predissociation yield was almost independent of the rotational quantum number J' and K'. Hepburn, Buss, Butler, and Lee[373] confirmed this result under collision free conditions. Osamura, Schaefer, Dupuis, and Lester[374] carried out *ab initio* calculations, and two primary processes

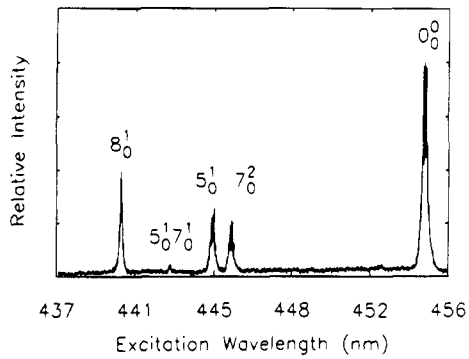

Figure 35. Fluorescence excitation spectrum of CHOCHO unnormalized for variations in the dye laser intensity. The normal modes are as follows: ν_8, C−H wagging; ν_5, C−C=O wagging; ν_7, torsion. (Reprinted from ref 375. Copyright 1987 American Institute of Physics.)

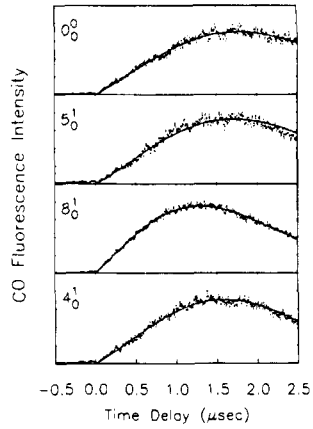

Figure 36. CO laser-induced fluorescence intensity as a function of delay time between the probe and photolysis lasers. CO was monitored on the $A^1\Pi(v'=2,J'=37) \leftarrow X^1\Sigma^+(v''=0,J''=37)$ transition. The label in each panel indicates the relevant predissociating vibronic band of CHOCHO. (Reprinted from ref 375. Copyright 1987 American Institute of Physics.)

$$CHOCHO(S_1{}^1A_u) \rightarrow H_2CO + CO \quad (I)$$

$$\rightarrow H_2 + 2CO \quad (II)$$

were proposed to take place via a planar transition state. I and II are called the *"formaldehyde channel"* and *"triple whammy channel"*, respectively. The predissociation of the $S_1{}^1A_u$ state was studied by measuring the PHOFEX spectrum.[375] The fluorescence excitation spectrum of CHOCHO using a supersonic jet is shown in Figure 35, where only the K' structure is resolved. The Q(37) line of the CO $A^1\Pi(v'=2) \leftarrow X^1\Sigma^+(v''=0)$ transition for the 0_0^0, 5_0^1, 8_0^1, and 4_0^1 excitations was observed. The appearance time of CO was in good agreement with the decay time of the excited vibronic level of CHOCHO, and was remarkably fast for the 8_0^1 band (see Figure 36). The rotational profiles of the fluorescence excitation and PHOFEX spectra were in good agreement. This indicated that the intersystem crossing to the $T_1{}^3A_u$ state was shown to be negligible.[376] Therefore, the observed vibrational and rotational dependence was attributed to the internal conversion and dissociation in the ground state. CO was not formed vibrationally excited, but the rotational levels were populated for $J'' = 0-65$. The averaged energy was much higher than the statistical distribution. From the Doppler profile, the velocity vector **v** of CO was observed to be nearly perpendicular to the total angular momentum **J**. This is expected if the transition state is planar. The CO velocity should be small in the triple whammy channel from energetic considerations, but low velocity components were not observed in the Doppler profile. Therefore, it was concluded that the main channel which yielded the CO fragments with high rotational energy was the formaldehyde channel.

E. CH_3SH

Selective fission of the strong S−H bond over the weak C−S bond was observed in the UV photolysis of methyl mercaptan CH_3SH, and a potential energy surface of the excited state was suggested to be repulsive.[377,378] However, Mouflih, Larrieu, and Chaillet[379] showed by *ab initio* SCF MO calculations that the $2^1A''$ potential energy surface accessed by the UV excitation was bound in the S−H coordinate.

Keller, Kash, Jensen, and Butler,[380] and Jensen, Keller, Waschewsky, Stevens, Graham, Freed, and Butler[381] studied both experimentally and theoretically the following photodissociation processes of CH_3SH in detail:

$$CH_3SH + h\nu \rightarrow CH_3S + H \quad (I)$$

$$\rightarrow CH_3 + SH \quad (II)$$

CH_3SH has two broad absorption bands at 235 and 205 nm.[382] CH_3SH in a molecular beam was excited at 248, 222, and 193 nm, and the photofragment velocity and angular distribution were measured. According to the *ab initio* calculations, there are two electronic states, $1^1A''$ and $2^1A''$, respectively, of repulsive and bound potentials with respect to the S−H coordinate. Photoexcitation at 248 and 222 nm accesses the lower potential energy surface near the saddle point, while excitation at 193 nm accesses the upper bound potential energy surface. By measuring the photofragments, it was shown that the C−S bond fission did not occur at 248 nm, but occurred slightly at 222 nm. Although the branching ratio between C−S bond fission and S−H bond fission was a factor of eight larger at 193 nm than at 222 nm, the S−H bond fission was still dominant. In the dispersed emission (resonance Raman) spectrum excited at 193 nm, a progression of peaks assigned to C−S stretching were observed in the spectrum, but S−H progressions were not observed. The initial motion on the upper potential energy surface was suggested to be along the C−S coordinate. Consequently, the S−H bond fission can occur by internal conversion to a lower dissociative surface. However, angular distribution of the fragments showed that the bond fission was strongly anisotropic and occurred on the time scale of rotation. It was concluded that the nonadiabatic coupling between the upper and lower states was important in the dissociation dynamics.

Yarkony[383] performed MCSCF calculations and pointed out that a conical intersection of potential surfaces exists between the two $^1A''$ states. Excitation at 193 nm accesses the $2^1A''$ state which is bound. CH_3SH does not dissociate adiabatically from this state. However, the nonadiabatic transition

$2^1A'' \rightarrow 1^1A''$ occurred on the surface of conical intersection involving states of mixed-valence–Rydberg character. It was concluded that the conical intersection facilitated the photodissociation of CH_3SH at wavelengths short enough to reach the $2^1A''$ state.

VII. Acknowledgments

This work is supported by a Grant-in-Aid for Specially Promoted Research from the Ministry of Education, Science and Culture of Japan. We thank Professor W. Demtröder for reading the manuscript and helpful discussions. We also thank Dr. E. Sekreta for improving the manuscript.

VIII. References

(1) Wentzel, G. *Z. Phys.* **1927**, *43*, 524; *Phys. Z.* **1928**, *29*, 321.
(2) Herzberg, G. *Z. Phys.* **1930**, *61*, 604.
(3) Rice, O. K. *J. Chem. Phys.* **1933**, *1*, 375.
(4) Kronig, R. L. *Z. Phys.* **1932**, *75*, 468.
(5) Van Vleck, J. H. *Phys. Rev.* **1932**, *40*, 544.
(6) Mulliken, R. S. *J. Chem. Phys.* **1960**, *33*, 247.
(7) Herzberg, G. *Molecular Spectra and Molecular Structure. I. Spectra of Diatomic Molecules*; Van Nostrand Reinhold: New York, 1950.
(8) Herzberg, G. *Molecular Spectra and Molecular Structure. III. Electronic Spectra and Electronic Structure of Polyatomic Molecules*; Van Nostrand Reinhold: New York, 1966.
(9) Kovács, I. *Rotational Structure in the spectra of Diatomic Molecules*; Adam Hilger: Bristol, 1969.
(10) Lefebvre-Brion, H.; Field, R. W. *Perturbations in the Spectra of Diatomic Molecules*; Academic Press: Orlando, 1986.
(11) Child, M. S. *Chem. Soc. Spe. Per. Rep. Mol. Spectrosc.* **1974**, *2*, 466.
(12) Erman, P. *Chem. Soc. Spe. Per. Rep. Mol. Spectrosc.* **1979**, *6*, 174.
(13) Schinke, R. *Photodissociation Dynamics*; Cambridge Univ. Press: Cambridge, 1993.
(14) Breford, E. J.; Engelke, F.; Ennen, G.; Meiwes, K. H. *Faraday Discuss. Chem. Soc.* **1981**, *71*, 233.
(15) Katô, H.; Kobayashi, T.; Chosa, M.; Nakahori, T.; Iida, T.; Kasahara, S.; Baba, M. *J. Chem. Phys.* **1991**, *94*, 2600.
(16) Fano, U. *Phys. Rev.* **1961**, *124*, 1866.
(17) Altick, P. L.; Moore, E. N. *Phys. Rev.* **1966**, *147*, 59.
(18) Bardsley, J. N. *J. Phys.* **1968**, *B1*, 349.
(19) Atabek, O.; Lefebvre, R. *Chem. Phys. Lett.* **1972**, *17*, 167.
(20) Tiemann, E. *Z. Phys.* **1987**, *D5*, 77.
(21) Abramowitz, M.; Stegun, I. A. *Handbook of Mathematical Functions*; Dover: New York, 1968; p 256.
(22) Child, M. S. *Mol. Phys.* **1976**, *32*, 1495.
(23) Lefebvre-Brion, H.; Colin, R. *J. Mol. Spectrosc.* **1977**, *65*, 33.
(24) Child, M. S.; Lefebvre, R. *Mol. Phys.* **1977**, *34*, 979.
(25) von Neumann, J.; Wigner, E. *Z. Phys.* **1929**, *30*, 467.
(26) Herzberg, G.; Longuet-Higgins, H. C. *Discuss. Faraday Soc.* **1963**, *35*, 77.
(27) Longuet-Higgins, H. C. *Proc. R. Soc. Ser. A* **1975**, *344*, 147.
(28) Herzberg, G. *Ergeb. Exakten Naturwiss.* **1931**, *10*, 207.
(29) Hougen, J. T. *NBS Monogr.* **1970**, *115*.
(30) Veseth, L. *Theor. Chim. Acta* **1970**, *18*, 368.
(31) Langhoff, S. R.; Kern, C. W. Molecular Fine Structure. In *Modern Theoretical Chemistry*; Schaefer, K. F., Ed.; Plenum: New York, 1977; Vol. 4, p 381.
(32) Vigué, J.; Broyer, M.; Lehmann, J. C. *J. Phys. (Paris)* **1981**, *42*, 937.
(33) Pique, J. P.; Bacis, R.; Hartmann, F.; Sadeghi, N.; Churassy, S. *J. Phys. (Paris)* **1983**, *44*, 347.
(34) Demtröder, W. *Laser Spectroscopy*; Springer: Berlin, 1981.
(35) Raab, M.; Höning, G.; Demtröder, W.; Vidal, C. R. *J. Chem. Phys.* **1982**, *76*, 4370.
(36) Ezekiel, S.; Weiss, R. *Phys. Rev. Lett.* **1968**, *20*, 91.
(37) Sinha, M. P.; Schultz, A.; Zare, R. N. *J. Chem. Phys.* **1973**, *58*, 549.
(38) Oldman, R. J.; Sander, R. K.; Wilson, K. R. *J. Chem. Phys.* **1971**, *54*, 4127.
(39) Rosker, M. J.; Dantus, M.; Zewail, A. H. *J. Chem. Phys.* **1988**, *89*, 6113.
(40) Khundkar, L. R.; Zewail, A. H. *Annu. Rev. Phys. Chem.* **1990**, *41*, 15.
(41) Loison, J.-C.; Kable, S. H.; Houston, P. L. *J. Chem. Phys.* **1991**, *94*, 1796.
(42) Reisler, H.; Noble, M.; Wittig, C. *Molecular Photodissociation Dynamics*; Ashfold, M. N. R., Baggott, J. E., Eds.; Roy. Soc. Chem.: London, 1987; p 139.
(43) Gerber, G.; Möller, R. *Phys. Rev. Lett.* **1985**, *55*, 814.
(44) Kolos, W.; Wolniewicz, L. *J. Chem. Phys.* **1965**, *43*, 2429; **1968**, *48*, 3672.
(45) Rothenberg, S.; Davidson, E. R. *J. Chem. Phys.* **1966**, *44*, 730.
(46) Namioka, T. *J. Chem. Phys.* **1964**, *40*, 3154; **1964**, *41*, 2141; **1965**, *43*, 1636.
(47) Monfils, A. *Acad. R. Belg. Sci.* **1961**, *47*, 816; **1968**, *54*, 44.
(48) Beutler, H.; Deubner, A.; Jüngen, H. O. *Z. Phys.* **1935**, *98*, 181.
(49) Rydberg, R. *Z. Phys.* **1931**, *73*, 376.
(50) Klein, O. *Z. Phys.* **1932**, *76*, 226.
(51) Rees, A. L. G. *Proc. Phys. Soc. (London)* **1947**, *A59*, 998.
(52) Dalgarno, A.; Allison, A. C. *J. Geophys. Res.* **1969**, *74*, 4178.
(53) Beyer, K.; Welge, K. H. *Z. Naturforsch.* **1967**, *22a*, 1161.
(54) Mentall, J. E.; Gentieu, E. P. *J. Chem. Phys.* **1970**, *52*, 5641.
(55) Comes, F. J.; Schumpe, G. *Z. Naturforsch.* **1971**, *26a*, 538.
(56) Julienne, P. S. *Chem. Phys. Lett.* **1971**, *8*, 27.
(57) Fiquet-Fayard, F.; Gallais, O. *Chem. Phys. Lett.* **1972**, *16*, 18.
(58) Glass-Maujean, M.; Breton, J.; Guyon, P. M. *Chem. Phys. Lett.* **1979**, *63*, 591.
(59) Dehmer, P. M.; Chupka, W. A. *Chem. Phys. Lett.* **1980**, *70*, 127.
(60) Glass-Maujean, M.; Breton, J.; Guyon, P. M. *Phys. Rev. Lett.* **1978**, *40*, 181.
(61) Borrell, P.; Guyon, P. M.; Glass-Maujean, M. *J. Chem. Phys.* **1977**, *66*, 818.
(62) Guyon, P. M.; Breton, J.; Glass-Maujean, M. *Chem. Phys. Lett.* **1979**, *68*, 314.
(63) Glass-Maujean, M.; Guyon, P. M.; Breton, J. *Phys. Rev.* **1986**, *A33*, 346.
(64) Glass-Maujean, M.; Breton, J.; Guyon, P. M. *Z. Phys.* **1987**, *D5*, 189.
(65) Rothschild, M.; Egger, H.; Hawkins, R. T.; Bokor, J.; Pummer, H.; Rhodes, C. K. *Phys. Rev.* **1981**, *A23*, 206.
(66) Glab, W. L.; Hessler, J. P. *Phys. Rev.* **1987**, *A35*, 2102.
(67) Rottke, H.; Welge, K. H. *J. Chem. Phys.* **1992**, *97*, 908.
(68) Eyler, E. E.; Pipkin, F. M. *Phys. Rev.* **1983**, *A27*, 2462.
(69) de Bruijn, D. P.; Helm, H. *Phys. Rev.* **1986**, *A34*, 3855.
(70) Lembo, L. J.; Huestis, D. L.; Keiding, S. R.; Bjerre, N.; Helm, H. *Phys. Rev.* **1988**, *A38*, 3447.
(71) Comes, F. J.; Wenning, U. *Z. Naturforsch.* **1969**, *24a*, 587.
(72) Mentall, J. E.; Guyon, P. M. *J. Chem. Phys.* **1977**, *67*, 3845.
(73) Borondo, F.; Eguiagaray, L. R.; Riera, A. *J. Phys.* **1982**, *B15*, 899.
(74) Beswick, J. A.; Glass-Maujean, M. *Phys. Rev.* **1987**, *A35*, 3339.
(75) MruGala, F. *Mol. Phys.* **1988**, *65*, 377.
(76) Jungen, C. *Phys. Rev. Lett.* **1984**, *53*, 2394.
(77) Comes, F. J.; Wenning, U. *Chem. Phys. Lett.* **1970**, *5*, 195.
(78) Qin, K.; Bistransin, M.; Glab, W. L. *Phys. Rev.* **1993**, *A47*, 4154.
(79) Uzer, T.; Dalgarno, A. *Chem. Phys.* **1980**, *51*, 271.
(80) Rice, S. F.; Xie, X.; Field, R. W. *Chem. Phys.* **1986**, *104*, 161.
(81) Linton, C.; Bacis, R.; Crozet, P.; Martin, F.; Ross, A. J.; Verges, J. *J. Mol. Spectrosc.* **1992**, *151*, 159.
(82) Preuss, W.; Baumgartner, G. *Z. Phys.* **1985**, *A320*, 125.
(83) Schmidt-Mink, I.; Meyer, W. *Chem. Phys. Lett.* **1985**, *121*, 49.
(84) Schmidt, I.; Meyer, W.; Krüger, B.; Engelke, F. *Chem. Phys. Lett.* **1988**, *143*, 353.
(85) Keller, J.; Weiner, J. *Phys. Rev.* **1984**, *A29*, 2943.
(86) Chawla, G. K.; Vedder, H. J.; Field, R. W. *J. Chem. Phys.* **1987**, *86*, 3082.
(87) Richter, H.; Knöckel, H.; Tiemann, E. *Chem. Phys.* **1991**, *157*, 217.
(88) Kasahara, S.; Baba, M.; Katô, H. *J. Chem. Phys.* **1991**, *94*, 7713.
(89) Meiwes, K. H.; Engelke, F. *Chem. Phys. Lett.* **1982**, *85*, 409.
(90) Brechignac, C.; Cahuzac, P. *Surf. Sci.* **1985**, *156*, 183.
(91) Brom, J. M., Jr.; Broida, H. P. *J. Chem. Phys.* **1974**, *61*, 982.
(92) Feldman, D. L.; Zare, R. N. *Chem. Phys.* **1976**, *15*, 415.
(93) Breford, E. J.; Engelke, F. *Chem. Phys. Lett.* **1980**, *75*, 132.
(94) Katô, H. *Faraday Discuss. Chem. Soc.* **1986**, *82*, 1.
(95) Katô, H.; Yoshihara, K. *J. Chem. Phys.* **1979**, *71*, 1585.
(96) Kraulinya, E. K.; Papernov, S. M.; Janson, M. L. *Chem. Phys. Lett.* **1979**, *63*, 531.
(97) Katô, H.; Onomichi, K. *J. Chem. Phys.* **1985**, *82*, 1642.
(98) Collins, C. B.; Anderson, J. A.; Popescu, D.; Popescu, I. *J. Chem. Phys.* **1981**, *74*, 1053.
(99) Collins, C. B.; Lee, F. W.; Anderson, J. A.; Vicharelli, P. A.; Popescu, D.; Popescu, I. *J. Chem. Phys.* **1981**, *74*, 1067.
(100) Raab, M.; Höning, G.; Demtröder, W.; Vidal, C. R. *J. Chem. Phys.* **1982**, *76*, 4370.
(101) Baba, M.; Nakahori, T.; Iida, T.; Katô, H. *J. Chem. Phys.* **1990**, *93*, 4637.
(102) Amiot, C.; Demtröder, W.; Vidal, C. R. *J. Chem. Phys.* **1988**, *88*, 5265.
(103) Katô, H.; Kobayashi, T.; Wang, Y. C.; Ishikawa, K.; Baba, M.; Nagakura, S. *Chem. Phys.* **1992**, *162*, 107.
(104) Katô, H.; Kumauchi, T.; Nishizawa, K.; Baba, M.; Ishikawa, K. *J. Chem. Phys.* **1993**, *98*, 6684.
(105) Heaven, M. C. *Chem. Soc. Rev.* **1986**, *15*, 405.
(106) Wasserman, E.; Falconer, W. E.; Yager, W. A. *J. Chem. Phys.* **1968**, *49*, 1971.
(107) Chutjian, A.; James, T. C. *J. Chem. Phys.* **1969**, *51*, 1242.
(108) Chutjian, A. *J. Chem. Phys.* **1969**, *51*, 5414.

(109) Mulliken, R. S. *J. Chem. Phys.* **1971**, *55*, 288.
(110) Busch, G. E.; Mahoney, R. T.; Morse, R. I.; Wilson, K. R. *J. Chem. Phys.* **1969**, *51*, 837.
(111) Brewer, L.; Tellinghuisen, J. *J. Chem. Phys.* **1972**, *56*, 3929.
(112) Tellinghuisen, J. *J. Chem. Phys.* **1972**, *57*, 2397.
(113) Tellinghuisen, J. *J. Chem. Phys.* **1973**, *58*, 2821.
(114) Vigue, J.; Broyer, M.; Lehmann, J. C. *J. Chem. Phys.* **1975**, *62*, 4941.
(115) Broyer, M.; Vigue, J.; Lehmann, J. C. *J. Chem. Phys.* **1975**, *63*, 5428.
(116) Broyer, M.; Vigue, J.; Lehmann, J. C. *J. Chem. Phys.* **1976**, *64*, 4793.
(117) Vigue, J.; Broyer, M.; Lehmann, J. C. *J. Phys.* **1977**, *B10*, L379.
(118) Brand, H.; Schulz, H. H.; Steudel, A. *Phys. Lett.* **1977**, *A63*, 235.
(119) Couillaud, B.; Ducasse, A. *Opt. Commun.* **1977**, *21*, 199.
(120) Borde, J.; Camy, G.; Decomps, B. *Phys. Rev.* **1979**, *A20*, 254.
(121) Vigue, J.; Broyer, M.; Lehmann, J. C. *J. Phys. (Paris)* **1981**, *42*, 949.
(122) Martinez, E.; Martinez, M. T.; Castano, F. *J. Mol. Spectrosc.* **1988**, *128*, 554.
(123) Tench, R. E.; Ezekiel, S. *Chem. Phys. Lett.* **1983**, *96*, 253.
(124) Steubing, W. *Verh. Dtsch. Phys. Ges.* **1913**, *15*, 1181.
(125) Turner, L. A. *Z. Phys.* **1930**, *65*, 464.
(126) Van Vleck, J. H. *Phys. Rev.* **1932**, *40*, 544.
(127) Degenkolb, E. O.; Steinfeld, J. I.; Wasserman, E.; Klemperer, W. *J. Chem. Phys.* **1969**, *51*, 615.
(128) Chapman, G. D.; Bunker, P. R. *J. Chem. Phys.* **1972**, *57*, 2951.
(129) Capelle, G. A.; Broida, H. P. *J. Chem. Phys.* **1972**, *57*, 5027.
(130) Broyer, M.; Vigue, J.; Lehmann, J. C. *Chem. Phys. Lett.* **1973**, *22*, 313.
(131) Vigue, J.; Broyer, M.; Lehmann, J. C. *J. Phys.* **1974**, *B7*, L158.
(132) Vigue, J.; Broyer, M.; Lehmann, J. C. *J. Phys. (Paris)* **1981**, *42*, 961.
(133) Baba, M.; Kimura, M.; Tsuboi, T.; Katô, H.; Nagakura, S. *Bull. Chem. Soc. Jpn.* **1989**, *62*, 17.
(134) Zener, C. *Proc. R. Soc.* **1933**, *A140*, 660.
(135) Sullivan, B. J.; Dows, D. A. *Chem. Phys.* **1980**, *46*, 231.
(136) Dalby, F. W.; Levy, C. D. P.; Vanderlinde, J. *Chem. Phys.* **1984**, *85*, 23.
(137) Capelle, G.; Sakurai, K.; Broida, H. P. *J. Chem. Phys.* **1971**, *54*, 1728.
(138) Clyne, M. A. A.; Heaven, M. C. *J. Chem. Soc., Faraday Trans. 2* **1978**, *74*, 1992.
(139) Luypaert, R.; Vlieger, G. D.; Craen, J. V. *J. Chem. Phys.* **1980**, *72*, 6283.
(140) Child, M. S. *J. Phys.* **1980**, *B13*, 2557.
(141) Clyne, M. A. A.; Heaven, M. C.; Tellinghuisen, J. *J. Chem. Phys.* **1982**, *76*, 5341.
(142) Bettin, N.; Knöckel, H.; Tiemann, E. *Chem. Phys. Lett.* **1981**, *80*, 386.
(143) Siese, M.; Tiemann, E.; Wulf, U. *Chem. Phys. Lett.* **1985**, *117*, 208.
(144) Peeters, F.; Craen, J. V.; Eisendrath, H. *J. Phys.* **1989**, *B22*, 2541.
(145) Katzenellenbogen, N.; Prior, Y. *J. Chem. Phys.* **1990**, *93*, 897.
(146) Booth, J. L.; Ozier, I.; Dalby, F. W. *Phys. Rev. Lett.* **1994**, *72*, 2371.
(147) Clyne, M. A. A.; McDermid, I. S. *J. Chem. Soc., Faraday Trans. 2* **1978**, *74*, 1935.
(148) Clyne, M. A. A.; McDermid, I. S. *J. Chem. Soc., Faraday Trans. 2* **1979**, *75*, 280.
(149) Clyne, M. A. A.; McDermid, I. S. *J. Chem. Soc., Faraday Trans. 2* **1979**, *75*, 1677.
(150) Heaven, M. C.; Clyne, M. A. A. *J. Chem. Soc., Faraday Trans. 2* **1982**, *78*, 1339.
(151) Billy, N.; Gouédard, G.; Girard, B.; Vigué, J. *J. Phys. II* **1991**, *1*, 323.
(152) Brown, W. G. *Phys. Rev.* **1932**, *42*, 355.
(153) Selin, L.-E. *Arkiv. Fysik.* **1962**, *21*, 529.
(154) Donovan, R. J.; Husain, D. *Trans. Faraday Soc.* **1968**, *64*, 2325.
(155) Knöckel, H.; Tiemann, E.; Zoglowek, D. *J. Mol. Spectrosc.* **1981**, *85*, 225.
(156) Siese, M.; Tiemann, E. *Z. Phys.* **1987**, *D7*, 147.
(157) Brown, W. G.; Gibson, G. E. *Phys. Rev.* **1932**, *40*, 529.
(158) Gordon, R. D.; Innes, K. K. *J. Chem. Phys.* **1979**, *71*, 2824.
(159) de Vries, M. S.; van Veen, N. J. A.; Hutchinson, M.; de Vries, A. E. *Chem. Phys.* **1980**, *51*, 159.
(160) Olson, C. D.; Innes, K. K. *J. Chem. Phys.* **1976**, *64*, 2405.
(161) Suzuki, T.; Kasuya, T. *J. Chem. Phys.* **1984**, *81*, 4818.
(162) Kitamura, M.; Kondow, T.; Kuchitsu, K.; Munakata, K.; Kasuya, T. *J. Chem. Phys.* **1985**, *82*, 4986.
(163) Durand, A.; Loison, J. C.; Bazalgette, G.; Gangler, E.; Dalby, F. W.; Vigué, J. *Chem. Phys.* **1994**, *181*, 209.
(164) Clyne, M. A. A.; McDermid, I. S. *J. Chem. Soc., Faraday Trans. 2* **1976**, *72*, 2252.
(165) Clyne, M. A. A.; McDermid, I. S. *J. Chem. Soc., Faraday Trans. 2* **1978**, *74*, 1644.
(166) Berry, R. S. *J. Chem. Phys.* **1957**, *27*, 1288.
(167) Davidovits, P.; Brodhead, D. C. *J. Chem. Phys.* **1967**, *46*, 2968.
(168) Busch, G. E.; Cornelius, J. F.; Mahoney, R. T.; Morse, R. T.; Schlosser, D. W.; Wilson, K. R. *Rev. Sci. Instrum.* **1970**, *41*, 1066.
(169) Van Veen, N. J. A.; DeVries, M. S.; Sokol, J. D.; Baller, T.; DeVries, A. E. *Chem. Phys.* **1981**, *56*, 81.
(170) Berg, R. A.; Skewes, G. W. *J. Chem. Phys.* **1969**, *51*, 5430.
(171) Schaefer, S. H.; Bender, D.; Tiemann, E. *Chem. Phys. Lett.* **1982**, *92*, 273.
(172) Schaefer, S. H.; Bender, D.; Tiemann, E. *Chem. Phys.* **1984**, *89*, 65.
(173) Bower, R. D.; Chevrier, P.; Das, P.; Foth, H. J.; Polanyi, J. C.; Prisant, M. G.; Visticot, P. *J. Chem. Phys.* **1988**, *89*, 4478.
(174) Bruhm, H.; Linder, J.; Tiemann, E. *J. Chem. Phys.* **1990**, *93*, 4556.
(175) Rose, T. S.; Rosker, M. J.; Zewail, A. H. *J. Chem. Phys.* **1988**, *88*, 6672.
(176) Rose, T. S.; Rosker, M. J.; Zewail, A. H. *J. Chem. Phys.* **1989**, *91*, 7415.
(177) Cong, P.; Mokhtari, A.; Zewail, A. H. *Chem. Phys. Lett.* **1990**, *172*, 109.
(178) Materny, A.; Herek, J. L.; Cong, P.; Zewail, A. H. *J. Phys. Chem.* **1994**, *98*, 3352.
(179) Choi, S. E.; Light, J. C. *J. Chem. Phys.* **1989**, *90*, 2593.
(180) Engel, V.; Metiu, H. *J. Chem. Phys.* **1989**, *90*, 6116.
(181) Lee, S. Y.; Pollard, W. T.; Mathies, R. A. *J. Chem. Phys.* **1989**, *90*, 6146.
(182) Meier, Ch.; Engel, V.; Briggs, J. S. *J. Chem. Phys.* **1991**, *95*, 7337.
(183) Chapman, S.; Child, M. S. *J. Phys. Chem.* **1991**, *95*, 578.
(184) Schaefer, S. H.; Bender, D.; Tiemann, E. *Chem. Phys.* **1986**, *102*, 165.
(185) Grice, R.; Herschbach, D. R. *Mol. Phys.* **1974**, *27*, 159.
(186) Flory, P. J. *J. Chem. Phys.* **1936**, *4*, 23.
(187) Murrell, J. N.; Taylor, J. M. *Mol. Phys.* **1969**, *16*, 609.
(188) Durmaz, S.; Murrell, J. N. *Mol. Phys.* **1971**, *21*, 209.
(189) Schaefer, H. F.; Miller, W. H. *J. Chem. Phys.* **1971**, *55*, 4107.
(190) Julienne, P. S.; Krauss, M. *J. Mol. Spectrosc.* **1975**, *56*, 270.
(191) Julienne, P. S. *J. Mol. Spectrosc.* **1976**, *63*, 60.
(192) Yang, X.; Wodtke, A. M.; Hüwel, L. *J. Chem. Phys.* **1991**, *94*, 2469.
(193) Lewis, B. R.; Berzins, L.; Carver, J. H.; Gibson, S. T. *J. Quant. Spectrosc. Radiat. Transfer* **1986**, *36*, 187.
(194) Cheung, A. S. C.; Yoshino, K.; Esmond, J. R.; Chiu, S. S. L.; Freeman, D. E.; Parkinson, W. H. *J. Chem. Phys.* **1990**, *92*, 842.
(195) Chiu, S. S. L.; Cheung, A. S. C.; Yoshino, K.; Fesmond, J. R.; Freeman, D. E.; Parkinson, W. H. *J. Chem. Phys.* **1990**, *93*, 5539.
(196) Cheung, A. S. C.; Yoshino, K.; Parkinson, W. H.; Freeman, D. E. *J. Mol. Spectrosc.* **1986**, *119*, 1.
(197) Cheung, A. S. C.; Yoshino, K.; Freeman, D. E.; Parkinson, W. H. *J. Mol. Spectrosc.* **1988**, *131*, 96.
(198) Cheung, A. S. C.; Yoshino, K.; Freeman, D. E.; Friedman, R. S.; Dalgarno, A.; Parkinson, W. H. *J. Mol. Spectrosc.* **1989**, *134*, 362.
(199) Chiu, S. S. L.; Cheung, A. S. C.; Finch, M.; Jamieson, M. L.; Yoshino, K.; Dalgarno, A.; Parkinson, W. H. *J. Chem. Phys.* **1992**, *97*, 1787.
(200) (a) Leahy, D. J.; Cyr, D. R.; Osborn, D. L.; Neumark, D. M. *Chem. Phys. Lett.* **1993**, *216*, 503. (b) Cosby, P. C.; Park, H.; Copeland, R. A.; Slanger, T. G. *J. Chem. Phys.* **1993**, *98*, 5117.
(201) Partridge, H.; Bauschlicher, C. W., Jr.; Langhoff, S. R.; Taylor, P. R. *J. Chem. Phys.* **1991**, *95*, 8292.
(202) van der Zande, W. J.; Koot, W.; Los, J.; Peterson, J. R. *J. Chem. Phys.* **1988**, *89*, 6758.
(203) van der Zande, W. J.; Koot, W.; Los, J. *J. Chem. Phys.* **1989**, *91*, 4597.
(204) Friedman, R. S.; Du, M. L.; Dalgarno, A. *J. Chem. Phys.* **1990**, *93*, 2375.
(205) Park, H.; Li, L.; Chupka, W. A. *J. Chem. Phys.* **1990**, *92*, 61.
(206) Yokelson, R. J.; Lipert, R. J.; Chupka, W. A. *J. Chem. Phys.* **1992**, *97*, 6153.
(207) Henri, V.; Teves, M. C. *Nature* **1924**, *114*, 895.
(208) van Iddekinge, H. H. *Nature* **1930**, *125*, 858.
(209) Lochte-Holtgreven, W. *Z. Phys.* **1936**, *103*, 395.
(210) Herzberg, G.; Mundie, L. G. *J. Chem. Phys.* **1940**, *8*, 263.
(211) Ricks, J. M.; Barrow, R. F. *Can. J. Phys.* **1969**, *47*, 2423.
(212) Matsumi, Y.; Suzuki, T.; Munakata, T.; Kasuya, T. *J. Chem. Phys.* **1985**, *83*, 3798.
(213) Quick, C. R.; Weston, R. E., Jr. *J. Chem. Phys.* **1981**, *74*, 4951.
(214) Narasimham, N. A.; Gopal, K. S. *Curr. Sci.* **1965**, *34*, 454.
(215) Carleer, M.; Colin, R. *J. Phys. B* **1970**, *3*, 1715.
(216) Olsson, E. *Z. Phys.* **1934**, *90*, 138.
(217) Rosen, B. *Physica* **1939**, *6*, 205.
(218) Barrow, R. F.; Chandler, G. G.; Meyer, C. B. *Philos. Trans. R. Soc. London Sect. A* **1966**, *260*, 395.
(219) Ackermann, F.; Miescher, E. *J. Mol. Spectrosc.* **1969**, *31*, 400.
(220) Miescher, E. *J. Mol. Spectrosc.* **1974**, *53*, 302.
(221) Callear, A. B.; Pilling, M. J. *Trans. Faraday Soc.* **1970**, *66*, 1618.
(222) Rottke, H.; Zacharias, H. *J. Chem. Phys.* **1985**, *83*, 4831.
(223) Tsukiyama, K.; Munakata, T.; Tsukakoshi, M.; Kasuya, T. *Chem. Phys.* **1988**, *121*, 55.
(224) de Vivie-Riedle, R.; van Hemert, M. C.; Peyerimhoff, S. D. *J. Chem. Phys.* **1990**, *92*, 3613.
(225) d'Azy, O. B.; Lopez-Delgado, R.; Tramer, A. *Chem. Phys.* **1975**, *9*, 327.
(226) Bubert, H. *J. Chem. Phys.* **1972**, *56*, 1113.

(227) Ashfold, M. N. R.; Dixon, R. N.; Prince, J. D.; Tutcher, B.; Western, C. M. *J. Chem. Soc., Faraday Trans. 2* **1986**, *82*, 1257.
(228) Miller, R. J.; Li, L.; Wang, Y.; Chupka, W. A.; Colson, S. D. *J. Chem. Phys.* **1989**, *90*, 754.
(229) Gadd, G. E.; Jusinski, L. E.; Slanger, T. G. *J. Chem. Phys.* **1989**, *91*, 3378.
(230) Fujii, A.; Morita, N. *J. Chem. Phys.* **1992**, *97*, 327.
(231) Fujii, A.; Morita, N. *J. Chem. Phys.* **1993**, *98*, 4581.
(232) Coster, D.; Brons, F. *Physica* **1934**, *1*, 155.
(233) Eidelsberg, M.; Rostas, F. *Astron. Astrophys.* **1990**, *235*, 472.
(234) Eidelsberg, M.; Roncin, J. Y.; Le Floch, A.; Launay, F.; Letzelter, C.; Rostas, J. *J. Mol. Spectrosc.* **1987**, *121*, 309.
(235) Cooper, D. M.; Langhoff, S. R. *J. Chem. Phys.* **1981**, *74*, 1200.
(236) Wolk, G. L.; Rich, J. W. *J. Chem. Phys.* **1983**, *79*, 12.
(237) Cooper, D. M.; Kirby, K. *J. Chem. Phys.* **1987**, *87*, 424.
(238) Tchang-Brillet, W. ÜL.; Julienne, P. S.; Robbe, J. M.; Letzelter, C.; Rostas, F. *J. Chem. Phys.* **1992**, *96*, 6735.
(239) Simmons, J. D.; Tilford, S. G. *J. Mol. Spectrosc.* **1974**, *49*, 167.
(240) Klopotek, P.; Vidal, C. R. *J. Opt. Soc. Am.* **1985**, *B2*, 869.
(241) Amiot, C.; Roncin, J. Y.; Verges, J. *J. Phys.* **1986**, *B19*, L19.
(242) Herzberg, G.; Johns, J. W. C. *Astrophys. J.* **1969**, *158*, 399.
(243) van Dishoeck, E. F. *J. Chem. Phys.* **1987**, *86*, 196.
(244) Brzozowski, J.; Bunker, P.; Elander, N.; Erman, P. *Astrophys. J.* **1976**, *207*, 414.
(245) Shidei, T. *Jpn. J. Phys.* **1936**, *11*, 23.
(246) Solomon, P. M.; Klemperer, W. *Astrophys. J.* **1972**, *178*, 389.
(247) Ubachs, W.; Meyer, G.; ter Meulen, J. J.; Dymanus, A. *J. Chem. Phys.* **1986**, *84*, 3032.
(248) Wang, Y.; Li, L.; Chupka, W. A. *Chem. Phys. Lett.* **1992**, *192*, 348.
(249) Smith, W. H.; Brzozowski, J.; Erman, P. *J. Chem. Phys.* **1976**, *64*, 4628.
(250) Kenner, R. D.; Kaes, A.; Browarzik, R. K.; Stuhl, F. *J. Chem. Phys.* **1989**, *91*, 1440.
(251) Goldfield, E. M.; Kirby, K. P. *J. Chem. Phys.* **1987**, *87*, 3986.
(252) Patel-Misra, D.; Parlant, G.; Sauder, D. G.; Yarkony, D. R.; Dagdigian, P. J. *J. Chem. Phys.* **1991**, *94*, 1913.
(253) Kenner, R. D.; Rohrer, F.; Stuhl, F. *J. Phys. Chem.* **1989**, *93*, 7824.
(254) Parlant, G.; Dagdigian, P. J.; Yarkony, D. R. *J. Chem. Phys.* **1991**, *94*, 2364.
(255) Bohn, B.; Stuhl, F.; Parlant, G.; Dagdigian, P. J.; Yarkony, D. R. *J. Chem. Phys.* **1992**, *96*, 5059.
(256) Gaydon, A. G.; Wolfhard, H. G. *Proc. R. Soc. London* **1951**, *A208*, 63.
(257) Sutherland, R. A.; Anderson, R. A. *J. Chem. Phys.* **1973**, *58*, 1226.
(258) Smith, W. H.; Elmergreen, B. G.; Brooks, N. H. *J. Chem. Phys.* **1974**, *61*, 2793.
(259) German, K. R. *J. Chem. Phys.* **1975**, *63*, 5252.
(260) Brzozowski, J.; Erman, P.; Lyyra, M. *Phys. Scr.* **1978**, *17*, 507.
(261) Bergeman, T.; Erman, P.; Haratym, Z.; Larsson, M. *Phys. Scr.* **1981**, *23*, 45.
(262) Gray, J. A.; Farrow, R. L. *J. Chem. Phys.* **1991**, *95*, 7054.
(263) Heard, D. E.; Crosley, D. R.; Jeffries, J. B.; Smith, G. P.; Hirano, A. *J. Chem. Phys.* **1992**, *96*, 4366.
(264) Sink, M. L.; Bandrauk, A. D.; Lefebvre, R. *J. Chem. Phys.* **1980**, *73*, 4451.
(265) Yarkony, D. R. *J. Chem. Phys.* **1992**, *97*, 1838.
(266) Bourguignon, B.; Gargoura, M. A.; Rostas, J.; Taieb, G. *J. Phys. Chem.* **1987**, *91*, 2080.
(267) Rostas, J.; Shafizadeh, N.; Taieb, G.; Bourguignon, B.; Prisant, M. G. *Chem. Phys.* **1990**, *142*, 97.
(268) Shafizadeh, N.; Rostas, J.; Taieb, G.; Bourguignon, B.; Prisant, M. G. *Chem. Phys.* **1990**, *142*, 111.
(269) Parlant, G.; Rostas, J.; Taieb, G.; Yarkony, D. *J. Chem. Phys.* **1990**, *93*, 6403.
(270) Brown, J. M.; Ramsay, D. A. *Can. J. Phys.* **1975**, *53*, 2232.
(271) Vasudev, R.; Zare, R. N. *J. Chem. Phys.* **1982**, *76*, 5267.
(272) Dixon, R. N. *Mol. Phys.* **1985**, *54*, 333.
(273) Kable, S. H.; Loison, J.-C.; Houston, P. L.; Burak, I. *J. Chem. Phys.* **1990**, *92*, 6332.
(274) Neyer, D. W.; Kable, S. H.; Loison, J.-C.; Houston, P. L.; Burak, I.; Goldfield, E. M. *J. Chem. Phys.* **1992**, *97*, 9036.
(275) Goldfield, E. M.; Gray, S. K.; Harding, L. B. *J. Chem. Phys.* **1993**, *99*, 5812.
(276) Manaa, M. R.; Yarkony, D. R. *J. Chem. Phys.* **1993**, *99*, 5251.
(277) Manaa, M. R.; Yarkony, D. R. *J. Chem. Phys.* **1993**, *100*, 473.
(278) Clement, M. J. Y.; Ramsay, D. A. *Can. J. Phys.* **1961**, *39*, 205.
(279) Bancroft, J. L.; Hollas, J. M.; Ramsay, D. A. *Can. J. Phys.* **1962**, *40*, 322.
(280) Dixon, R. N.; Jones, K. B.; Noble, M.; Carter, S. *Mol. Phys.* **1981**, *42*, 455.
(281) Dixon, R. N.; Rosser, C. A. *Chem. Phys. Lett.* **1984**, *108*, 323.
(282) Petersen, J. C. *J. Mol. Spectrosc.* **1985**, *110*, 277.
(283) McNesby, J. R.; Tanaka, I.; Okabe, H. *J. Chem. Phys.* **1971**, *36*, 605.
(284) Tsurubuchi, S. *Chem. Phys.* **1975**, *10*, 335.
(285) Hodgson, A.; Simons, J. P.; Ashfold, M. N. R.; Bayley, J. M.; Dixon, R. N. *Chem. Phys. Lett.* **1984**, *107*, 1.
(286) Hodgson, A.; Simons, J. P.; Ashfold, M. N. R.; Bayley, J. M.; Dixon, R. N. *Mol. Phys.* **1985**, *54*, 351.
(287) Ashfold, M. N. R.; Bayley, J. M.; Dixon, R. N. *Chem. Phys.* **1984**, *84*, 35.
(288) Meijer, G.; ter Moulen, J. J.; Andresen, P.; Bath, A. *J. Chem. Phys.* **1986**, *85*, 6914.
(289) Kuge, H. H.; Kleinermanns, K. *J. Chem. Phys.* **1989**, *90*, 46.
(290) Herzberg, G.; Innes, K. K. *Can. J. Phys.* **1957**, *35*, 842.
(291) Hsu, Y.-C.; Smith, M. A.; Wallace, S. C. *Chem. Phys. Lett.* **1984**, *111*, 219.
(292) Peric, M.; Peyerimhoff, D.; Buenker, R. J. *Can. J. Chem.* **1977**, *55*, 3664.
(293) Meenakshi, A.; Innes, K. K. *J. Chem. Phys.* **1986**, *84*, 6550.
(294) Chamberlain, G.; Simons, J. P. *J. Chem. Soc., Faraday Trans. 2* **1975**, *71*, 2043.
(295) Ashfold, M. N. R.; Simons, J. P. *J. Chem. Soc., Faraday Trans. 2* **1978**, *74*, 280.
(296) MacPherson, M. T.; Simons, J. P. *Chem. Phys. Lett.* **1978**, *55*, 84.
(297) MacPherson, M. T.; Simons, J. P. *J. Chem. Soc., Faraday Trans. 2* **1978**, *74*, 1965.
(298) Kanamori, H.; Butler, J. E.; Kawaguchi, K.; Yamada, C.; Hirota, E. *J. Chem. Phys.* **1985**, *83*, 611.
(299) Ebata, T.; Nakazawa, O.; Ito, M. *Chem. Phys. Lett.* **1988**, *143*, 31.
(300) Stevens, C. G.; Brand, J. C. D. *J. Chem. Phys.* **1973**, *58*, 3324.
(301) Vasudev, R.; McClain, W. M. *J. Mol. Spectrosc.* **1981**, *89*, 125.
(302) Becker, S.; Braatz, C.; Lindner, J.; Tiemann, E. *Chem. Phys. Lett.* **1993**, *208*, 15.
(303) Bonhoeffer, K. F.; Farkas, L. *Z. Phys. Chem.* **1928**, *A134*, 337.
(304) Douglas, A. E. *Discuss. Faraday Soc.* **1963**, *35*, 158.
(305) McCarthy, M. I.; Rosmus, P.; Werner, H. J.; Botschwina, P.; Vaida, V. *J. Chem. Phys.* **1987**, *86*, 6693.
(306) Ashfold, M. N. R.; Bennett, C. L.; Dixon, R. N. *Chem. Phys.* **1985**, *93*, 293.
(307) Dixon, R. N. *Mol. Phys.* **1989**, *68*, 263.
(308) Endo, Y.; Iida, M.; Ohshima, Y. *Chem. Phys. Lett.* **1990**, *174*, 401.
(309) Ashfold, M. N. R.; Dixon, R. N. *Chem. Phys. Lett.* **1990**, *177*, 597.
(310) Biesner, J.; Schnieder, L.; Schmeer, J.; Ahlers, G.; Xie, X.; Welge, K. H.; Ashfold, M. N. R.; Dixon, R. N. *J. Chem. Phys.* **1988**, *88*, 3607.
(311) Biesner, J.; Schnieder, L.; Ahlers, G.; Xie, X.; Welge, K. H.; Ashfold, M. N. R.; Dixon, R. N. *J. Chem. Phys.* **1989**, *91*, 2901.
(312) Okabe, H. *J. Chem. Phys.* **1983**, *78*, 1312.
(313) Wodtke, A. M.; Lee, Y. T. *J. Phys. Chem.* **1985**, *89*, 4744.
(314) Ingold, C. K.; King, G. W. *J. Chem. Soc.* **1953**, 2702.
(315) Innes, K. K. *J. Chem. Phys.* **1954**, *22*, 863.
(316) Fujii, M.; Haijima, A.; Ito, M. *Chem. Phys. Lett.* **1988**, *150*, 380.
(317) Haijima, A.; Fujii, M.; Ito, M. *J. Chem. Phys.* **1990**, *92*, 959.
(318) Osamura, Y.; Mitsuhashi, F.; Iwata, S. *Chem. Phys. Lett.* **1989**, *164*, 205.
(319) Nadler, I.; Pfab, J.; Reisler, H.; Wittig, C. *J. Chem. Phys.* **1984**, *81*, 653.
(320) Nadler, I.; Reisler, H.; Noble, M.; Wittig, C. *Chem. Phys. Lett.* **1984**, *108*, 115.
(321) Nadler, I.; Noble, M.; Reisler, H.; Wittig, C. *J. Chem. Phys.* **1985**, *82*, 2608.
(322) Noble, M.; Nadler, I.; Reisler, H.; Wittig, C. *J. Chem. Phys.* **1984**, *81*, 4333.
(323) Qian, C. X. W.; Noble, M.; Nadler, I.; Reisler, H.; Wittig, C. *J. Chem. Phys.* **1985**, *83*, 5573.
(324) Pechukas, P.; Light, J. C. *J. Chem. Phys.* **1965**, *42*, 3281.
(325) Pechukas, P.; Light, J. C.; Rankin, C. *J. Chem. Phys.* **1966**, *44*, 794.
(326) Wittig, C.; Nadler, I.; Reisler, H.; Noble, M.; Catanzarite, J.; Radhakrishnan, G. *J. Chem. Phys.* **1985**, *83*, 5581.
(327) Qian, C. X. W.; Ogai, A.; Reisler, H.; Wittig, C. *J. Chem. Phys.* **1989**, *90*, 209.
(328) Khundkar, L. R.; Knee, J. L.; Zewail, A. H. *J. Chem. Phys.* **1987**, *87*, 77.
(329) Dekoven, B. M.; Fung, K. H.; Levy, D. H.; Hoffland, L. D.; Spears, K. G. *J. Chem. Phys.* **1981**, *74*, 4755.
(330) Spears, K. G.; Hoffland, L. D. *J. Chem. Phys.* **1981**, *74*, 4765.
(331) Bower, R. D.; Jones, R. W.; Houston, P. L. *J. Chem. Phys.* **1983**, *79*, 2799.
(332) Dyet, J. A.; McCoustra, M. R. S.; Pfab, J. *J. Chem. Soc., Faraday Trans. 2* **1988**, *84*, 463.
(333) Ellis, H. B.; Ellison, G. B., Jr. *J. Chem. Phys.* **1983**, *78*, 6541.
(334) McCoustra, M. R. S.; Dyet, J. A.; Pfab, J. *Chem. Phys. Lett.* **1987**, *136*, 231.
(335) Dyet, J. A.; McCoustra, M. R. S.; Pfab, J. *J. Chem. Soc., Faraday Trans.* **1990**, *86*, 2049.
(336) Reisler, H.; Pessine, F. B. T.; Haas, Y.; Wittig, C. *J. Chem. Phys.* **1983**, *78*, 3785.
(337) Noble, M.; Qian, C. X. W.; Reisler, H.; Wittig, C. *J. Chem. Phys.* **1986**, *84*, 3573.
(338) Noble, M.; Qian, C. X. W.; Reisler, H.; Wittig, C. *J. Chem. Phys.* **1986**, *85*, 5763.

(339) Moortgat, G. K.; Seiler, W.; Warneck, P. *J. Chem. Phys.* **1983**, *78*, 1185.
(340) Moore, C. B.; Weisshaar, J. C. *Annu. Rev. Phys. Chem.* **1983**, *34*, 525.
(341) Ho, P.; Bamford, D. J.; Buss, R. J.; Lee, Y. T.; Moore, C. B. *J. Chem. Phys.* **1982**, *76*, 3630.
(342) Hayes, D. M.; Morokuma, K. *Chem. Phys. Lett.* **1972**, *12*, 539.
(343) Jaffe, R. L.; Hayes, D. M.; Morokuma, K. *J. Chem. Phys.* **1974**, *60*, 5108.
(344) Jaffe, R. L.; Morokuma, K. *J. Chem. Phys.* **1976**, *64*, 4881.
(345) Goddard, J. D.; Schaefer, H. F., III. *J. Chem. Phys.* **1979**, *70*, 5117.
(346) Goddard, J. D.; Yamaguchi, Y.; Schafer, H. F., III. *J. Chem. Phys.* **1981**, *75*, 3459.
(347) Frisch, M. J.; Krishnan, R.; Pople, J. A. *J. Phys. Chem.* **1981**, *85*, 1467.
(348) Weisshaar, J. C.; Moore, C. B. *J. Chem. Phys.* **1979**, *70*, 5135.
(349) Henke, W. E.; Selzle, H. L.; Hays, T. R.; Schlag, E. W.; Lin, S. H. *J. Chem. Phys.* **1982**, *76*, 1327.
(350) Frisoli, J. K.; Moore, C. B. *J. Phys. Chem.* **1988**, *92*, 5425.
(351) Henke, W. E.; Selzle, H. L.; Hays, T. R.; Schlag, E. W.; Lin, S. H. *J. Chem. Phys.* **1982**, *76*, 1335.
(352) Bamford, D. J.; Filseth, S. V.; Foltz, M. F.; Hepburn, J. W.; Moore, C. B. *J. Chem. Phys.* **1985**, *82*, 3032.
(353) Houston, P. L.; Moore, C. B. *J. Chem. Phys.* **1976**, *65*, 757.
(354) Debarre, D.; Lefebvre, M.; Pealat, M.; Taran, J. P. E.; Bamford, D. J.; Moore, C. B. *J. Chem. Phys.* **1985**, *83*, 4476.
(355) Apel, E. C.; Lee, E. K. C. *J. Chem. Phys.* **1986**, *84*, 1039.
(356) Waite, B. A.; Gray, S. K.; Miller, W. H. *J. Chem. Phys.* **1983**, *78*, 259.
(357) Miller, W. H. *J. Am. Chem. Soc.* **1983**, *105*, 216.
(358) Weisshaar, J. C.; Moore, C. B. *J. Chem. Phys.* **1980**, *72*, 5415.
(359) Orita, H.; Morita, H.; Nagakura, S. *Chem. Phys. Lett.* **1981**, *81*, 409.
(360) Orita, H.; Morita, H.; Nagakura, S. *Chem. Phys. Lett.* **1982**, *86*, 123.
(361) Horowitz, A.; Calvert, J. G. *J. Phys. Chem.* **1982**, *86*, 3105.
(362) Baba, M.; Hanazaki, I.; Nagashima, U. *J. Chem. Phys.* **1985**, *82*, 3938.
(363) Kono, T.; Takayanagi, M.; Nishiya, T.; Hanazaki, I. *Chem. Phys. Lett.* **1993**, *201*, 166.
(364) Kono, T.; Takayanagi, M.; Hanazaki, I. *J. Phys. Chem.* **1993**, *97*, 12793.
(365) Benson, S. W.; Kistiakowsky, G. B. *J. Am. Chem. Soc.* **1942**, *64*, 80.
(366) Denshlag, H. O.; Lee, E. K. C. *J. Am. Chem. Soc.* **1968**, *90*, 3628.
(367) Lee, N. E.; Denschlag, H. O.; Lee, E. K. C. *J. Chem. Phys.* **1968**, *48*, 3334.
(368) Lee, N. E.; Lee, E. K. C. *J. Chem. Phys.* **1969**, *50*, 2094.
(369) Hemminger, J. C.; Rusbult, C. F.; Lee, E. K. C. *J. Am. Chem. Soc.* **1971**, *93*, 1867.
(370) Hemminger, J. C.; Lee, E. K. C. *J. Chem. Phys.* **1972**, *56*, 5284.
(371) Tang, K. Y.; Lee, E. K. C. *J. Phys. Chem.* **1976**, *80*, 1833.
(372) Loge, G. W.; Parmenter, C. S. *J. Phys. Chem.* **1981**, *85*, 1653.
(373) Hepburn, J. W.; Buss, R. J.; Butler, L. J.; Lee, Y. T. *J. Phys. Chem.* **1983**, *87*, 3638.
(374) Osamura, Y.; Schaefer, H. F.; Dupuis, M.; Lester, W. A., Jr. *J. Chem. Phys.* **1981**, *75*, 5828.
(375) Burak, I.; Hepburn, J. W.; Sivakumar, N.; Hall, G. E.; Chawla, G.; Houston, P. L. *J. Chem. Phys.* **1987**, *86*, 1258.
(376) Parmenter, C. S.; Seaver, M. *Chem. Phys.* **1980**, *53*, 333.
(377) Callear, A. B.; Dickson, D. R. *Trans. Faraday Soc.* **1970**, *66*, 1987.
(378) Bridges, L.; White, J. M. *J. Phys. Chem.* **1973**, *77*, 295.
(379) Mouflih, B.; Larrieu, C.; Chaillet, M. *Chem. Phys.* **1988**, *119*, 221.
(380) Keller, J. S.; Kash, P. W.; Jensen, E.; Butler, L. J. *J. Chem. Phys.* **1992**, *96*, 4324.
(381) Jensen, E.; Keller, J. S.; Waschewsky, G. C. G.; Stevens, J. E.; Graham, R. L.; Freed, K. F.; Butler, L. J. *J. Chem. Phys.* **1993**, *98*, 2882.
(382) Vaghjiani, G. L. *J. Chem. Phys.* **1993**, *99*, 5936.
(383) Yarkony, D. R. *J. Chem. Phys.* **1994**, *100*, 3639.

CR940048T